Occupant Monitoring using Footstep-Induced Floor Vibration

Submitted in partial fulfillment of the requirements for

the degree of

Doctor of Philosophy

in

Civil and Environmental Engineering

Mostafa Mirshekari

B.S., Civil Engineering, University of Tehran

M.S., Project and Construction Management, University of Tehran

M.S., Civil-Structural Engineering, University of Technology, Malaysia

M.S., Civil and Environmental Engineering, Carnegie Mellon University

Carnegie Mellon University

Pittsburgh,PA

November 2019

Acknowledgements

I would like to acknowledge various forms of support that I received throughout my PhD at Carnegie Mellon. That support has permanent and constructive influence on my both academical life and personal life.

First, I would like to express my utmost gratitude to my wife, Sareh, for her unconditional support and patience during my PhD. Without her support, none of this would have been possible.

I would also thank my advisors, Prof. Hae Young Noh and Prof. Pei Zhang, for their continuous support of my Ph.D study and related research, for being a source of motivation and for pushing me to go beyond what I thought possible. Their guidance helped me in all the time of research and writing of this thesis. Further, I also want to thank them for introducing me to new realms in food! I have enjoyed some of the best foods of my life with them.

Besides my advisor, I would like to thank the rest of my thesis committee: Prof. Irving Oppenheim, Prof. Daniel Siewiorek, and Dr. Eve Schooler, for their insightful comments and encouragement, but also for the insightful questions which helped me widen my research from various perspectives.

This dissertation work was supported by several funding sources. First, I am grateful for the financial support I received from the Dean's Fellowship from Carnegie Institute of Technology and for the Bertucci fellowship. Second, I would like to acknowledge the funding we received from NSF (CMMI-1653550), Google, Intel, and Highmark.

I also want to thank all my fellow office-mates in the past few years. I like to thank my senior PhD students, Shijia Pan, George Lederman, and Frank Mokaya for being awesome and inspiring mentors. Thanks to my friend and colleague Jonathon Fagert who has always there when I needed

help with anything! Thanks to Irem Velibeyoglu for all her support and for always reminding me of important meetings! I still believe that Irem knows my schedule better than myself. Thanks to Jingxiao Liu for all the energy and positive vibes and all the insightful discussions! Thanks to Mahnoosh Babaei for all the philosophical discussions about the future of science and humanity. Finally, thanks to Adeola Bannis, Amelie Bonde, Carlos Ruiz, and Ankit Shrivastava for being an important part of my life.

I would also like to thank Civil and Environmental Engineering staff, Maxine Leffard, Cornelia Moore, Andrea Rooney, Jodi Russo, Ronald Ripper, Brian Belowich, Marilu Lundeen, and Marc Peretti for their logistical help throughout my PhD. Last but not the least, I would like to thank my family: my parents, my brothers, and my in-laws for supporting me throughout writing this thesis and my life in general.

Abstract

The overall objective of this research is to monitor occupants in indoor settings using their footstep-induced floor vibration. Some of the current sensing approaches for occupant monitoring include vision-based, radio-frequency-based, pressure-based, and mobile-based sensing. However, maintenance and installment requirements, such as dense deployment and requiring the occupants to carry a device, limit their application. To overcome these limitations, we have introduced vibration-based sensing as a sparse and non-intrusive alternative for occupant monitoring which does not require carrying a device. The intuition behind this sensing approach is that occupant footsteps cause floor vibration waves which travel through the structure and reach our sensors. These vibrations can be used for extracting information about the occupants (e.g., location and presence). However, because these vibration waves travel through the structure, they are also affected by the structural characteristics which result in various research challenges for occupant monitoring. In this dissertation, I have focused on three research contributions which are based on structure-related challenges.

First, we present a floor-vibration-based occupant detection approach which enables detection across different structures through "model transfer". The structural effects on the signals results in footstep models being different in different structures which consequently adds to the labeled data and calibration requirements. To address this challenge, we characterize the effect of the structure on the footstep-induced floor vibration responses to develop a physics-driven model transfer approach that enables step-level occupant detection across structures. Specifically, our model transfer approach projects the data into a feature space in which the structural effects are minimized. By minimizing the structure effect in this projected feature space, the footstep

models mainly represent the differences in the excitation types and therefore are transferable across structures. In other words, in this projected space, a footstep model trained in a source structure in which labeled data is available can be used for target structures in which no labeled data is available. By only requiring labelled data from a few source structures, this approach significantly reduces the labeled data and calibration requirements. We analytically show that the structural effects are correlated to the Maximum-Mean-Discrepancy (MMD) distance between the source and target marginal data distributions. Therefore, to reduce the structural effect, we minimize the MMD between the distributions in the source and target structures. We evaluated the robustness of our approach through field experiments in three types of structures. Our evaluation consists of training a footstep model in a set of structures and testing it in a different structure. As the performance metric, we have utilized F1 score which is the harmonic mean of the precision and recall rate and has been commonly used for evaluating classification algorithms. Across the three structures, the evaluation results show footstep detection F1-score of up to 99 percent for our approach, corresponding to 29X improvement compared to a baseline approach which does not transfer the model.

Second, we characterize dispersive wave propagation to localize occupants using their footstep-induced floor vibrations and without extensive calibration. To localize the footsteps, we utilize the Time Differences of Arrival (TDoA) and the propagation velocity of the footstep-induced vibration waves. To this end, the main challenges are: 1) the vibration wave propagation in the floor is of dispersive nature (i.e., different frequency components travel at different velocities) and 2) due to floor heterogeneity, these wave propagation velocities vary in different structures as well as in different locations in a structure. These challenges result in signal distortions which in turn reduce the TDoA and propagation velocity estimation accuracy and lead to large localization inaccuracies or calibration requirements. We present a "decomposition-based dispersion mitigation technique" which extracts specific components (which have similar propagation characteristics) for localization. Further, we introduce an "adaptive multilateration approach" that employs heuristics to constrain the search space and robustly locate the footsteps when the propagation velocity is unknown. We evaluated our approach using field experiments in 3 different types of buildings (both commercial

and residential) with human participants. The results show an average localization error of 0.34 meters, which corresponds to a 6X reduction in error compared to a baseline method (which will be defined in the thesis). Furthermore, our approach resulted in standard deviation of as low as 0.18 meters, which corresponds to a 8.7X improvement in precision compared to the baseline approach.

Third, we model the obstruction effect on the footstep-induced floor vibration waves to enable robust occupant localization in obstructive indoor settings. obstructions such as walls and furniture add mass to the structure which affect the structural characteristics, the wave propagation velocity, and in turn, reduce the localization performance. To address this challenge, we localize footsteps by considering different velocities between the footsteps and sensors depending on the existence and mass of obstruction on the wave path. Specifically, we 1) detect and estimate the mass of the obstruction by characterizing the wave attenuation rate, and 2) use this estimated mass to find the propagation velocities for localization by modeling the velocity-mass relationship through the lamb wave characteristics. Finally, we leverage these propagation velocities to locate the footsteps (and the occupants) using our non-isotropic multialteration approach. In field experiments, we achieved average localization error of 0.61 meters, which is 1) the same as the average localization error when there is no obstruction and 2) 1.6X improvement compared to a baseline approach which does not consider the effect of the obstruction.

List of Figures

List of Tables

Contents

Chapter 1

Introduction

1.1 Motivation

The objective of this research is to develop a framework for monitoring occupants inside buildings using their footstep-induced structural vibration. Monitoring occupants in indoor settings involves tracking their information such as presence and location. This information is important in many smart building applications such as efficient energy management [1, 2] and senior/healthcare [3, 4]. Knowing the presence and location of the occupants in different rooms of the building enables efficient assignment of the heating and cooling. Furthermore, detecting and localizing the occupant footsteps is useful for estimating gait-health-related features such as step time, stride length, and step frequency. These features can then be used for predicting and tracking the progression of many medical conditions [5–7]. Current sensing approaches for occupant monitoring include vision-based [8, 9], RF-based [10–12], pressure-based [13, 14], and mobile-based [15–19] sensing approaches. These application of these approaches are limited due to installation and maintenance requirements. Vision-based sensing is sensitive to visual occlusions such as furniture and column which exist in indoor settings. Non-wearable RF-based approaches and pressure-based approaches require dense deployment for step-level occupant monitoring. Mobile approaches require the occupants to carry or wear a device which limits their application in applications such as senior/healthcare.

To overcome these limitations, we have introduced vibration-based sensing for occupant monitoring. This approach is robust to visual occlusions, enables sparse sensing, and does not require the occupants to carry a device. The intuition behind this approach is that footsteps cause vibrations in the floor. These vibrations travel through the structure and reach our vibration sensors at different times. These structural vibrations contain occupant information which can be utilized for monitoring them in a step-level manner. However, by travelling through the structure, these vibration signals are also affected by the underlying structure characteristics which introduces challenges for extracting information from them. In the next section, I will discuss the main structure-induced research questions and challenges that are investigated in this dissertation.

1.2 Research Questions

The high-level research question that we answer is: "How can we detect and locate the occupants using the floor vibrations caused by their footsteps?" This high-level research question can be divided into the following sub-questions:

- "How to model the structural effect on footstep-induced vibration responses to enable footstep modelling across different structures?"

  Due to structure-dependent vibration characteristics, a footstep model trained through supervised learning in one structure is not accurate in other structures. In other words, the distribution of the vibration data is different across various structures and hence, the footstep model does not transfer well between them. Furthermore, acquiring labeled data in every structure and possibly different locations in the same structure is costly and difficult. We have addressed this challenge in the context of occupant detection by introducing a model transfer approach which projects the data in a space with reduced structural effect. Lower structural effect means that in this projected space, the footstep model mainly represents the excitation differences and is similar across structures (i.e., transfers well between them).

- "How to characterize the dispersive wave propagation in the floor to localize occupants without extensive calibration?"

The wave propagation in the floors is dispersive (i.e., different frequency components have different propagation velocity). Signal distortion due to dispersive floor characteristics results in drastically dissimilar signal shapes for the same footstep signals measured from multiple sensors. Thus, the comparison of those signals become difficult, which leads to inaccurate Time-Difference-of-Arrival (TDoA) estimation and occupant localization. Furthermore, wave propagation velocities are important parameters in multilateration for estimating the footstep location, but they are unknown and differ greatly across different locations of the floor and also across different buildings due to structural heterogeneity. Unknown propagation velocity either requires extensive calibration, which is time-consuming and costly, or adds to the dimension (i.e., number of unknowns) of the multilateration (which is a highly non-convex problem) and results in large localization errors.

We mitigate the effect of the dispersion by decomposing the signal into frequency components and localize the footsteps using various components. By separating signals into different components each of which has similar wave propagation characteristics, we reduce the dispersion-induced signal distortions. To eliminate the need for velocity calibration, we introduce an adaptive multilateration approach which employs heuristics about the space configuration to define a novel formulation to be minimized across a constrained search space (i.e., footstep location and propagation velocity). By constraining the search space, we reduce the effect of non-convexity (which might result in erroneous local minima) to robustly estimate location when the propagation velocity is unknown and changes for different locations.

- "How to model the effect of obstructions on the footstep responses to improve the sensing sparsity?"

  Obstructions such as walls and furniture affect the wave propagation characteristics which in turn cause localization errors. We have observed that the obstruction mass is one of the key factors that affect the wave propagation velocity and reduce the localization accuracy. Therefore, to overcome the obstruction challenge, we localize footsteps by considering different

velocities between the footsteps and sensors depending on the existence and mass of obstruction on the wave path. Specifically, we 1) detect and estimate the mass of the obstruction by characterizing the wave attenuation rate and 2) use this estimated mass to find the propagation velocities for localization by modeling the velocity-mass relationship through the lamb wave characteristics. Then, we leverage these obstructed propagation velocities to locate the footsteps (and the occupants) using our non-isotropic and grid-search-based multilateration approach which estimates the footstep location when the propagation velocities between the footstep and different sensors are different..

1.3 Dissertation Overview

The structure of this dissertation is as follows: in Chapter 2, I discuss our vibration-based data acquisition and impulse detection procedures which are common in all of the applications. In Chapter 3, I answer the first research question by discussing our model transfer approach. In Chapter 4, I discuss the dispersive wave propagation research question and our solution. In Chapter 5, I address the obstruction effect research question to enable occupant localization in obstructed indoor environments. Finally, in Chapter 6, I provide a brief summary of this dissertation and discuss the future research directions.

Chapter 2

Structural Vibration Sensing

For vibration data acquisition, we measure the vertical floor vibrations which is a mixture of footsteps, other impulsive excitations (such as falling objects, door shutting, etc.), and background noise (such as fan, machinery, and sensor noise). The details of our sensing approach are discussed in Section 2.1. To ensure that we analyze the footstep-induced part of the signals, we first need to detect and extract them in the signals. To this end, we first separate the impulsive excitations from the stationary background noise. To this end, we use the assumption that these impulsive vibration signals are of higher variation than the background noise and perform an anomaly detection to separate them. The details of this procedure is discussed in Section 2.2 and an example is presented in Figure 2.2. Then, we classify the extracted impulsive vibration events into footsteps and non-footsteps, which is discussed in Section 3.

2.1 Vibration Data Acquisition

The structural vibration is measured using geophone sensors placed on the floor at different locations. Compared to accelerometers, geophones are low-cost and low-distortion sensors which convert the velocity of the floor vibration to voltage. Generally, the footstep-induced vibrations have low energy and amplitude. Therefore, to improve their resolution, the vibration signals are then amplified using an op-amp [20]. Higher signal resolution results in more information and

more robust and accurate monitoring. Empirically, we have found that a 200-2000X amplification rate provides high signal resolution and avoids signal clipping. Of course, this ratio also depends on the underlying structure and its stiffness.

Then, the vibration signals are digitized and transferred to a Personal Computer (PC) for further analysis. To transfer the data, we have two options: 1) wired sensing system (presented in Figure 2.1a) and 2) wireless system (presented in Figure 2.1b). The wired sensors transfer the data through wires and are generally suitable in applications for which fine-grained synchronization is necessary (e.g., occupant localization). On the other hand, wireless sensors transfer the data through radio and are suitable for other applications due to the their implementation ease. Batteries or power plugs are used for powering these sensors. Power plugs are better suited for a long-term deployment as they do not require maintenance and replacement (like batteries). However, they are harder to implement as they require configuring the sensors considering the available power plugs and also increase the wiring requirements.

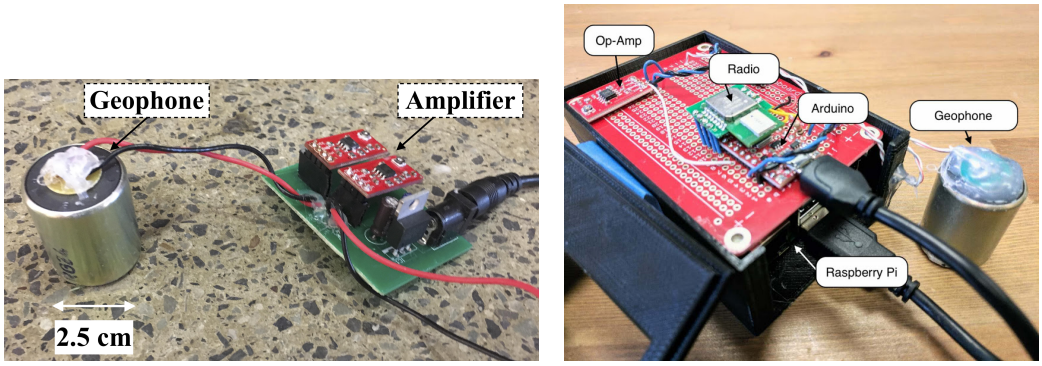

(a) Our Wired System **(b)** Our Wireless System

Figure 2.1: The Sensing Unit. The geophone measures the velocity of vertical vibration on the floor which then will be amplified, digitized, and transferred to a PC for further analysis. Part (a) and (b) show our wired and wireless sensing units.

2.2 Impulse Detection

To extract the impulsive vibration events, we conduct a chi-squared hypothesis test. The main intuition is that the variance of the impulsive event signal is larger than the variance of the ambient

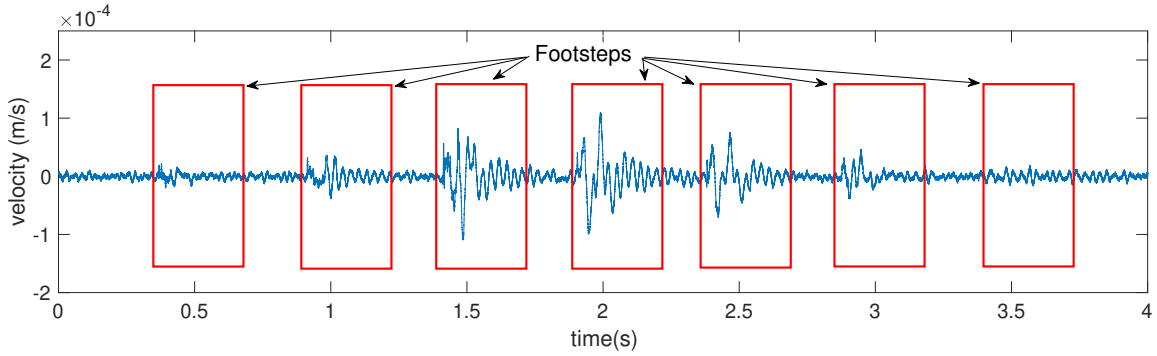

Figure 2.2: An Example of Footstep-induced Floor Vibration Signals Measured by a Geophone.

noise signal. To this end, we use the Chi-squared test that determines whether the signal has the same variance as the ambient noise. In other words, the Chi-squared test evaluates the null hypothesis $H_0 : \sigma_w^2 = \sigma_n^2$ (i.e., signal is a noise) against the alternative hypothesis $H_1 : \sigma_w^2 > \sigma_n^2$ (i.e., signal is an impulsive event), where σ_w^2 is the variance of the signal window and σ_n^2 is the variance of the ambient noise. We use the sliding window on the signal and conduct the hypothesis test for each window to detect impulsive vibration events. We have empirically chosen one tenth of a second as the window size to ensure that the beginning part of the footstep vibration signal is detected. The reason behind choosing the Chi-squared test is that the variance of the ambient noise signal follows a scaled Chi-squared distribution. Specifically, assuming normally distributed and independent noise measurements, the following statistics (i.e., χ^2-statistics) for each window has a Chi-squared distribution [21]

$$\chi_w^2 = (m-1)\frac{s_w^2}{\sigma_n^2}, \tag{2.1}$$

where m is the number of samples in the signal window, and s_w is the sample variance of the signal within the window.

We continuously and incrementally [22] learn and update the population variance of the ambient noise, σ_n^2, from the sensed data using the following equations.

$$\mu_n[h] = \mu_n[h-1] + \frac{1}{h}(x_n[h] - \mu_n[h]) \tag{2.2}$$

$$\sigma_n^2[h] = \frac{(h-1)\sigma_n^2[h-1] + (x_n[h] - \mu_n[h-1])(x_n[h] - \mu_n[h])}{h}, \tag{2.3}$$

where $x_n[h]$ is the h^{th} measurement for ambient noise signal, $\mu_n[h]$ and $\sigma_n^2[h]$ are the updated mean and variance of the ambient noise signal after adding the h^{th} measurement.

When the signal form deviates from the ambient noise, the corresponding statics, χ_w^2, also deviates from the chi-square distribution. Thus, for every signal window, we compare the χ_w^2-statistics with χ_α^2, which is the statistic value corresponding to the significance levels of α (i.e., the probability of having samples with χ^2-statistics higher than χ_α^2 given the null hypothesis). Specifically, we reject the H_0 if $\chi_w^2 \geq \chi_\alpha^2$ [21]. The significance level is the false positive rate of the test (i.e., the probability of rejecting the null hypothesis when it is true). In this work, we empirically choose the significance value of 0.01. The windows in which the null hypothesis is rejected correspond to the vibration events.

Chapter 3

Footstep Modelling across Structures using Model Transfer

The objective of footstep modelling is to distinguish vibrations caused by the footsteps from the ones caused by other impulsive excitations. Conventionally, a set of labelled data (footsteps and non-footsteps) are used to train a footstep model through supervised learning. However, the vibration responses are affected by the underlying structure. Therefore, the footstep models trained in one structure do not transfer and will be unable to distinguish the footsteps and non-footsteps in other structures. Thus, labelled data is required in different structures (and different locations in the same structure) which is costly and time-consuming to acquire. To address this challenge, we introduce a model transfer approach which first models the structural effect and then finds a projected space in which the structural effect on the data is minimized. In the projected space, the models are similar across structures and hence transfer well. Our model transfer approach does not require labelled data in every structure and hence reduces the labelled data requirement. In this section, we first review the related literature in Section 3.1. Then, we discuss the physical intuition behind our approach including our analytic physical characterization of model transfer in Section 3.2. Then, we describe our step-level occupant detection approach in Section 3.3 and evaluate it in Section 3.4.

3.1 Literature Review

In recent years, footstep-induced floor vibration sensing has been used for many occupant monitoring applications such as occupant localization [23–26], activity monitoring [27–29], occupant identification [30], and occupant balance estimation [31]. In this paper, we introduce a model transfer approach for step-level occupant detection using this sensing approach. Here, we first discuss the current floor-vibration-based occupant detection approaches and their limitations. Then, we review the literature for model transfer (sometimes also referred to as transfer learning).

3.1.1 Conventional Learning Approaches for Floor-Vibration-Induced Occupant Detection

The current floor-vibration-based approaches for occupant detection use signal processing and machine learning approaches to distinguish the footsteps from the non-footstep excitations. Some examples of these approaches include: 1) statistics-based signal analysis, using features such as kurtosis [32, 33], Chi-squared [24, 34], and auto-correlation [35], 2) matched filtering [25, 36], and 3) supervised learning (e.g., neural networks [37] and support vector machines [38]). However, these approaches require calibration in every structure or at every noise level. For example, the statistics-based approaches require a threshold which may change in various structures. Furthermore, the matched filtering and supervised learning approaches require labelled data in every new structure, as well as various locations in the same structure. Due to these calibration requirements, these approaches are difficult and expensive to implement in real applications.

3.1.2 Transfer Learning

Model transfer or transfer learning has been introduced in machine learning to reduce labeled data requirements. The idea behind transfer learning for vibration-based occupant detection is to use the labeled vibration data in a specific structure (source) to train a footstep model in other structures (target) in which only unlabeled data is available. In the literature, this specific context corresponds to transductive transfer learning [39]. Similar to model transfer, unsupervised learning

approaches assume no labeled data in the structure. However, they do not utilize the labeled data in the other structures (i.e., source structures) which results in lower model performance. Furthermore, semi-supervised and supervised learning algorithms assume that at least some labeled data is available for the structure [40]. The main categories of transductive transfer learning are instance-based and feature-based approaches.

Instance-Based Transductive Transfer Learning. The main idea behind the instance-based approaches is to assign higher weights to a subset of the source instances which are more likely to happen in the target structure for model training [41–44]. Therefore, these approaches assume an overlap between the source and target data distribution in the original data space. In our application, various structures have drastically different signal characteristics that typically do not overlap in the original data space and hence instance-based transfer is not suitable.

Feature-Based Transductive Transfer Learning. The feature-based approaches aim to find a feature space (i.e., the projection of the original data) in which the distributions of data in the source and target share similarities [45–49]. It is possible to find such a feature space even if in the original data space the source and target distributions are different and therefore, these approaches are more suitable for our problem. To demonstrate this point, we consider a set of input vibration responses $\mathbf{Y_S} \in \mathbb{R}^{n_s \times n_b}$ and $\mathbf{Y_T} \in \mathbb{R}^{n_t \times n_b}$ for the source and target structures where n_s and n_t are the number of samples in the source and target structures and n_b is the length of each input vector. Assuming $n_s = n_t$ and to ensure similarity in the projected space, we aim to find the solutions for $\mathbf{Y_S W} = \mathbf{Y_T W}$ where $\mathbf{W} \in \mathbb{R}^{n_b \times n_d}$ projects the source and target data into a n_d-dimensional feature space. Here, without loss of generality, we consider the simplest case of $n_d = 1$. Existence of solutions for this equation means that regardless of the differences in the original data space, the source and target distributions in the projected feature space share similarities. We can rewrite the equation as a homogeneous set of simultaneous equations $(\mathbf{Y_S} - \mathbf{Y_T})\mathbf{W} = 0$. This set of equations always have non-trivial solutions as long as there are more unknowns than equations ($n_b > n$) [50]. This condition is generally true in our application as the length of the sample vectors (e.g., the number of bins in frequency domain representation) are much higher than the number of samples. This proof shows that there exists a projected space in which the source and target distribution

share similarity. However, this similarity does not ensure separable classes (e.g., footsteps and non-footsteps) nor high performance of the model in the projected feature space.

Furthermore, the current feature-representation-based approaches only ensure that the marginal distribution of the data are similar across the source and target structure. In other words, there is no guarantee that in the projected feature space the source structure features for the footsteps are close to the target structure features for the footsteps and the non-footsteps close to the non-footsteps. Therefore, even after projection, the footstep models are not necessarily transferable across various structures. To overcome these limitations, we reduce the structural effect which ensures that the footstep models in the projected feature space mainly represent the excitation characteristics. To this end, we utilize physical insights to 1) characterize the structural effect on the floor vibration response and its distribution and 2) introduce a model transfer approach which reduces the structural effect to make the footstep models useful across various structures. By mainly representing the excitation effect, the features for footsteps in the source and target structure are close to each other and similarly, the features for non-footsteps are close in source and target structures. Hence, in the projected feature space, the footstep models are transferable across various structures.

3.2 Analytic Physical Characterization of Model Transfer for Occupant Detection

Our approach models the footstep floor vibrations to distinguish the signals caused by them from the ones caused by non-footsteps. These floor vibrations depend on the underlying structure and therefore the the footstep models trained in one structure are significantly different from other structures. In this section, we first describe the excitation mechanism and the structural effects by showing a set of footstep and balldrop signals in two structures. Then, we characterize the structural effect on the vibration responses to transfer the models across various structures.

Structure-Dependent Excitation Mechanism. Intuitively, impulsive excitations cause deformations in the floor structure. The floor is then restored to its original position due to the elasticity of the structure. The repeated cycle of applied force and restoration force results in a deformation

cycle and oscillations in the floor structure, which are commonly referred as "vibrations". Various excitations result in different deformation patterns and hence vibration signals. Therefore, if we have labeled footstep and non-footstep signals from a structure, we can train a classifier to distinguish them.

However, the vibration signals are also affected by the underlying structure and its characteristics. To illustrate this point, Figure 3.1 shows sample balldrop and footstep signals from two structures. Figures 3.1a-3.1b show the balldrops and Figures 3.1c-3.1d show the footsteps. In each structure, the footstep and balldrop are different in shape which enables training the footstep model. However, the differences between the footstep and the balldrop are not consistent in these two structures. Therefore, the model we train using the labeled signals from one of the structures is not applicable to the other structure. To better understand this problem and our solution, in the rest of this section, we first analytically describe the effect of the structure and the excitation type on the vibration signals. Then, we show that our model transfer approach minimizes the effect of the structural differences on the vibration signals. This minimization enables us to use the same footstep model from the source structure for footstep prediction in the target structure.

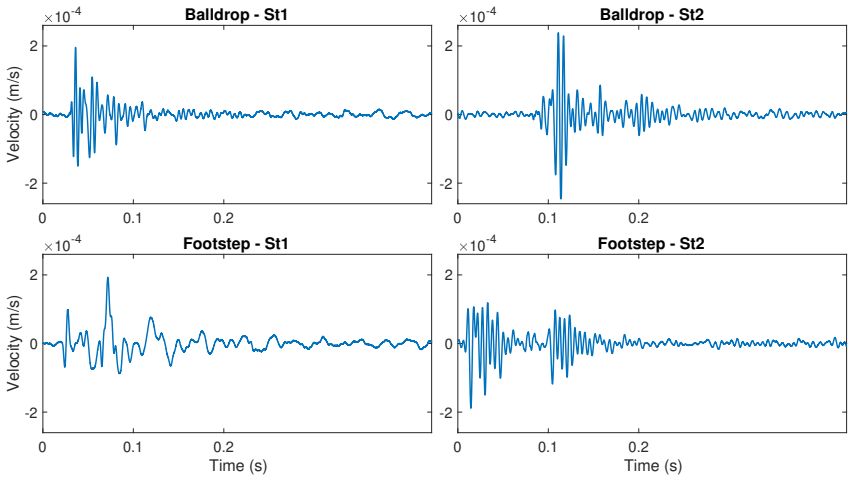

Figure 3.1: Sample Signals of Balldrop and Footstep Impulses in Two Structures. The differences between the footstep and the balldrop are not consistent in these two structures. Therefore, the model trained in one structure is not suitable in the other structure.

Structural Effect Formulation. To transfer the models across structures, we first formulate the structural effects on the vibration responses through the convolution theorem assuming Linear

Time-Invariant (LTI) system [51]. Specifically, in frequency domain, a specific sample (e.g., i^{th}) can be described as,

$$\mathbf{Y_i} = \mathbf{H_i}\mathbf{X_i} \tag{3.1}$$

where $\mathbf{Y_i} \in \mathbb{R}^{n_b \times 1}$ is the vibration frequency representation in which n_b is the number of frequency bins and $\mathbb{R}$ is the set of real numbers, $\mathbf{X_i} \in \mathbb{R}^{n_b \times 1}$ is the input force spectrum, and $\mathbf{H_i} \in \mathbb{R}^{n_b \times n_b}$ is the frequency response function (FRF) of the structure which can be described as the following diagonal matrix.

$$\mathbf{H_i} = \begin{pmatrix} h_1 & & & \\ & h_2 & & \\ & & \ddots & \\ & & & h_{n_b} \end{pmatrix}. \tag{3.2}$$

Minimizing the Structural Effect. The vibration responses depend on the structure and the excitation, as shown in Equation 3.1. Therefore, by minimizing the structural effect, the trained model mainly represents the excitation effect and transfers across structures. To this end, in the rest of this section, we show that the structural effect is correlated to the Maximum-Mean-Discrepancy (MMD) distance between the source and target structure in a given kernel space. This insight implies that by minimizing the MMD distance between the source and target distributions, we achieve our objective of minimizing the structural effect which enables transferring models across the structures.

To show the aforementioned correlation, we analytically describe the MMD distance with respect to the structural effects. MMD is a non-parametric distribution distance metric which does not require an intermediate density estimate and hence does not require distribution type assumption [52, 53]. Given the datasets $\mathbf{S} = \{\mathbf{Y_i^s}\}$ and $\mathbf{T} = \{\mathbf{Y_i^t}\}$ from the source and target structures respectively, the empirical estimate of the MMD can be described as in [54]

$$MMD(\mathbf{S}, \mathbf{T}, \phi) = \left\| \frac{1}{n_s} \sum_{i=1}^{n_s} \phi(\mathbf{Y_i^s}) - \frac{1}{n_t} \sum_{i=1}^{n_t} \phi(\mathbf{Y_i^t}) \right\|_{\mathcal{H}} \tag{3.3}$$

where ϕ is a kernel-induced feature map, n_s and n_t are the number of samples in the source and target

structures, $\mathbf{Y_i^s}$ and $\mathbf{Y_i^t}$ are the i^{th} samples in the source and target structures, and $\|.\|_{\mathcal{H}}$ is the norm in the Reproducing Kernel Hilbert Space (RKHS). RKHS is a Hilbert space with two properties: 1) the feature map of every point is in the feature space and 2) it has reproducing property meaning that for the values of the functions can be evaluated through an inner product [55]. The kernel matrix can be defined as $K = [\phi(\mathbf{Y_i})^T \phi(\mathbf{Y_j})]$ to rewrite the Equation 3.3 through the kernel trick as in [48]

$$MMD(\mathbf{S}, \mathbf{T}, \mathbf{K}) = tr(\mathbf{KL}) \tag{3.4}$$

where $\mathbf{K} \in \mathbb{R}^{(n_s+n_t)\times(n_s+n_t)}$ is the kernel matrix for the dataset consisting of the data from both the target and source structures. The submatrices forming the kernel matrix are shown in Equation 3.5.

$$\mathbf{K} = \begin{bmatrix} \mathbf{K_{S,S}} & \mathbf{K_{S,T}} \\ \mathbf{K_{T,S}} & \mathbf{K_{T,T}} \end{bmatrix} \tag{3.5}$$

where $\mathbf{K_{S,S}} \in \mathbb{R}^{n_s \times n_s}$ and $\mathbf{K_{T,T}} \in \mathbb{R}^{n_t \times n_t}$ are the kernel matrices between the source samples and target samples, respectively. Furthermore, $\mathbf{K_{S,T}} \in \mathbb{R}^{n_s \times n_t}$ and $\mathbf{K_{T,S}} \in \mathbb{R}^{n_t \times n_s}$ are the kernels across the samples in source and target structures. $\mathbf{L} \in \mathbb{R}^{(n_s+n_t)\times(n_s+n_t)}$ is a matrix of coefficients which is found by

$$\mathbf{L_{ij}} = \begin{cases} \frac{1}{n_s^2} & \mathbf{Y_i}, \mathbf{Y_j} \in \mathbf{S} \\ \frac{1}{n_t^2} & \mathbf{Y_i}, \mathbf{Y_j} \in \mathbf{T} \\ -\frac{1}{n_s n_t} & otherwise \end{cases} \tag{3.6}$$

Knowing that the trace of a product of two matrices can be rewritten as the sum of element-wise product of them, we can use the Equations 3.5 and 3.6 to rewrite Equation 3.4 as,

$$MMD(\mathbf{S}, \mathbf{T}, \mathbf{K}) = \frac{1}{n_s^2}\mathbf{K_{S,S}} + \frac{1}{n_t^2}\mathbf{K_{T,T}} - \frac{2}{n_t n_s}\mathbf{K_{T,S}} \tag{3.7}$$

The distance defined by Equation 3.7 is correlated to the structural effects. To show this, we first describe the kernel matrix in terms of the input force spectrum and the frequency response function. For better understanding, we start with the simpler case of assuming a linear kernel for which $\phi(\mathbf{Y_i}) = \mathbf{Y_i}$. In this case, the MMD distance from Equation 3.3 is equivalent to the Euclidean

distance between the mean of the source and target samples in the original data space. Using the expression in Equation 3.1, the linear kernel matrix for a set of n samples can be found using

$$\mathbf{K} = \mathbf{X^T H^T H X} \tag{3.8}$$

where $\mathbf{H} \in \mathbb{R}^{n_b \times (n_b \times n)}$ and $\mathbf{X} \in \mathbb{R}^{(n_b \times n) \times n}$ are matrices containing the FRF and input force spectrum for all the samples and can be described as

$$\mathbf{H} = \begin{pmatrix} \mathbf{H_1} & \mathbf{H_2} & \dots & \mathbf{H_n} \end{pmatrix} \tag{3.9}$$

$$\mathbf{X} = \begin{pmatrix} \mathbf{X_1} & & & \\ & \mathbf{X_2} & & \\ & & \ddots & \\ & & & \mathbf{X_n} \end{pmatrix}. \tag{3.10}$$

The next step is to rewrite Equation 3.7 in terms of the structural and input responses using the kernel matrix in Equation 3.8. Assuming that the input matrix is similar for the source and target structures (i.e., $\mathbf{X_T} = \mathbf{X_S} = \mathbf{X}$) and using the kernel description from Equation 3.8, we can rewrite Equation 3.7 as

$$MMD(\mathbf{S}, \mathbf{T}) = \frac{1}{n_s^2}\mathbf{X^T H_S^T H_S X} - \frac{2}{n_t n_s}\mathbf{X^T H_S^T H_T X} + \frac{1}{n_t^2}\mathbf{X^T H_T^T H_T X}. \tag{3.11}$$

Equation 3.11 can be rewritten in the following format.

$$MMD(\mathbf{S}, \mathbf{T}) = \mathbf{X^T}(\frac{1}{n_s^2}\mathbf{H_S^T H_S} - \frac{2}{n_t n_s}\mathbf{H_S^T H_T} + \frac{1}{n_t^2}\mathbf{H_T^T H_T})\mathbf{X} \tag{3.12}$$

Equation 3.12 represents the distance between the source and the target structure data distributions. The term $\mathbf{H_S^T H_T}$ shows the cross-similarity between the structure FRFs. According to this equation, the MMD between the source and target distributions is negatively correlated to the cross-similarity of the structures. In other words, assuming that the norms of $\mathbf{H_S}$ and $\mathbf{H_T}$ are fixed, lower distance

corresponds to higher cross-similarity between the structures and lower structural effect.

To generalize this derivation to other kernels, we use the more general description of the kernel, $\mathbf{K} = [\phi(\mathbf{Y_i})^T \phi(\mathbf{Y_j})]$. In this case, we rewrite Equation 3.8 as

$$\mathbf{K} = \phi_M(\mathbf{HX})^T \phi_M(\mathbf{HX}) \tag{3.13}$$

where ϕ_M is a function which maps each column of the matrix using the ϕ mapping. Using this definition of the kernel matrix, we rewrite Equation 3.11 as

$$MMD(\mathbf{S}, \mathbf{T}, \phi) = \frac{1}{n_s^2}\phi_M(\mathbf{H_S X})^T \phi_M(\mathbf{H_S X}) - \frac{2}{n_t n_s}\phi_M(\mathbf{H_S X})^T \phi_M(\mathbf{H_T X}) + \frac{1}{n_t^2}\phi_M(\mathbf{H_S X})^T \phi_M(\mathbf{H_S X}). \tag{3.14}$$

By defining $\phi_{MX}(\mathbf{H}) = \phi_M(\mathbf{XH})$, equation 3.14 can be rewritten in the following format.

$$MMD(\mathbf{S}, \mathbf{T}, \phi) = \frac{1}{n_s^2}\phi_{MX}(\mathbf{H_S})^T \phi_{MX}(\mathbf{H_S}) - \frac{2}{n_t n_s}\phi_{MX}(\mathbf{H_S})^T \phi_{MX}(\mathbf{H_T}) + \frac{1}{n_t^2}\phi_{MX}(\mathbf{H_S})^T \phi_{MX}(\mathbf{H_S}). \tag{3.15}$$

In equation 3.15, $\phi_{MX}(\mathbf{H_S})^T \phi_{MX}(\mathbf{H_T})$ represents the cross-similarity of a projected version of the structure FRFs. Equation 3.15 shows that the MMD between the source and target structure is negatively correlated to the projected version of the cross-similarity of the structures, assuming that the norms of $\phi_{MX}(\mathbf{H_T})$ and $\phi_{MX}(\mathbf{H_S})$ are fixed. Therefore, to reduce the structural effects, our model transfer projects the data into a feature space in which the MMD between the source and target data distributions is minimized.

However, just minimizing the MMD might not be satisfactory because: 1) it might result in a trivial solution for which there is zero distance between the distributions and all the data points are projected to the origin and 2) in these derivations, we assume that the data is noise-free which is not the case in real applications. In these cases, we might end up in a projected feature space in which the footstep and non-footsteps are mixed and not distinguishable. When introducing our method, we will discuss other objectives which will be combined with distribution distance minimization to overcome these limitations.

Footstep Models Before and After Projection. Due to the reduced structural effect, in the

projected feature space the trained models mainly represent the excitation effects and hence transfer well between the structures. In other words, in the projected feature space, the footsteps and non-footsteps from the source and target structures are close to the other footsteps and non-footsteps, respectively. Figures 3.2a and 3.2b show the data from a target and source structure before and after projection. Before projecting the data, the distance between the data distributions caused by the structural effect is significant. Therefore, the footsteps models in the target source structures are not similar. In this figure, the frequency feature A and B are the log amplitudes of the fft at 42 and 260 Hz. These specific frequencies are chosen for better illustration of the model transfer intuition. Furthermore, we use the log transform of the fft amplitudes to reduce the right-skewness of the data and improve the model training. After the projection, this structural effect and the distance between the distributions are reduced. Thus, the model trained in the source structure well represent the data in the target structure.

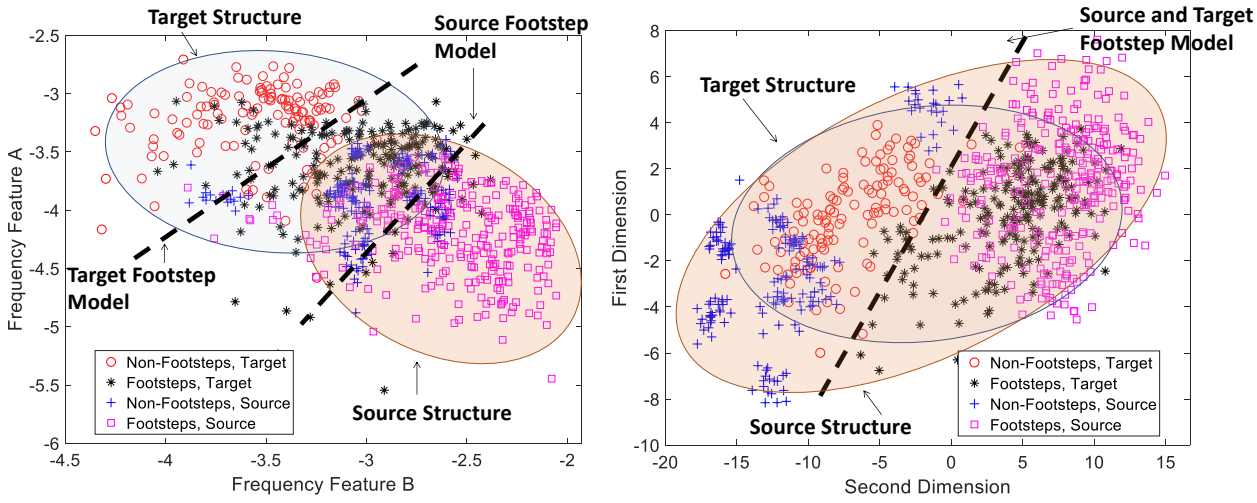

(a) Before Projection **(b)** After Projection

Figure 3.2: The Structural Effect Before and After Projection. Part (a) shows that before projection the distance between the distributions caused by the structural effects results in major differences in the footstep model. However, part (b) shows the distributions after projection where the footstep models are aligned.

3.3 Model Transfer for Step-Level Occupant Detection Across Structures

In this section, we describe our floor-vibration-based approach for step-level occupant detection across different structures through model transfer. Our approach has two main modules: 1) impulse detection module which measures the structural vibration and distinguishes possible footstep-induced vibration signals from the background noise and 2) structure-informed model transfer module which utilizes the data from the source structure to train a footstep model in the target structure. An overview of the approach is presented in Figure 3.3. The impulse detection has been discussed in Section 2. However, as shown in Figure 3.4, the separated impulses include both footsteps and other impulsive vibration events. The next modules distinguish the footsteps from other impulsive excitations.

3.3.1 Structure-Informed Model Transfer

The main objective of the structure-informed model transfer module is to use the labelled data in the source structures to develop a footstep model in the target structure. This model distinguishes the footsteps from the other impulsive excitations and therefore, enables step-level occupant detection. This objective is achieved by 1) extracting the frequency features, 2) projecting the features from the source and target structures to a new feature space in which the structural effect is reduced, 3) train a footstep model using the labelled source data in the projected feature space, and 4) predict the sample labels in the target structure by combining the predictions of the models from different source structures.

Frequency Feature Extraction

Our model transfer approach takes the frequency representation of the vibration signals as the original data features. As shown in Equation 3.1, in the frequency domain, the excitation and structure effect can be simply separated using matrix multiplication which enables the formulation of the relationship between the MMD and the structural effect. Therefore, we develop the features

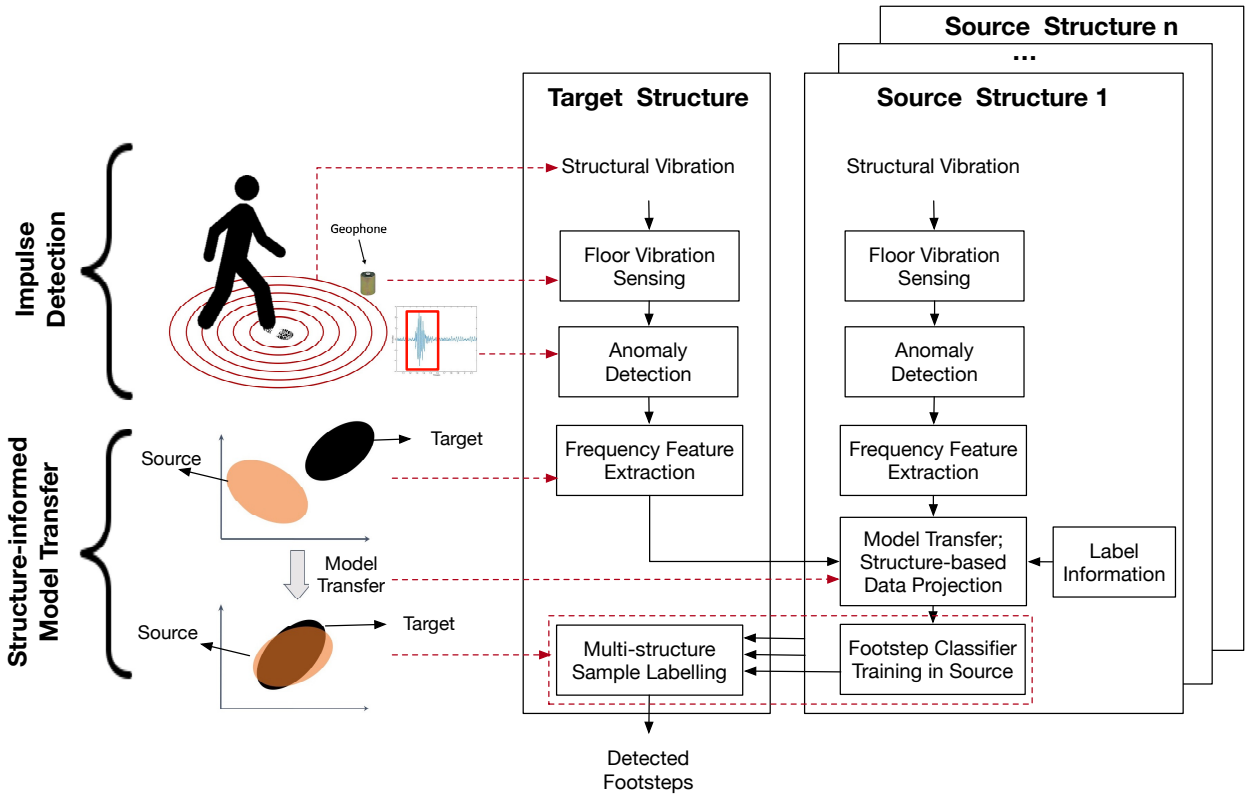

Figure 3.3: System Overview. Our approach consists of Impulse Detection and Structure-Informed Model Transfer. The figures on the left conceptually shows the steps of our approach. The red arrows relate the conceptual figures to the different steps shown in the flow chart. The black arrows in the flowchart show the relationship between different steps.

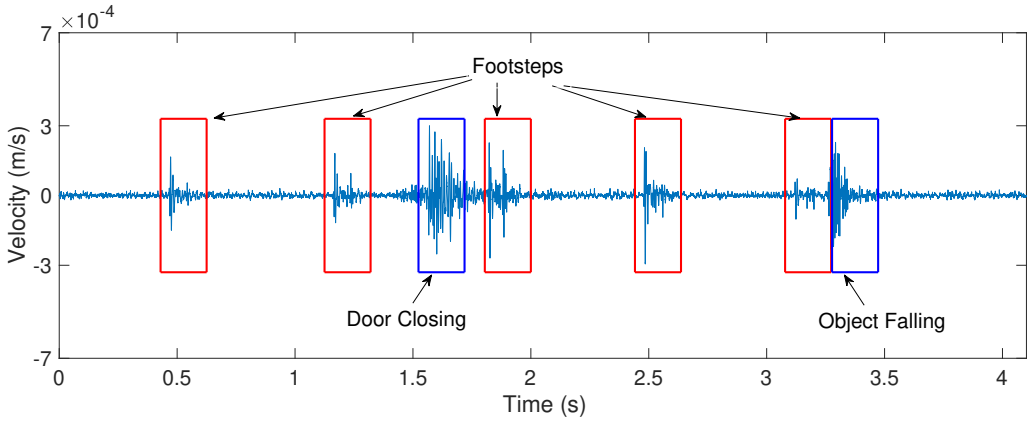

Figure 3.4: An Example of Impulse Detection. This figure shows that the detected impulses can be footsteps or other impulsive excitations such as a door closing.

for model training using the frequency domain representation which is more suitable for our problem compared to time domain and time-frequency domain representations.

However, directly using the frequency representation estimated through Fast-Fourier-Transform (FFT) has two limitations. First, the overall amplitude of the measured signals shows how much the signal is attenuated which is location-dependent and does not represent the excitation type. Therefore, before estimating the FFT of the signal, we normalize the signals to ensure the same energy for all the signals by multiplying the signal by $constant/\sqrt{\sum s_i^2}$ in which s_i is the i^{th} element of the signal. Second, the frequency data distribution is right-skewed which is caused by the fact that the values of signal amplitude in each frequency are positive. This right-skewness results in a data distribution which is less similar to Gaussian distribution and reduces the classifier training performance. To reduce this right-skewness and improve the classifier training, we perform the log transform of the frequency data by finding the logarithm of the signal amplitude in each frequency [56].

Structure-Based Data Projection

The objective of structure-based data projection is to find a a feature space in which structural effects are minimized while keeping the footsteps and non-footsteps separable. Due to reduced structural effects in this projected feature space, the footstep models trained in various structures are similar and successfully transfer between the structures. In real-life applications, minimizing only the structural effects might not be enough for model transfer because of the noise in the data and the possibility of ending up with a trivial solution. In these situations, even though the projected feature space has lower structural effect, the footsteps and non-footsteps are not separable and this results in low model performance. In the following sections, we further discuss the structural effect minimization objective and then address the aforementioned limitations by adding additional terms to the objective function using the Semi-Supervised Transfer Component Analysis (SSTCA) [48] model transfer framework.

Minimizing the Structural Effect. To minimize the structural effect, the Maximum-Mean-Discrepancy (MMD) across the source and target structures is minimized. In Equations 3.12 and 3.15, we have shown that the MMD between the source and target data distributions is correlated to the structural effect in the kernel space. MMD is a non-parametric distribution distance metric which does not make distributional assumptions about the data. Hence, it is more suitable to our

problem compared to alternative approaches (e.g., KL-divergence) because the distribution of the vibration data is unknown [57]. This MMD can be defined as $tr(\mathbf{KL})$, where $\mathbf{K}$ is the kernel matrix for the dataset consisting of the data from the target and source structures and L is a coefficient matrix. To find a feature space with lowest structural effect, instead of assuming a fixed kernel, we can solve for the kernel matrix $min_{\mathbf{K}\geq 0} tr(\mathbf{KL})$ through semi-definite programming (SDP) [54]. However, there are three limitations using this formulation:

1. SDP is computationally expensive.
2. for each new unseen test sample in the target structure, a new kernel matrix needs to be computed which adds to the computational cost.
3. to reduce the dimension of the final projected feature space (and consider a subspace with lower structural effects), additional dimensionality reduction approach (such as PCA) is necessary [48].

To overcome these limitations, an alternative representation of the objective function is formed based on the SSTCA model transfer approach [48]. Assuming positive definite (and hence invertible) kernel, we can decompose $\mathbf{K}$ and rewrite the objective function as

$$min_{\mathbf{K}} tr((\mathbf{K}\mathbf{K}^{-1/2})(\mathbf{K}^{-1/2}\mathbf{K})\mathbf{L}) \tag{3.16}$$

This decomposition is generally known as an empirical kernel map [58]. We decompose $\mathbf{K}\mathbf{K}^{-1/2} = \bar{\mathbf{K}}\bar{\mathbf{K}}^{-1/2}\widetilde{\mathbf{W}}$ where $\bar{\mathbf{K}} \in \mathbb{R}^{(n_s+n_t)\times(n_s+n_t)}$ is a fixed kernel matrix (e.g., linear, RBF, etc.) and $\widetilde{\mathbf{W}} \in \mathbb{R}^{(n_s+n_t)\times(n_s+n_t)}$ is a weight matrix. This decomposition holds as $\mathbf{K}$, $\bar{\mathbf{K}}$, $\mathbf{K}^{-1/2}$, and $\bar{\mathbf{K}}^{-1/2}$ are positive definite and invertible. Similarly, we decompose $\mathbf{K}^{-1/2}\mathbf{K} = \widetilde{\mathbf{W}}^{\mathbf{T}}\bar{\mathbf{K}}^{-1/2}\bar{\mathbf{K}}$. Based on these decompositions, the objective function is rewritten as

$$min_{\widetilde{\mathbf{W}}} tr((\bar{\mathbf{K}}\bar{\mathbf{K}}^{-1/2})\widetilde{\mathbf{W}}\widetilde{\mathbf{W}}^{\mathbf{T}}(\bar{\mathbf{K}}^{-1/2}\bar{\mathbf{K}})\mathbf{L}) \tag{3.17}$$

Next, we simplify the equations by defining $\mathbf{W} = \bar{\mathbf{K}}^{-1/2}\widetilde{\mathbf{W}}$, which results in

$$min_{\mathbf{W}} tr((\bar{\mathbf{K}}\mathbf{W}\mathbf{W}^{\mathbf{T}}\bar{\mathbf{K}})\mathbf{L}) \tag{3.18}$$

Finally, the cyclic property of the trace can be used to rewrite the equation as

$$min_{\mathbf{W}} tr(\mathbf{W}^{\mathbf{T}}\bar{\mathbf{K}}\mathbf{L}\bar{\mathbf{K}}\mathbf{W}) \tag{3.19}$$

This new representation addresses the limitations of the previous objective function. First, this representation enables finding a close-form solution which is computationally inexpensive as it does not require solving the SDP, as will be described later. Second, for new samples, the corresponding kernel values can be computed and added to the kernel matrix and there is no need to resolve the optimization problem. Finally, the dimensions of $\mathbf{W}$ can be defined as $\mathbb{R}^{(n_s+n_t)\times m}$ to project the kernel data into a m-dimensional feature space. Therefore, additional dimensionality reduction approach might not be necessary.

However, only minimizing the distance between the distributions is not enough for successful model transfer. First, the derivation in Equations 3.3 to 3.15 is based on the assumption that the data is noise-free. Existence of noise in real life applications might result in noise-governing low-variance projected features spaces. Second, it results in the trivial solution for which all the data points are projected to the origin (i.e., zero distance between the distributions). In these cases, we end up with a feature space in which the footsteps and non-footsteps are mixed and not separable. To avoid these challenges, additional terms are added to the objective function. Specifically, to avoid the challenges regarding the trivial solution and noisy data, a term is added to preserve the distance pattern of the samples (i.e., to ensure that the neighbor samples in the original data space are close to each other after projection). Furthermore, to improve the classification accuracy, another term is added to utilize the source label data by maximizing the dependence between the labels and the projected data. The following sections discuss these additional terms, the final objective function, and the close-form solution to the objective function.

Maintaining the Data Variation. In the cases of trivial solution and noisy data, we might

end up in projected spaces in which data has low variance. In these low-variance spaces, even though the distance between the distributions is small, the footsteps and non-footsteps are mixed and inseparable which in turn results in low classification accuracy. Therefore, the second term in SSTCA aims to maintain the variation and the distance pattern of the data through locality preservation. The intuition is that, if there are two samples, $\mathbf{Y_i}$ and $\mathbf{Y_j}$, which are neighbors in the original data space, they should be close to each other after projection. To ensure locality preservation, first, the data is considered as a graph with affinity of $m_{ij} = exp(-d_{ij}^2/2\sigma^2)$. This affinity is then used to form $\mathcal{N} = (\mathbf{Y_i}, \mathbf{Y_j})$ which is the set of sample pairs that are k-nearest neighbors of each other. Then, we can minimize

$$\sum_{i,j \in \mathbf{N}} m_{ij} \left\| \left[\mathbf{W^T \bar{K}}\right]_i - \left[\mathbf{W^T \bar{K}}\right]_j \right\|^2 \tag{3.20}$$

where $\left\| \left[\mathbf{W^T \bar{K}}\right]_i - \left[\mathbf{W^T \bar{K}}\right]_j \right\|^2$ is the distance between the samples $\mathbf{Y_i}$ and $\mathbf{Y_j}$ the projected feature space, respectively. Equation 3.20 can be rewritten as

$$tr(\mathbf{W^T \bar{K} \mathcal{L} \bar{K} W}) \tag{3.21}$$

where $\mathcal{L} = \mathbf{D} - \mathbf{M}$, $\mathbf{M} = [m_{ij}]$ and $\mathbf{D}$ is a diagonal matrix with entries $d_{ii} = \sum_{j=1}^{n} m_{ij}$.

Using the Label Information. To improve the classification accuracy, the third objective aims to take advantage of the labelled data in the source structure. To this end, SSTCA maximizes the dependence of the projected data and the labels using Hilbert-Schmidt Independence Criterion (HSIC) which is a non-parametric approach for estimating the dependence between two sets [59]. Specifically, SSTCA considers the HSIC between the original dataset containing all of the data in source an target, D, and the label set, L, is

$$HSIC(\mathbf{D}, \mathbf{L}) = \frac{1}{(n-1)^2} tr(\mathbf{C \bar{K} C K_L}) \tag{3.22}$$

where $\mathbf{K_L}$ is a kernel matrix representing the label dependence, $\mathbf{C}$ is a centering matrix defined as $\mathbf{C} = \mathbf{I} - (1/n_s + n_t)\mathbb{1}\mathbb{1}^\mathbf{T}$, and n is the number of all the samples in the source and target structure

and is equal to $n_s + n_t$. Furthermore, $\mathbf{K_L}$ can be described as

$$\widetilde{\mathbf{K}}_{\mathbf{L}} = \gamma \mathbf{K_l} + (1 - \gamma)\mathbf{K}_\nu \tag{3.23}$$

where $[\mathbf{K_l}]_{ij}$ is the kernel value between the i^{th} and j^{th} sample labels in the labelled source data, $\mathbf{K}_\nu = \mathbf{I}$, and γ is a trade-off parameter. It has been shown empirically that $\gamma = 0.5$ works well on all the datasets [48]. Replacing the kernel matrix definition from Equation 3.19 in Equation 3.22 and removing the constant coefficient results in

$$HSIC(\mathbf{D}, \mathbf{L}) = \mathbf{W^T}\bar{\mathbf{K}}\mathbf{C}\widetilde{\mathbf{K}}_{\mathbf{L}}\mathbf{C}\bar{\mathbf{K}}\mathbf{W}. \tag{3.24}$$

Updating the Objective Function and Finding a Solution. Finally, the three objectives shown in Equations 3.19, 3.21, 3.24 are combined to form the SSTCA optimization problem [48] which is

$$\begin{aligned} \underset{\mathbf{W}}{\text{minimize}} \quad & tr(\mathbf{W^T}\bar{\mathbf{K}}\mathbf{L}\bar{\mathbf{K}}\mathbf{W}) + \mu tr(\mathbf{W^T}\mathbf{W}) + \frac{\lambda}{n^2} tr(\mathbf{W^T}\bar{\mathbf{K}}\mathcal{L}\bar{\mathbf{K}}\mathbf{W}) \\ \text{subject to} \quad & \mathbf{W^T}\bar{\mathbf{K}}\mathbf{C}\widetilde{\mathbf{K}}_{\mathbf{L}}\mathbf{C}\bar{\mathbf{K}}\mathbf{W} = \mathbf{I} \end{aligned} \tag{3.25}$$

where $\lambda \geq 0$ is a trade-off parameter and $n^2 = (n_s + n_t)^2$ is a normalization term in which n_s and n_t are the number of samples in the source and target structures. Furthermore, $tr(\mathbf{W^T}\mathbf{W})$ is the regularization term which aims to control the complexity of $\mathbf{W}$ and avoid overfitting. The solutions of this problem are the eigenvectors of $(\bar{\mathbf{K}}(\mathbf{L} + \lambda\mathcal{L})\bar{\mathbf{K}} + \mu\mathbf{I})^{-1}\bar{\mathbf{K}}\mathbf{C}\widetilde{\mathbf{K}}_{\mathbf{L}}\mathbf{C}\bar{\mathbf{K}}$ [48]. The steps of structure-informed data projection is summarized in Algorithm 1. These eigenvectors are the dimension components which can be used for projecting the data. Furthermore, the order of the corresponding eigenvalues shows how well the data projected using the dimension components satisfy the objective function. Therefore, to project the data into a m-dimensional feature space, we choose the m eigenvectors with leading eigenvalues for data projection. The number of the projected data dimensions m affect the performance of the model transfer and is evaluated in the evaluation section.

Algorithm 1 The Structure-Informed Data Projection

$\mathbf{Y} \leftarrow [\mathbf{Y^s}; \mathbf{Y^t}]$
$n_s \leftarrow size(\mathbf{Y^s}, 1); n_t \leftarrow size(\mathbf{Y^t}, 1)$
Estimate $\bar{\mathbf{K}}(\mathbf{Y})$ *(e.g., for linear kernel* $\bar{\mathbf{K}}(\mathbf{Y}) = \mathbf{Y}\mathbf{Y^T}$*)*
for $i, j \leq n_s, n_t$ **do**
    if $\mathbf{Y_i}, \mathbf{Y_j} \in \mathbf{S}$ **then**
        $\mathbf{L_{ij}} \leftarrow \frac{1}{n_s^2}$
    else if $\mathbf{Y_i}, \mathbf{Y_j} \in \mathbf{T}$ **then**
        $\mathbf{L_{ij}} \leftarrow \frac{1}{n_t^2}$
    else
        $\mathbf{L_{ij}} \leftarrow -\frac{1}{n_s n_t}$
    end if
end for
$\mathbf{M} = [m_{ij}] \leftarrow exp(-d_{ij}^2/2\sigma^2)$ ▷ For k-nearest neighbors
$\mathbf{D} = [d_{ii}] \leftarrow \sum_{j=1}^{n} m_{ij}$ ▷ $\mathbf{D}$ is Diagonal
$\mathcal{L} \leftarrow \mathbf{D} - \mathbf{M}$ ▷ *Laplacian Matrix*
Estimate the label kernel $[\mathbf{K_l}]_{ij}$.
$\mathbf{K}_\nu \leftarrow \mathbf{I}$
$\widetilde{\mathbf{K}}_\mathbf{L} \leftarrow \gamma\mathbf{K_l} + (1-\gamma)\mathbf{K}_\nu$ ▷ *Label Dependence Matrix*
$\mathbf{C} \leftarrow \mathbf{I} - (1/n_s + n_t)\mathbb{1}\mathbb{1}^\mathbf{T}$
$eig((\bar{\mathbf{K}}(\mathbf{L} + \lambda\mathcal{L})\bar{\mathbf{K}} + \mu\mathbf{I})^{-1}\bar{\mathbf{K}}\mathbf{C}\widetilde{\mathbf{K}}_\mathbf{L}\mathbf{C}\bar{\mathbf{K}})$
return the first m eigenvectors

Footstep Classifier Training in Source

To distinguish the footstep-induced vibrations from vibration caused by non-footsteps, we utilize binary classifiers. Without loss of generality, we use Support Vector Machine (SVM), a common classification approach that does not make distributional assumptions about the data. Instead, SVM maximizes the distance (i.e., margin) of the sample points to the decision boundary [40]. After finding the suitable $\mathbf{W}$, we project the source and target data by finding the $\mathbf{W}\bar{\mathbf{K}}$. In this projected space, the structural effects on the vibration data is minimized and the source and target data distributions are similar. Therefore, the SVM classifier is trained on the labeled projected data from the source structure(s) and is used for predicting the target structure data labels. The output of the SVM classifier for each vibration sample is a score whose value and sign represent the distance of the sample to the decision boundary and whether the sample is a footstep or a non-footstep, respectively.

Multi-structure Sample Labeling

When there are more than one source structures available, each one of them is used for data projection and developing SVM classifiers for the target structure. To improve the accuracy and robustness of footstep classification (and occupant detection), we combine the scores across these classifiers. To this end, we add the SVM scores for target samples from these classifiers from all the source structures. The sign and magnitude of the final score represents the predicted label (footstep or non-footstep) and the prediction confidence.

3.4 Occupant Detection Evaluation

To evaluate the performance of our model transfer for step-level occupant detection, we have conducted a set of experiments with two human participant in real-world structures. We first introduce the experimental setup and define the metrics used for evaluation. For evaluation, we first present and analyze the step-level occupant detection results based on the whole approach (as shown in Figure 3.3) which combines the results of multiple source structures. We also aim to analyze the

model transfer part without combining the results for multiple sources to show that transferring the model improves the classification performance regardless of the choice of the source structure. To this end, we evaluate the model transfer performance for single source structure cases. Finally, we also evaluate the approach for the sensitivity to the number of available data in the target structure and in the source structures, as well as the sensitivity to the dimension of the projected feature space.

3.4.1 Experimental Setup in Three Buildings

To explore the effect of using various types of structure as the source and target structure, we have conducted experiments in three types of structures, as shown in Figure 3.5. These three structures, located in Pittsburgh, PA, include: 1) a wooden floor in the third floor of the Baptist senior care, 2) a concrete hallway on the ground level of the Porter hall, which is a campus building at Carnegie Mellon University, 3) and a metal deck floor on the second floor of the Vincentian senior care facility. The first observed natural frequency of these structures are 16.02, 23.83, and 14.84 Hz, respectively. We obtain these natural frequency estimations using the Basic Frequency Domain (BFD) or "peak-picking" approach [60], where we identify the first observed natural frequency as the first peak in the Fourier transform of ambient vibration data. The varying natural frequency of the three structures reinforces that their vibration responses will vary and justifies the use of our model transfer approach. Furthermore, to evaluate how accurate our approach is in distinguishing footsteps from other impulsive excitations, we collected footsteps as well as other impulsive excitations, such as door closings, dropping objects (ball and keychain) on the floor, and hammer striking in the experiments. Specifically, we included 220, 100, and 290 footsteps and 130, 70, and 190 non-footsteps in Baptist, Porter, and Vincentian, respectively. The impact locations are within the 5 meters around the sensor. Figure 3.6 presents the experimental setup used for all the structures.

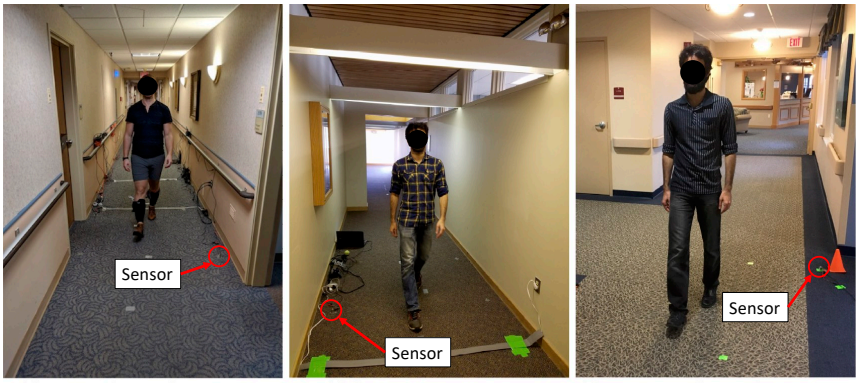

(a) Baptist Senior Care Facility (b) CMU Porter Hall - A18 (c) Vincentian Senior Care Facility

Figure 3.5: Experiment Locations.

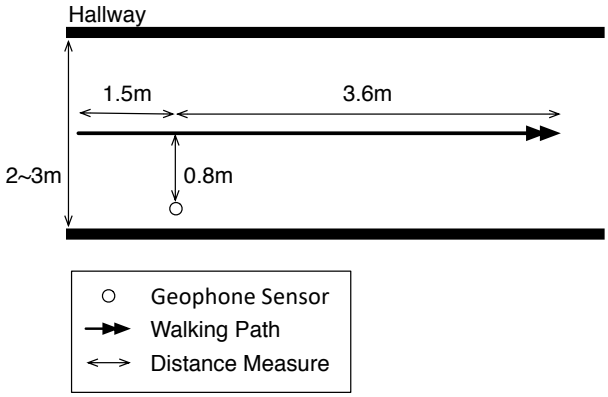

Figure 3.6: Experimental Setup. This figure shows the sensor configuration and the footstep trace utilized in all the structures.

3.4.2 Evaluation Metric and Model Parameters

As the performance metric, we have utilized the F1 score which has been commonly used for evaluating classification algorithms. The F1 score is the harmonic mean of the precision and recall rate and can be found through the following equation [61]:

$$Recall = \frac{True\ Positives}{True\ Positives + False\ Negatives} \tag{3.26}$$

$$Precision = \frac{True\ Positives}{True\ Positives + False\ Positives} \tag{3.27}$$

$$F1 = 2 \cdot \frac{precision \cdot recall}{precision + recall} \tag{3.28}$$

where True Positives mean the number of correctly detected footsteps, False Positives mean the number of non-footstep which are by mistake detected as footsteps, and False Negatives mean the number of missed footstep events. The F1 score is estimated using the k-fold cross-validation approach using $k = 10$. Using the fitcsvm MATLAB function [62], the training of the SVM model for 300 samples takes approximately 0.009 seconds using a Macbook pro with 8 GB Ram and 2.7 GHz Intel Core i5. With respect to the SVM parameters, the regularization term C (or the box constraint) is empirically set as 1. We have used a simple linear kernel to ensure that the SVM model does not overfit to the data in the source structure. Further, the software divides the input data by an appropriate scale factor which is estimated using a heuristic procedure before applying the kernel [62].

3.4.3 Overall Footstep Classification Robustness

In this section, we evaluate the accuracy and robustness of the overall footstep classification approach. To this end, we discuss and compare the robustness of our approach with two baseline approaches in three structures. The two baseline approaches utilize the time-domain (TD) and frequency-domain (FD) representations of the signal. Both TD-based and FD-based baseline approaches first train an SVM classifier in one structure and then test the model in a different structure (i.e., without model transfer). Then, each sample in the target structure is labeled by combining the SVM scores from multiple sources.

Figure 3.7a shows the comparison of the F1 score for each structure as the target. For the results of each structure, the other two structures are the source structures. For example, the Baptist results represent the case with Baptist as the target structure and Porter and Vincentian as the source structures. Based on these results, in Baptist nursing home, our approach has resulted in 0.96 F1-score which is equivalent to 9.25X and 7.5X reduction in classification error over the TD-based and FD-based approaches which results in 0.63 and 0.7 F1 score, respectively. Similarly, in Porter

Hall, our approach results in 0.97 F1-score compared to 0.71 and 0.76 F1-score using the TD-based and FD-based approach which is equivalent to 9.7X and 8X reduction in error, respectively. Finally, in Vincentian nursing home, our approach results in F1-score of 0.99 compared to the F1-score of 0.71 and 0.84 using the TD-based and FD-based approaches, equivalent to 29X and 16X reduction in error, respectively.

These higher improvements in Vincentian is due to larger separation between the footsteps and non-footsteps in this structure. To explore this effect, we define a separation metric as the mean of $\mu_f - \mu_{nf}$ where μ_f and μ_{nf} are the mean of the fft of footstep and non-footstep samples, respectively. This separation metric is 0.029 in Vincentian compared to 0.019 in Baptist and 0.018 in Porter. The models trained in the structures with smaller separation metric contain more information about the lower-confidence samples which are closer to the decision surface compared to the models trained in structures with larger separation metric. Therefore, the models trained in Baptist and Porter which have smaller separation metric perform well in the Vincentian which has larger separation metric. This effect will be described in more detail in Section3.4.4 which discusses model transfer with one source structure.

To provide more detail, Figures 3.7b and 3.7c show the evaluation results for recall and precision rate, respectively. These figures show that the baseline approaches generally have higher recall rate than precision rate. Specifically, the recall rate is between 0.92 and 1 for TD-based and between 0.84 and 1 for FD-based approaches. In comparison, the precision rate is between 0.48 and 0.58 for the TD-based and between 0.59 and 0.72 for FD-based approach. High recall rate and low precision rate implies that the baseline approaches cause a large number of false positives and detect non-footsteps as footsteps. This high false positive rate is caused by the higher variation in the footstep-induced excitations which results in distribution imbalance between the footstep and non-footsteps. In this case, the model will be biased toward classifying the samples as footsteps because the higher-variance footstep class account for more of the data space than the lower-variance non-footstep class. In comparison, our approach results in recall rate of 0.98, 0.94, and 1 and precision rate of 0.95, 1, and 0.98 for Baptist, Porter, and Vincentian, respectively. Consistent improvement in the F1-score in all the three structures shows that our approach is more robust to

the changes in the structure. Furthermore, the combined high recall and high precision rates using our approach shows that it is more robust to the footstep variations.

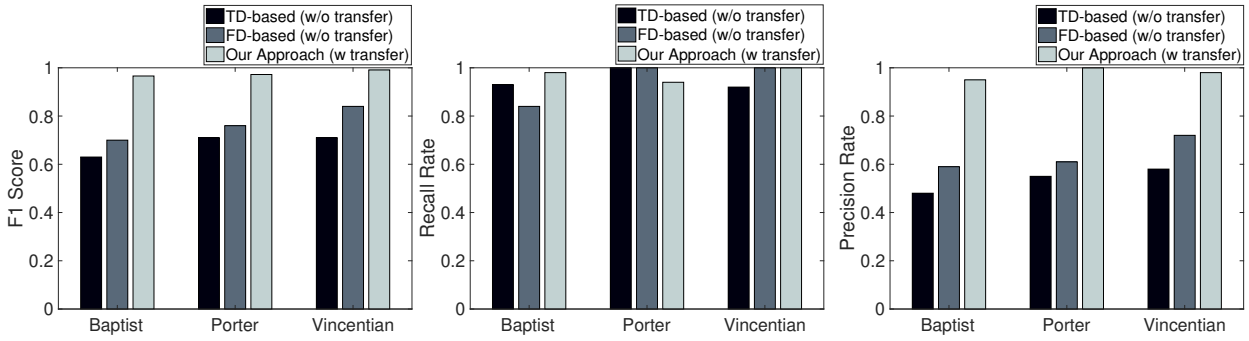

(a) F1-Score **(b)** Recall Rate **(c)** Precision Rate

Figure 3.7: The Evaluation Results in Three Structures. Part(a)-(c) compare the F1-score, recall rate, and precision rate using our transfer-based approach with two methods which utilize the time-domain and frequency-domain signals in the source without transfer to predict the sample labels in the target structure.

3.4.4 Model Transfer Evaluation for Different Source Structures

By reducing structural effects through ensuring similar data distribution in the target and source structures, the structure-informed model transfer enables footstep modelling and classification in the target structure with no labelled data. In this section, we focus on the model transfer performance by comparing the results of our approach with the TD and FD-based baseline approaches when there is only one source structure. Figures 3.8a-3.8c shows the results in Baptist, Porter, and Vincentian, respectively.

Figure 3.8a shows the F1-scores for the Baptist as the target structure. It can be seen that when the source structure is Vincentian, our approach achieves a F1-score of 0.95 compared to 0.61 and 0.65 using the TD-based and FD-based approaches, respectively, which is a 7.8X and 7X improvement in error. On the other hand, when the source structure is Porter, our approach results in F1-score of 0.89 compared to 0.64 and 0.68 using the TD-based and FD-based approaches, equivalent to 3.3X and 2.9X improvement in error.

Figure 3.8b shows the F1-scores for the case with Porter as the target structure. Our approach

achieves a F1-score of 0.98 compared to 0.67 and 0.76 using the TD-based and FD-based approaches which is equivalent to 16.5X and 12X improvement in error when the source structure is Baptist. On the other hand, when the source structure is Vincentian, our approach results in F1-score of 0.94 compared to 0.73 and 0.74 using the TD-based and FD-based approaches which correspond to 4.5X and 4.3X improvement in error, respectively.

Figure 3.8c shows the F1-scores for the case with Vincentian as the target structure. In this case, when the source structure is Baptist, our approach results in a F1-score of 0.99 compared to 0.67 and 0.79 using the TD-based and FD-based approaches which is equivalent to 33X and 21X improvement in error. On the other hand, when the source structure is Porter, our approach results in F1-score of 0.98 compared to 0.73 and 0.8 using the TD-based and FD-based approaches, which is equivalent to 13.5X and 10X improvement in error, respectively.

The first observation in these results is that the model performance is higher when the Vincentian is the source structure compared to when it is the target structure. As discussed in the previous section, the reason behind this effect is the larger separation between the footsteps and non-footsteps in Vincentian. Specifically, the separation metric is 0.029 in Vincentian compared to 0.019 in Baptist and 0.018 in Porter. Models with smaller separation metric contain more information about the low-confidence samples which are closer to the decision surface. Therefore, the models trained in Baptist and Porter perform well in Vincentian (which is shown by f1-score of 0.99 and 0.98, respectively). However, the models trained in Vincentian have lower performance in Baptist and Porter (shown by f1-score of 0.95 and 0.94, respectively).

The second observation is that using the Baptist as the source and Porter as the target outperforms using the Porter as the source and Baptist as the target. This is true even though the separation metric is similar in Baptist and Porter. The reason behind this observation is that the heterogeneity of the wooden floor in Baptist results in higher variance in the data distribution. To explore this effect, we defined a metric as the mean of the σ/μ where σ and μ are the standard deviation and the mean of the frequency representation (FFT) of the samples in each structure. The values of this metric are 1.29, 1.06, and 1.05 in Baptist, Porter, and Vincentian, respectively. The higher value of the metric show the higher data variance and heterogeneity of the data from Baptist.

Therefore, the model trained in Baptist is more informative than the model trained in Porter and works well in Porter (f1-score of 0.98), whereas the model trained in Porter has lower performance in Baptist (f1-score of 0.89).

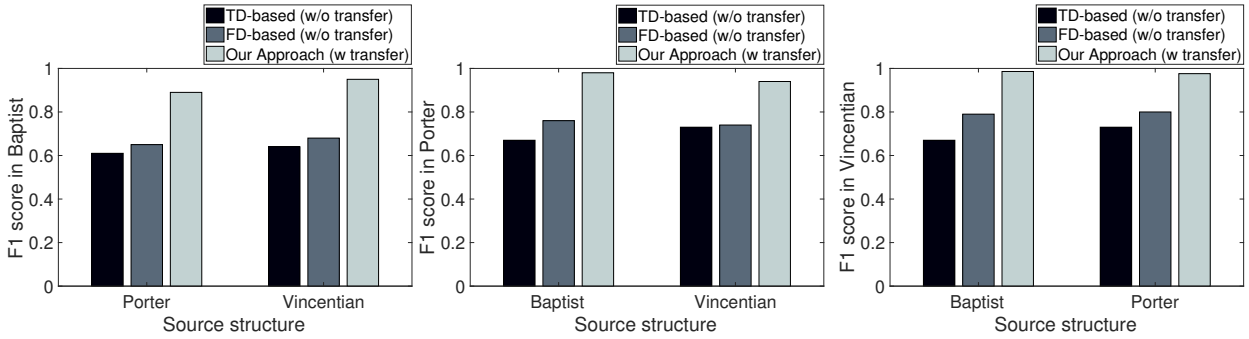

(a) Baptist Building **(b)** Porter Hall **(c)** Vincentian Building

Figure 3.8: The F1 Score using One Structure as the Source. Part(a)-(c) compare the F1-score for our transfer-based approach with the baseline approaches when different source targets are utilized.

Using more than one source structure improves the robustness of the results. In other words, the combined source structure case outperforms the source structure with lower model performance; however, the improvement over the source structure with higher performance is not substantial. Specifically, for Baptist, Vincentian, and Porter, the f1-scores are 0.96, 0.99, and 0.97 when using two source structures, 0.89, 0.98, and 0.94 when using the source structure with lower performance which is equivalent to 2.75X, 2X, and 2X improvement, respectively. However, the f1-scores when using the source structure with the higher performance are 0.95, and 0.99, and 0.98 for Baptist, Vincentian, and Porter which are equivalent to 1.25X, 0X, and -1.5X change in the error, respectively.

In summary, although model transfer performance depends on the source structure, our model transfer approach results in 0.89-0.99 F1-score and 2.9X-33X improvement in the error compared to the baseline approaches in different cases of source and target structures. Therefore, our approach successfully transfers the footstep model between the structures.

3.4.5 Sensitivity to the amount of target data

The amount of the available data in the target structure potentially affects the performance of the model transfer approach. To evaluate this effect, we have first kept 10 percent of the target data as the test data. Then, among the rest of the target data, we randomly choose varying amount of the remaining target data (unlabeled) and use it with the source data (labeled) for training. The trained model is then used for labelling the test samples and finding the F1-scores.

Figures 3.9a- 3.9c show the results of this evaluation. As expected, having a dataset with more target data results in higher F1-scores in the target structure because it better represents the target structure data distribution in model transfer. Specifically, in Baptist, Porter, and Vincentian, the F1-score is increased from 0.87 and 0.91, and 0.95 to 0.97, 0.97, and 0.99, respectively. The number of samples necessary to reach to the maximum accuracy is 240, 55, and 85 samples in Baptist, Porter, and Vincentian, respectively. The reason behind the need for more target data in Baptist is the higher variance of the target data distribution caused by higher structural heterogeneity in Baptist as discussed in the previous section. Higher structural heterogeneity results in different characteristics for the impulse signals in different locations of the structure. Therefore, more samples are necessary to represent the data distribution in the Baptist location.

Furthermore, having more target data decreases the variance of the estimated F1-scores and hence increases the robustness of the footstep model in the target structure. These variances for Baptist, Porter, and Vincentian are reduced from 0.07, 0.11, and 0.03 to 0.03, 0.04, and 0.016, respectively. These evaluation results can be used for determining the amount of target data necessary for different applications.

3.4.6 Sensitivity to the amount of source data

One of the factors affecting the performance of the model transfer approach is the amount of the data which is available in the source structure. To evaluate this effect, we have randomly kept a varying amount of the source data and estimated the F1-scores in the target data. Furthermore, to find the variance of the F1-score, we have repeated the analysis for 10 subsets of the source data.

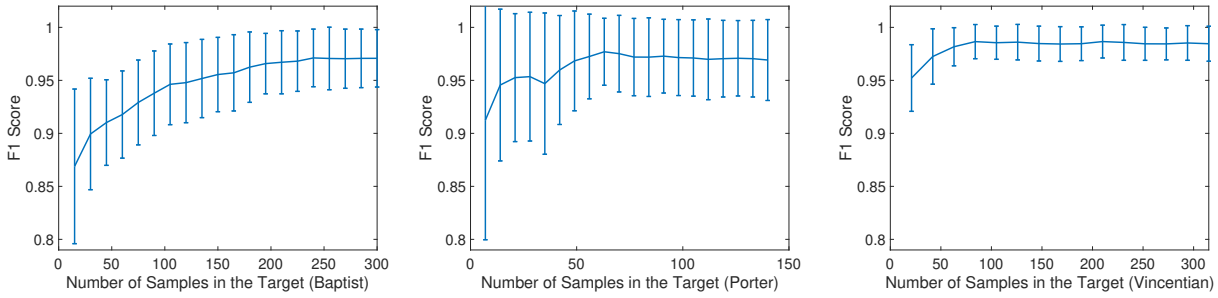

(a) Baptist Building **(b)** Porter Hall **(c)** Vincentian Building

Figure 3.9: The Sensitivity of the F1-score to the Amount of Data in the Target Structures. Part (a)-(c) show the results for the case with Baptist, Porter, and Vincentian buildings as the target structure, respectively. As expected, these figures show that in general, increasing the amount of target data results in better performance (i.e., higher F1-score) and lower standard deviation of F1-scores.

Figures 3.10a-3.10c show the results of evaluation. For the sake of comparison, these figures also present the same evaluation for the TD-based and FD-based baseline approaches.

Having a dataset with more source data generally results in higher F1-scores in the target structure because it better represents the source structure data distribution. In Vincentian, the F1-score is increased from 0.83 from cases with 15 samples to 0.98 for cases with 150 samples, respectively. In Porter, the F1-score is increased from 0.83 from cases with 15 samples to 0.95 for cases with 150 samples, respectively. As discussed in the previous section, Vincentian and Porter, which are the source structures for Baptist results are less heterogeneous. Therefore, high accuracy is achieved even with lower number of source samples for Baptist.

Furthermore, having more source data decreases the variance of the estimated F1-scores and hence increases the robustness of the footstep model in the target structure. These variances for Baptist, Porter, and Vincentian are reduced from 0.03, 0.1, and 0.065 for cases with 15 source samples to 0.007, 0.01, and 0.007 for cases with 150 samples. These results show that using 50 or more samples from the source structure results in the F1-score greater than 0.9.

3.4.7 Sensitivity to the Projected Feature Space Dimension

An important factor in the model transfer performance is the number of dimensions in the projected feature space. The dimension components for model transfer approach are ordered

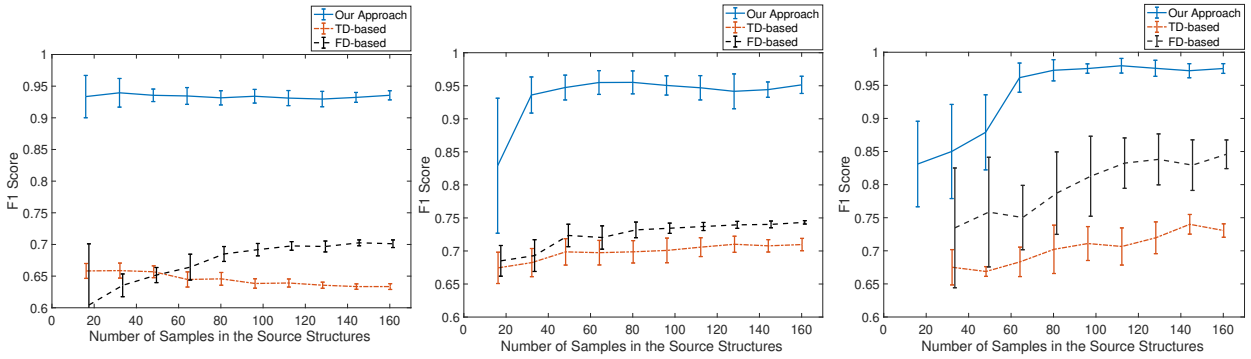

(a) Baptist Building **(b)** Porter Hall **(c)** Vincentian Building

Figure 3.10: The Sensitivity of the F1-score to the Amount of Data in the Source Structures. Part (a)-(c) show the results for the case with Baptist, Porter, and Vincentian buildings as the target structure, respectively. As expected, these figures show that in general, increasing the amount of source data results in better performance (i.e., higher F1-score) and lower standard deviation of F1-scores.

with respect to the objective function. Therefore, the effect of the number of dimensions on model transfer is a trade-off between better satisfaction of the objective function and higher model flexibility. On the one hand, as we add to the number of dimensions, we add components for which the objective function is less satisfied and this might decrease the model performance. On the other hand, using more dimensions can potentially result in higher model flexibility and performance.

We evaluated the model performance through finding the F1-score in the target structure using different numbers of dimensions. Figures 3.11a-3.11c show the results of this evaluation. The general trend of F1-score in all the three structures shows an initial increase which is caused by higher model flexibility using more dimensions. However, after the initial increase, the F1-score for Vincentian and Baptist decrease, whereas in Porter hall, the F1-score does not show significant change.

To understand this trend, the cumulative normalized eigenvalues are depicted in Figure 3.12. As discussed when describing Equation 3.25, these eigenvalues show how well the data projected using a specific dimension components satisfy the objective function. To make the eigenvalues comparable across the structures, we normalized them through dividing them by the summation of the eigenvalues for each structure. The range of the normalized eigenvalues is between 0 and 1 where higher values show higher contribution of the dimension component. This figure shows that

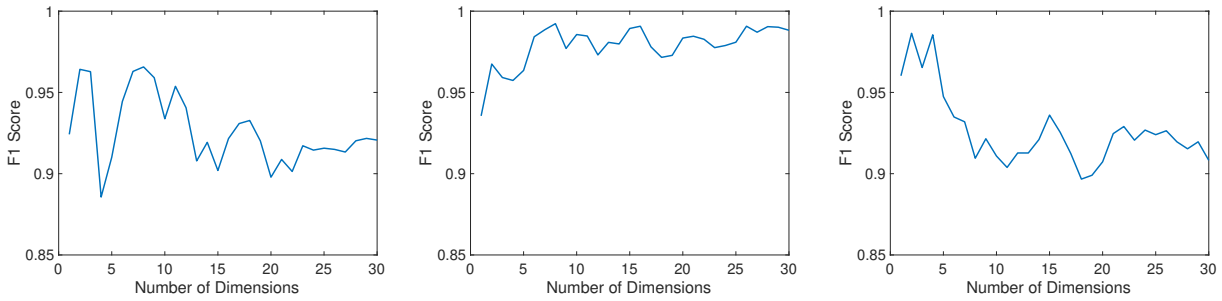

(a) Baptist Building **(b)** Porter Hall **(c)** Vincentian Building

Figure 3.11: The Sensitivity of the F1-score to the Number of Dimensions. Part (a)-(c) show the results for the case with Baptist, Porter, and Vincentian buildings as the target structure, respectively.

the first few dimensions has more contribution compared to Baptist and Vincentian. For example, 4 initial dimensions count for 0.82 of the total value in Porter. The corresponding values for the same number of dimensions in Baptist and Vincentian are 0.76 and 0.68. The higher contribution of the initial components with lower noise results in a model which is less affected by the later noisier dimensions. Therefore, in Porter, the performance of the model does not decrease by adding more dimensions. Furthermore, the largest decrease is happening in Vincentian where the initial dimensions show the lowest contribution.

Furthermore, for Baptist, the trend is mostly decreasing after the initial part. However, there is an outlier with low F1-score for the case of 4 dimensions which means that the fourth basis projects the data into a feature space in which the footsteps and non-footsteps are not separable. This effect is caused by higher noise in the wooden floor which results in some errors in the model transfer. In this paper, to ensure good performance in all the structures, we have chosen the first two dimensions for model transfer.

3.4.8 Sensitivity to the Signal-to-Noise-Ratio (SNR)

The existence of environmental and measurement noise can affect the model performance. To evaluate this factor, we have studied the relationship between the Signal-to-Noise-Ratio (SNR) and the model F1-score. Specifically, we compare this relationship for our model transfer approach with the ones using the TD and FD-based approaches. For each impulsive event, SNR values are

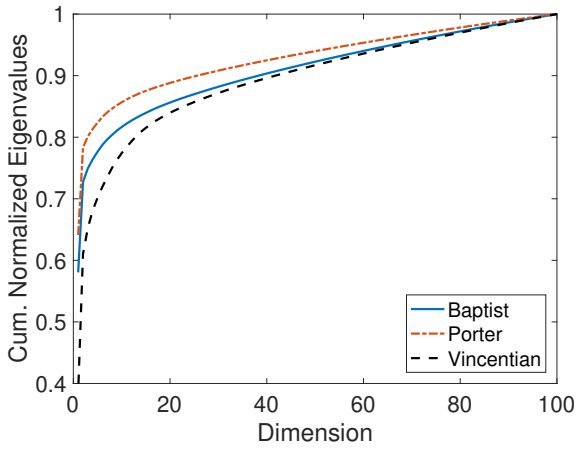

Figure 3.12: Dimension Contribution through Normalized Eigenvalue.

computed as the ratio of the summed squared magnitude of the event signal to that of the noise (of the same length) and is described in decibel (db). Higher SNR values indicate high level of event signal and low level of noise, and vice versa. The noise consists of ambient vibration measurements which does not include impulsive excitation and footstep events. Figure 3.13 shows the F1-score for 10 different levels of SNR. The results show that our approach outperforms other approaches in all the SNR ranges with F1-scores between 0.91 and 1.00. In comparison, the baseline TD-based and FD-based approaches result in F1-score ranges of [0.4, 0.63] and [0.05, 0.92], respectively. Consistent improvement in the performance using our approach compared to the baseline approaches shows that our approach is more robust to the changes in the SNR.

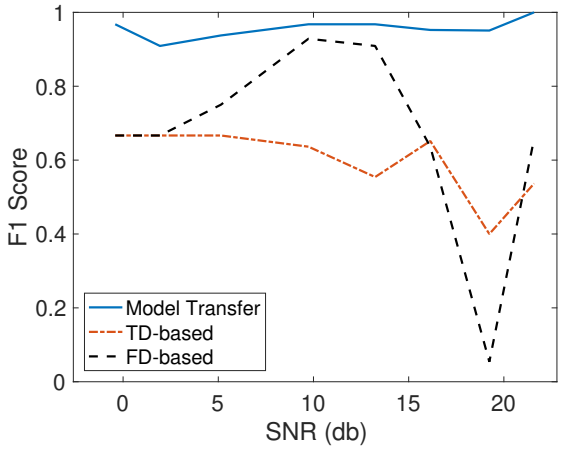

Figure 3.13: Sensitivity to the SNR. This figure shows that our model transfer higher F1-score compared to the baseline approaches in various SNR ranges.

Chapter 4

Characterizing Dispersive Wave Propagation without Prior Calibration

In this chapter, we characterize dispersive wave propagation for occupant localization purpose. Wave propagation in a floor structure is of dispersive nature. In other words, the wave propagation properties change across various wave frequency components. Dispersion results in signal distortions which make analyzing the signal challenging. Specifically, for occupant localization, this signal distortion results in inaccurate TDoA estimation and localization. Further challenge for occupant localization is that the wave propagation velocities are unknown and different across structures which result in a time-consuming and costly calibration phase. To address these challenges, we characterize dispersive wave propagation to develop a vibration-based occupant localization approach which addresses dispersion without requiring calibration. In this section, we first review the related literature in Section 4.1. Then, we describe our localization approach in Section 4.3 and evaluate it in Section 4.4.

4.1 Literature Review

The occupant localization using footstep-induced floor vibrations can be seen as a source localization problem in dispersive media. Here, we explore the existing approaches and remaining

research gap for vibration-based occupant localization.

4.1.1 Dispersion-Induced Signal Distortion Reduction

Floor structures are dispersive which causes waves of different frequency to travel at different speed. This results in signal distortions which decrease the accuracy of TDoA estimation and localization (see Section 4.2 for details). The two main approaches to mitigate such distortions are physics-based approaches [63–66] and signal-based approaches [67–72]. The physics-based approaches require a priori information (e.g., stiffness and mass) of the underlying structure to estimate dispersion curves. However, their application is limited in real environments as this information varies for different structures and requires extensive calibration. Signal-based approaches address dispersion by decomposing the signals using time-frequency representations (TFR) and do not require detailed prior information about the floor.

Among the TFR approaches, wavelet decomposition has been successfully utilized for impulsive excitations (such as footstep-induced vibration) because it is suitable for representing non-stationary signals [23, 68–71, 73, 74]. The main wavelet-based approaches for source localization either utilize: 1) the ridge [68, 69, 71, 74] (i.e., peak amplitude in scale-time plane) which is difficult to robustly estimate in real floors with environmental noise or 2) highest energy scale components [23, 73] which potentially have large noise (ambient vibration) because this scale might correspond to the fundamental frequency of the floor. Therefore, these approaches are not well-suited for source localization and result in large errors. To improve localization, We introduce a new approach which directly chooses the components with the highest localization performance for signal recovery (localization performance will be described in Section 4.3.2).

4.1.2 Source Localization

Source localization problems consider signals induced by a source of unknown location and received in several sensors at known locations to find the source location. Source localization is of vital importance in several domains such as sonar [75, 76], mobile communications [77, 78],

wireless sensor networks [79, 80], structural health monitoring [81–83], and robotics [84, 85]. Existing approaches include beamforming, fingerprinting, and multilateration.

Beamforming delays/shifts the received signals based on an assumed waveform and propagation velocity and then finds the location by identifying the time-shift that maximizes the similarity in the delayed signals [83, 86–88]. These approaches in general focus on propagation in homogeneous media where the propagation velocity is well known (e.g., sound in air). In these approaches, unknown propagation velocity and dispersion-related signal distortions would result in large localization errors.

Fingerprinting (or signature-based) approaches are an alternative when the propagation characteristics are unknown. These approaches first construct a database of received signals for source excitation in different known locations through site surveying. For every new excitation, the measured signals will be compared to the signals in the database to find the location corresponding to the most similar signal [89–91]. Unfortunately, the site surveying can be a time-consuming and laborious process, especially for fine-grained localization.

Range-based localization estimates the range between the source and sensors and leverage such information for estimating source location. Two methods introduced for range estimation are Received Signal Strength (RSS)-based and Multilateration. RSS-based [92–94] methods estimate the range between the source and the sensors based an attenuation pattern for wave propagation. However, these methods do not perform well in real floors for which such attenuation pattern is not previously known or accurately modeled by a parametric model (such as exponential models as assumed in [94]). This becomes more problematic especially when reflections can create constructive or destructive interference. Multilateration, on the other hand, leverages the differences in time of arrival for signals received by different sensors, referred to as TDoA, to estimate the location of the source [74, 95–102]. For a specific value of TDoA between two sensors, the possible solutions (i.e., source locations) form a hyperbola. The location of the source can be estimated by adding more sensors and their TDoAs, which result in more hyperbolas, and then finding their intersection. In this regard, a cost function for each potential source location is defined as the error between 1) the distance difference between the potential source location and the known sensor

locations and 2) their expected distance difference computed from the TDoA and wave propagation velocity. The solution of multilateration is obtained by minimizing this function. In this paper, we adopted the multilateration approach as it locates the source in a fine-grained manner without laborious site surveying and does not assume a known waveform.

A key challenge in multilateration is that if the wave propagation velocity is unknown and varies across different locations and buildings, which is often the case in practice, it increases the number of unknowns and the non-convexity of the multilateration cost function. The severe non-convexity of the cost function makes finding the global minimum difficult. Therefore, we introduce an adaptive multilateration approach that is more robust to irrelevant local minima by incorporating space configuration information to heuristically limit the search space.

4.2 The Physics Behind Footstep-induced Dispersive Wave Propagation

Our localization approach utilizes wave propagation in floor structures. In this section, we provide a brief background of the physics behind footstep-induced structural vibration and describe the main challenges we address: 1) dispersion-related signal distortions and 2) unknown wave propagation velocity across different locations due to floor heterogeneity.

The impact due to each footstep strike is of an impulsive nature. These impulses result in deformation (and restoration due to elasticity) in the floor. This combined deformation and restoration results in waves propagating outward from the footstep location through the floor. These waves are plate waves (i.e., lamb waves) because building floors are generally solid plates with free boundaries on top and bottom and the ratio of wavelength to thickness of the floor is large in our application [103]. As an example, if the wave have a frequency component of 100 Hz and wave propagation at a velocity of 300 m/s, the wavelength is equal to 3 meters, which is much larger than the common floor thickness (on the order of 0.2-0.3 meters).

However, lamb wave propagation in floor structure is of a dispersive nature, which causes different frequency components to have different phase velocities [104, 105]. Due to this dispersion

effect, the same footstep will induce dissimilar signals in sensors in different parts of the floor. In other words, dispersion introduces distortion in the vibration signal, which makes vibration-based occupant localization a challenging task. Figure 4.1 shows a simple and intuitive illustration of dispersion to better understand how it distorts the signals. In this figure, we assume that the wave consists of two linearly attenuative sinusoidal components of 2 and 8 Hz. Figures 4.1a and 4.1b show the waves propagated through a non-dispersive medium in which wave propagation velocity is the same for all frequency components. Figures 4.1c and 4.1d show the waves propagated through a dispersive medium in which wave propagation velocities are different for different frequency components. Figures 4.1a and 4.1c show the wave measured at a closer sensor and Figures 4.1b and 4.1d show the resulting wave measured at a further sensor. As shown in these figures, in a non-dispersive medium, the waves arrive at a later time (with delay of Δ) in the further sensor, but the shape of the signal is the same as the one measured at the closer sensor. In contrast, in the dispersive medium, the further sensor observes the more dispersed waves, and for the same excitation, the shape of the received signals are different for the two sensors. The difference is caused by the different delays for these two components (Δ_1, Δ_2). For example, the maximum cross-correlation values between the two sensor measurements decrease from 1 to 0.69 when the floor becomes dispersive.

In real life applications, these effects are aggravated due to reasons such as having more frequency components, different attenuation rates, and noise [23]. These dispersion-related distortions make it difficult to estimate the TDoA between different sensors, thereby decreasing the localization accuracy.

Furthermore, lamb wave propagation velocity (for each frequency component) depends on structural and material characteristics, such as modulus of elasticity, density, Poisson's ratio, and slab thickness [106]. Due to structural heterogeneity, these characteristics (and thus the propagation velocity) vary greatly across different sections of the floor and different buildings. To handle this velocity variations, we assume that heterogeneous floors are locally isotropic. In other words, the structural characteristics and wave propagation velocity differ across different footstep locations; however, in the vicinity of each footstep location, these characteristics (and propagation velocity

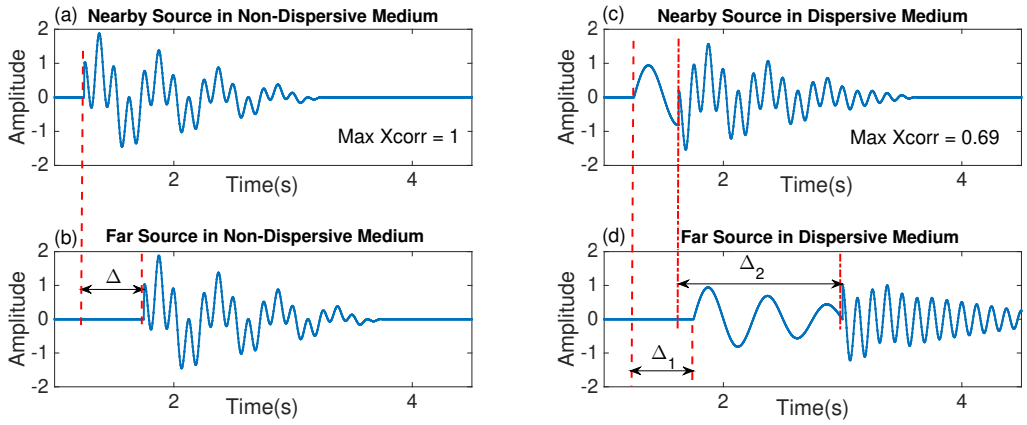

Figure 4.1: Dispersion Illustration: This figure illustrates how dispersion distorts the shape of the received signals by considering two attenuative sinusoidal components. These distortions decrease the localization accuracy. The red lines show the arrival time of sinusoidal components.

to the sensors) are assumed to be similar. Then to eliminate extensive calibration to obtain wave propagation velocity in different footstep locations, we introduce our adaptive multilateration approach in the next section.

4.3 Adaptive Occupant Localization in Dispersive Medium

Our fine-grained floor vibration-based occupant localization approach has two main modules: 1) Footstep Detection; 2) Dispersion-invariant TDoA Estimation; and 3) Locally Adaptive Footstep Localization. We have discussed Footstep Detection in detail in Sections 2 and 3. After detecting footsteps, in the Dispersion-invariant TDoA Estimation module, our approach mitigates the dispersion-induced signal distortion through signal decomposition and then estimates the TDoAs for different components. Section 4.3.1 provides more details on the dispersion mitigation approach. Finally, in the Locally Adaptive Footstep Localization module our method selects a subset of sensors which are closest to the footstep to further reduce signal distortion effects and estimates component-level footstep location using our adaptive multilateration approach. Then, it selects a subset of components with best multilateration performance and averages these component-level location estimations to obtain the final estimation of the footstep location. The details of this

module are discussed further in Section 4.3.2.

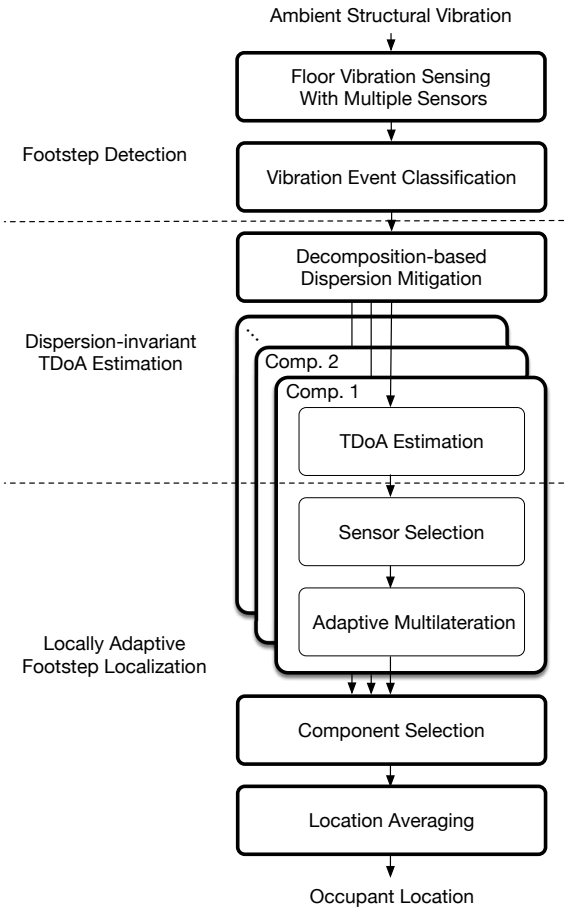

Figure 4.2: Occupant Localization Approach Overview

4.3.1 Dispersion-invariant TDoA Estimation

To mitigate dispersion-related signal distortion, we decompose the vibration signal using a time frequency representation (TFR) and extract scale components from each sensor data [23]. Separately analyzing each component, which has similar wave propagation characteristics (e.g., phase velocities), mitigates the effects of dispersion as shown in Figure 4.3. This figure shows the signals received in two sensors from the same footstep excitation. After decomposition (and extracting a specific component), the shapes of the signals become more similar to each other (the maximum cross-correlation value increases from 0.49 to 0.95, which corresponds to 1.9X improvement in similarity) and show more clear peak correspondence.

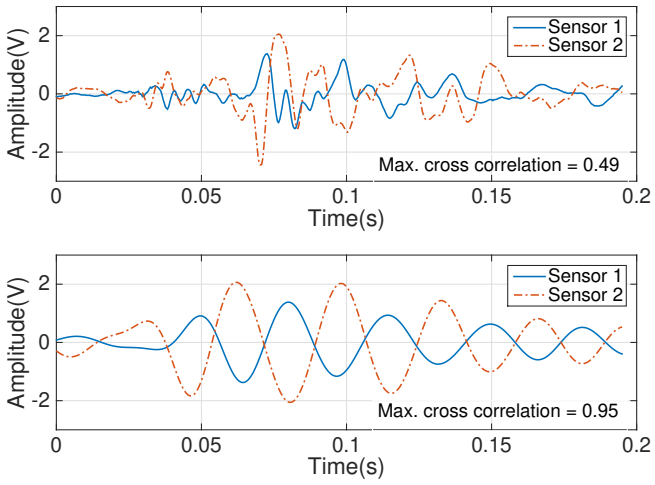

Figure 4.3: An Example of Dispersion Mitigation by Signal Decomposition. This figure shows that the decomposed signals (bottom) are more similar, and the peaks clearly correspond with each other the improvement compared to the raw signals (top) received in two sensors for the same excitation.

Decomposition-based Dispersion Mitigation To decompose the signal, we use wavelet transform, which is well suited for non-stationary signals such as impulses and footsteps [69, 70, 107] (as discussed in Section 4.1.1). We decompose the signal into frequency components using continuous wavelet transform. Mathematically, continuous wavelet decomposition of signal x can be represented as,

$$T(a,b) = w(a) \int_{-\infty}^{+\infty} x(s)\Psi^*_{b,a}(s)ds \tag{4.1}$$

in which $w(a)$ is a weighting function and $\Psi_{b,a}(s)$ is the dilated and time-shifted version of the basis function (mother wavelet $\Psi(s)$), which can be represented as,

$$\Psi_{b,a}(s) = \Psi\left(\frac{s-b}{a}\right) \tag{4.2}$$

in which b is the unit of translation in time and a is the amount of dilation (commonly called a scale.). This dilation (i.e., scale) is inversely proportional to the frequency components of the signal. In other words, higher scales correspond to lower frequency components and the relationship between them can be described using [107],

$$F_a = \frac{F_c}{a\delta} \tag{4.3}$$

in which δ is the sampling frequency (Hz), F_a is the (pseudo-)frequency (Hz) corresponding to scale of a, and F_c is the center frequency of the wavelet (Hz).

Mexican hat wavelet is chosen as the mother wavelet as it is a good representation of the footstep-induced vibration signals due to its similarity in shape [108]. To reduce the computational cost of performing the continuous wavelet transform, we choose a limited range of scales. To limit the range (while keeping the useful information in the signal), we use two notions: 1) floor vibration signals caused by footsteps typically contain frequencies below 100 Hz [109] and 2) geophones are naturally a second-order high pass filter for frequencies less than 10 Hz [110, 111] (i.e., when the frequency decreases from 10Hz to 1Hz, the geophone's response may become 100 times weaker). Therefore, we choose the range of 10-100Hz for wavelet decomposition. Using Mexican hat wavelet, for sampling frequency of 25 kHz, which we used for evaluation, this range translates to a scale range of 64 to 640. We have observed in our prior experiments that footwear can affect the frequency range. For example, high heels are more similar to impulses (e.g., ball drops) than flat-bottom shoes and hence, generally result in higher frequency components compared to, for example, someone wearing flat-bottom shoes [30]. However, while we did not control the footwear of the subjects, there was little variation in the footwear of the experimental subjects (all variants of flat-bottom shoes). The defined range works well for the structures and footwear we consider in Section 4.4. This range can be modified to accommodate different applications with different floor types or footwear with different response frequencies.

TDoA Estimation To estimate the TDoAs between different pairs of sensors for every scale components, we utilize a threshold-based method[27]. This method detects the first peaks of the signals, which correspond to the wave arrival time at each sensor location. Note that the wave arrival time does not provide the time of flight because the start time (i.e., time of footstep excitation) is unknown. Instead, the TDoA is obtained by comparing the wave arrival times of each sensor pairs. We have chosen the peak detection method over the cross-correlation to compute the TDoA because it is less affected by signal distortions due to multipath and reflections [112]. The peaks are determined using the anomaly detection approach, which assumes that the signal has a Gaussian distribution for the background noise (i.e., when there is no footstep). This assumption is then used

to find the threshold for detecting an anomaly (i.e., time of arrival for a footstep event). We chose 3σ as a threshold, in which σ is the standard deviation of the decomposed background noise, to allow 1% detection false alarm. This threshold value is adjustable according to the application.

4.3.2 Locally Adaptive Footstep Localization

To enable footstep localization in different structures and heterogeneous floors, we present a locally adaptive multilateration approach which robustly estimates the footstep location when the propagation velocity is unknown. We take a two-step approach to first obtain the component-level location estimation through sensor selection and adaptive multilateration and then combine those results to make the system-level location estimation.

Sensor Selection The key intuition behind choosing the closest sensors is that the less distance waves propagate through the floor, the less it gets affected by the floor's attenuative characteristics. This in turn results in higher SNR, less signal distortion, and consequently more accurate TDoA and location estimation. To choose the closest sensors, we utilize the relative time of arrival for footstep signals to reach different sensors. We first sort the detected times of arrival for first peaks for different sensors obtained in the previous module and then select the sensors with earlier times of arrival. Note that each scale component may lead to different set of "closest sensors" due to the errors in the first peak detection; however, the components with such erroneous peak estimations often lead to large localization errors and get filtered out through the component selection in the next module. Assuming unknown wave propagation velocity, at least four sensors are necessary for localizing the footsteps. Using more sensors has the potential to reduce the noise and improve the accuracy; however, including additional sensors means including the sensors further away from the footstep (because of our sensor selection approach), which result in more attenuated signals and lower localization accuracy. Thus, in this paper, we use four sensors, whose performance is compared with systems with different number of sensors in Section 4.5.3.

Adaptive Multilateration These selected sensors and their corresponding TDoAs are then utilized in our adaptive multilateration approach to estimate the location of the footstep for each scale component (component-level location estimation). Our approach does not require prior knowledge

on wave propagation velocity; therefore, it can adapt to different locations in a heterogeneous floor (with different structural characteristics).

The main challenge in achieving the adaptive localization is the large search space for solutions, due to the model flexibility (e.g., extra unknown parameters on wave propagation velocity). As discussed in Section 4.2, we assume different propagation velocities across different locations (i.e., heterogeneous floor) and same velocity between each footstep and the sensors (i.e., locally isotropic). However, due to the non-convexity of the problem, deviation from local isotropy assumption causes the multilateration to get stuck in local minimas and therefore result in large localization errors.

To make the multilateration approach more robust, we employ heuristics on physical space configurations to constrain the solution search space (i.e., possible locations and velocities). We constrain the search space by considering the propagation velocities for which every pair of hyperbolas have an intersection in the room boundary. As discussed in Section 4.1.2, the possible locations of a footstep for specific TDoA between two sensors and propagation velocity form a hyperbola. Ideally, these hyperbolas from multiple sensor pairs meet at one intersection, which is the solution of multilateration; however, signal noise and errors in TDoA estimation lead to hyperbolas that meet at multiple points or do not intersect. To this end, we define the localization cost function as: 1) the area of the polygon between intersections of hyperbolas when all pairs of hyperbolas intersect in the room boundary or 2) an arbitrarily large value when they do not intersect (e.g., ∞). This cost function is then minimized across different propagation velocities to robustly estimate the location of footsteps.

The advantages of our approach are that: 1) it does not require wave propagation velocity to be known and fixed and 2) constraining search space makes it less-prone to vastly out of range local minima. Figures 4.4a-4.4c visualize an example of the multilateration procedure. These figures show the hyperbolas for three different velocities (100, 150, and 200 m/s), where the true velocity is 200 m/s. For each velocity, we construct the hyperbolas and find their intersections. We can see from the figures that by minimizing the area, its center point (found by averaging the intersection locations) gets closer to the actual location of the footstep (represented by a star sign). In other words, the case with minimum area between intersections also has the lowest localization error.

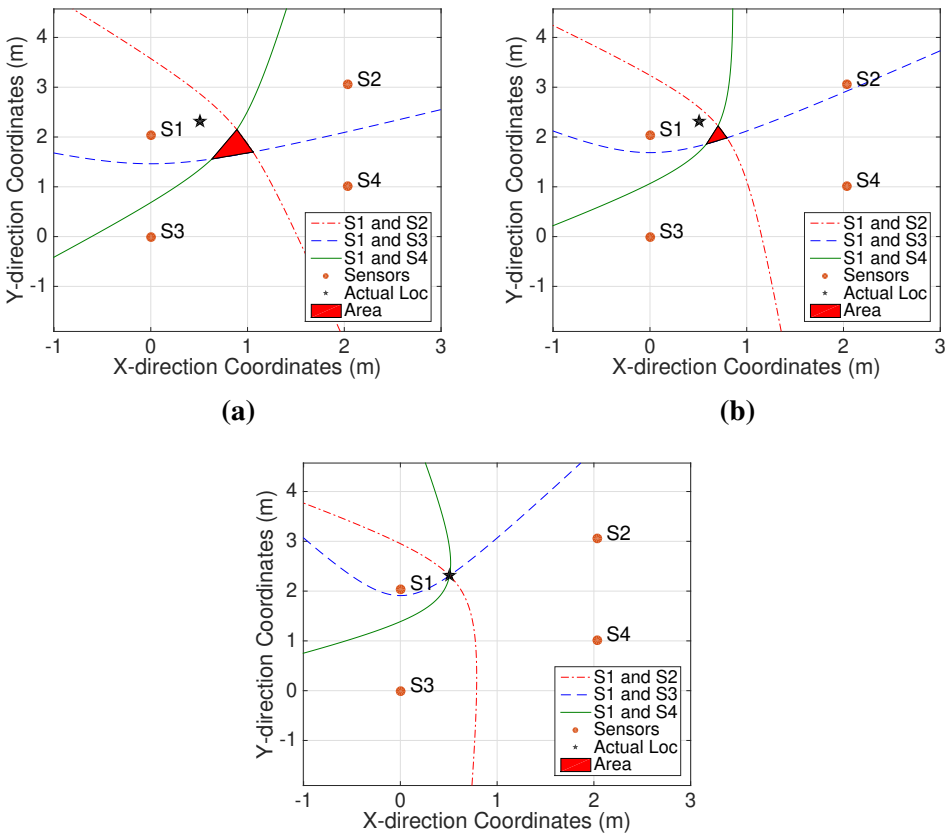

Figure 4.4: An Example of the Solution Procedure. The footstep location can be found by changing the velocity values and finding the velocity value which minimizes the area between intersections. Parts a-c show an example of such a procedure for three values of wave propagation velocity. We can see that the case with minimum area between intersections also has the lowest localization error.

Our approach uses a closed-form formulation for constructing the hyperbolas, finding their intersections, and forming the polygon between the intersections. In the closed-form formulation, for a specific value of wave propagation velocity, the hyperbola between a pair of sensors is defined in the following format [113].

$$x = \frac{p_{ix} + p_{jx}}{2} + Xcos\alpha - Ysin\alpha \tag{4.4}$$

$$y = \frac{p_{iy} + p_{jy}}{2} + Xsin\alpha + Ycos\alpha \tag{4.5}$$

where α is the rotation angle of the hyperbola, $[x, y]$ are the coordinates of the hyperbola, and p_{ix}, p_{iy}, p_{jx}, and p_{jy} are the coordinates of the sensors i and j. Also,

$$cos\alpha = \frac{p_{ix} - p_{jx}}{2c}; \qquad sin\alpha = \frac{p_{iy} - p_{jy}}{2c}; \qquad X = a * cosh(\theta); \qquad Y = b * sinh(\theta) \tag{4.6}$$

in which θ is a parameter which can range $[-\infty, +\infty]$. Furthermore, a, b, and c are defined as,

$$a = \frac{v\tau_{ji}}{2}; \qquad b = \sqrt{c^2 - a^2}; \qquad c = \frac{1}{2}\left\|p_j - p_i\right\|_2 \tag{4.7}$$

in which v is the propagation velocity and τ_{ji} is the time difference of arrival between the i^{th} and j^{th} sensor. Using this formulation, one of the sensors is considered as the anchor sensor and a hyperbola is found between the anchor sensor and every other sensor. We then use a grid-search based method [114] to find the intersections of the hyperbolas.

The final step of our solution is to minimize the area of the resulting polygons across a range of velocity values. Let the intersections between different pairs of hyperbolas which are in the boundary of the room be stored in an array called P in which $P_k = [x_k, y_k]$. Then the optimization objective is defined as

$$min_v \left(\begin{cases} \sqrt{\frac{1}{2}\sum_{k,l=1}^{3} \|P_l - P_k\|_2^2} & if\ |P| = \frac{n(n-1)}{2} \\ \infty & if\ |P| \neq \frac{n(n-1)}{2} \end{cases} \right) \tag{4.8}$$

where, $\|P_l - P_k\|_2$ is the Euclidean distance between the k^{th} and l^{th} intersections, $|P|$ is the cardinality (number of elements) in the set P, and $\frac{n(n-1)}{2}$ is the number of different combinations of two hyperbolas (each representing one intersection) when there are n hyperbolas. By minimizing this cost function, we ensure that: 1) all pairs of hyperbolas intersect in the room boundary and 2) the area between these intersections is minimized. The center of the smallest area, found by averaging the intersection locations, is the component-level location estimation.

Component Selection and Location Averaging Finally, we choose a subset of component-level location estimations and use their average as the final footstep location estimation. By averaging

several estimated locations, we reduce the effect of noise and outliers. The components with best localization performance are selected (i.e., components with lowest values of minimum localization cost function value as defined in Eq. 4.8. The lower minimum localization cost function means that the localization has been more successful (i.e., higher localization performance). In ideal scenarios and when there is no noise in the TDoAs, the minimum of this cost function is equal to zero (high localization performance). However, having noise in the TDoAs results in a larger minimum of cost function, as the hyperbolas might not intersect at one point. Therefore, we choose a subset of component-level estimated locations which result in lowest minimum localization cost function. The number of the estimated locations to be included in the subset poses a trade-off. On one hand, utilizing more scale components reduces the effect of noise and improves localization. On the other hand, including scale components with large noise decreases the localization accuracy. In this paper, we utilize eight scale components based on empirical evaluation, which is discussed further in Section 4.5.5.

4.4 Footstep Localization Evaluation

To understand the system performance, we conducted a set of experiments with human participants. We first introduce the sensor configuration (Section 4.5). Next, we present and analyze the footstep localization accuracy and robustness using our approach (in Sections 4.5.1- 4.5.4). Then, we explore the effect of decomposition-based dispersion mitigation on localization (in Section 4.5.5). Finally, we validate our locally adaptive localization approach using experiments in categorically different structures (in Section 4.5.6- 4.5.8).

4.5 Experimental Setup

To evaluate our localization approach, we utilize a sensing system which measures the footstep-induced vibration using nine floor-mounted geophones [111]. As discussed in Section 4.3.2, four sensors are necessary for localization in a real applications. However, to explore the effects

of different number of sensors on localization performance, we deliberately installed a dense configuration. The collected signals are amplified by the orders of 200-2000X using an op-amp to improve the resolution of signals while reducing the amount of signal clipping. Higher signal resolution in turn improves TDoA and localization accuracy. After amplification and depending on the structure type and footstep strike energy, the effective sensing range of our system for footstep detection is up to 20 meters in diameter. Amplified signals are then digitized and transferred to a server using a 24 bit A/D converter. Figure 2.1 shows one of the sensing units. Sampling frequency is chosen as 25 kHz to ensure enough time resolution for accurate TDoA estimation.

The experiments include having three subjects walk in three buildings of different structural types to show that our approach is robust to different structures. All the subjects wear variants of flat-bottom footwear. The chosen structures represent common types of structures for residential and commercial buildings and include a non-carpeted concrete hallway on the ground level of the campus building at Carnegie Mellon University (with the first observed natural frequency of 23.83 Hz), a carpeted metal deck floor on the second floor of a senior care facility (with the first observed natural frequency of 14.84 Hz), and a wooden floor in the second floor of a residential building (with the first observed natural frequency of 16.02 Hz). The tested areas did not include obstructions such as structural walls underneath or beams. Twenty walking traces, each consisting of six footsteps, are collected from each structure. The averages and standard deviations of subjects walking speed are 1.09 and 0.115 m/s for subject 1, 0.66 and 0.03 m/s for subject 2, and finally 0.84 and 0.06 m/s for subject 3. Figure 4.5 presents the sensor configuration and footstep locations. Figure 4.6 shows the 3 experiment locations with our system set up. The dimensions of sensor configuration represent hallways in common residential and commercial buildings. Furthermore, to obtain the ground truth, the locations of the footsteps were taped on the floor and the participants were asked to walk on these locations.

4.5.1 Overall Localization Accuracy Evaluation

To evaluate the accuracy of our approach, we compare the overall localization errors in all three structures using our approach and a baseline approach. The baseline approach is a method

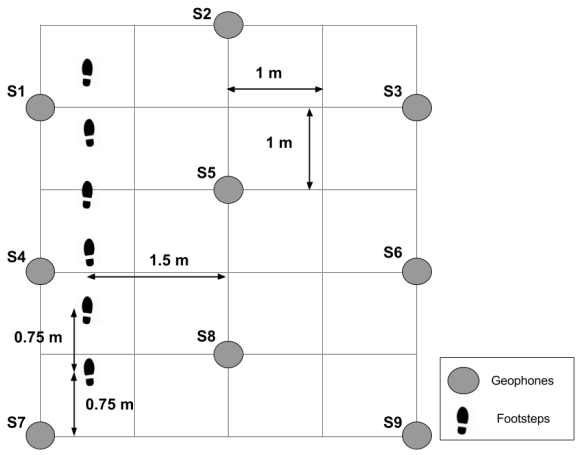

Figure 4.5: Experimental Setup. This figure shows the sensor configuration and the location of footstep excitations. The database includes 20 traces of six footsteps.

Figure 4.6: Experiment Locations. Part (a) shows a concrete non-carpeted hallway on the ground level in the campus building of Carnegie Mellon University. Part (b) is a hallway on the second floor of a senior care facility with a concrete metal deck floor. Finally, Part(c) is a room with a wooden floor on the second floor of a residential building.

commonly used for localization which utilizes the raw signal for TDoA estimation and then performs multilateration through Nonlinear Least Square (NLS) solution. The metric used for this purpose is the Euclidean distance of the actual location of the footstep from the estimated location. Table 4.1 and Figure 4.7 show the overall results of this comparison for all three structures' data combined. Based on these results, our approach results in 0.41 meters average accuracy which is equivalent to approximately 5X improvement over the conventional approach which has 2.04 meters of accuracy. Similarly, our approach results in 0.23 meters standard deviation which is 6.70X precision improvement over the conventional approach. Similarly, our approach results in 3.08X

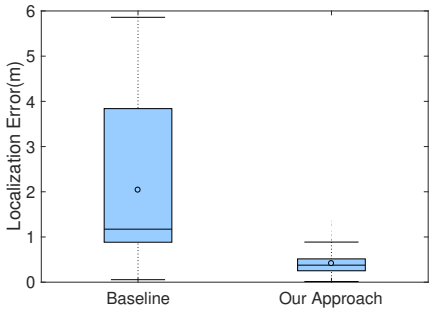

Figure 4.7: Localization Accuracy of Our Approach. This figure compares the accuracy of our localization approach with a baseline approach. Median of the results using our approach is 0.38 meters which shows 3.08X improvement over the baseline approach.

and 11.38X improvement in the median and 25-75 percentile of the localization error, respectively. This level of occupant localization accuracy and robustness makes our approach more suitable for smart building applications.

4.5.2 Robustness to Sensor-Footstep Distance

Sensor-footstep distance is an important factor in localization performance. To evaluate this factor, we use four sensors and evaluate the errors for footsteps of different locations. The metric used to define the sensor-footstep distance is the root mean square (RMS) of the the Euclidean distances of the footstep to each sensor. Furthermore, we consider two different sensor configurations to evaluate whether it is important for the footstep to be inside the polygon formed by the sensors. The first configuration consists of S4, S5, S7, and S8 and considers the three footsteps outside the polygon formed by the 4 sensors, as shown in Figure 4.5. Figure 4.8a depicts the changes in localization error for this configuration with respect to the defined metric. The correlation coefficient of 0.82 shows that there is a strong linear relationship between the distances and the localization error. The positive slope of 1.44 shows that higher distances result in lower localization accuracy.

Table 4.1: Localization Results (For All Three Structures)

	Mean	St. Dev.	Median	Quartile
Conv. Approach	2.04	1.54	1.17	2.96
Our Approach	0.41	0.23	0.38	0.26
Improvement	4.98X	6.70X	3.08X	11.38X

The second configuration consists of S1, S2, S7, and S8. As can be seen in Figure 4.5, for this configuration all the footsteps are inside the sensor polygon. Figure 4.8b presents the changes in the localization error with varying sensor to footstep distances in this sensor configuration. In this case, compared to the results outside the polygon, both the slope (i.e., 0.16) and the correlation coefficient (i.e., 0.05) are smaller. Inside the polygon, the localization results are not as significantly affected by the distances as outside the polygon. For example, in the cases outside the polygon, increasing the distance from 2 meters to 2.6 meters causes the error to increase from 0.6 to 1.5 meters; whereas, for a similar range of distances (2.3 meters to 2.6 meters) and for the cases inside the polygon, the error increases from 0.53 meters to 0.64 meters. Finally, Figures 4.8b and 4.8c show that as the sensors are further apart (Figure 4.8b), the average localization errors are larger (0.53-0.83 meters) than when we apply the sensor selection algorithm (Figure 10c, 0.2-0.49 meters). The reason is that our sensor selection algorithm chooses the closest sensors from the footstep location.

Increasing the distance the wave propagates through the floor results in more attenuation of the signal which in turn causes larger localization errors. Therefore, selecting the sensors closest to the footstep for localizing the footsteps improves the performance of localization approach and therefore is adopted in this paper (discussed in Section 4.3.2). In addition, choosing the sensor configuration (and the distance between the sensors) depends on the desirable localization accuracy (which is application-dependent). For example, in our setup and according to Figures 4.8b and 4.8c, a 5 meters by 2 meters sensor configuration achieves 0.63 meters accuracy whereas a 2.5 meters by 2 meters achieves 0.34 meters localization accuracy. This means that, for example, six sensors are required to achieve approximately 0.63 meters accuracy in a 10 meters by 2 meters hallway (or six sensors to cover an 8 meters by 8 meters room). The required number of sensors increase if the desired localization accuracy is 0.34 meters.

4.5.3 Robustness to the Sensor Configuration

The number of sensors and the distances between them affect localization accuracy and is important for sensor selection, as described in Section 4.3.2. Generally, the trade-off is: 1) having more sensors mitigates the effect of noisy sensors and increases localization accuracy; 2) high

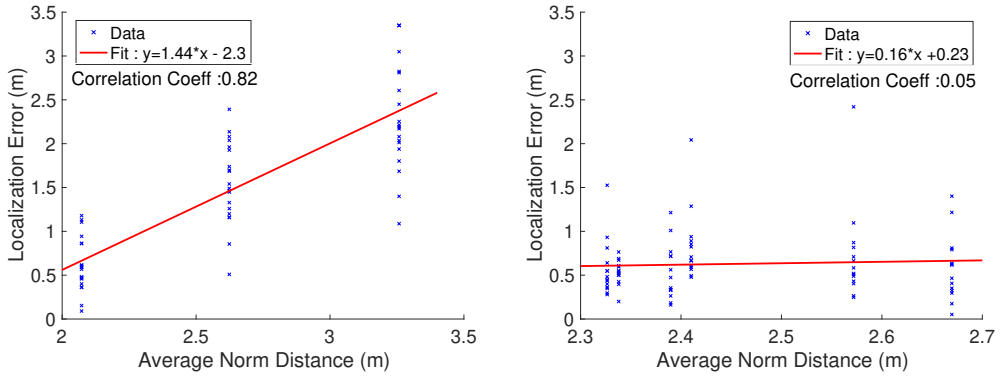

(a) S4, S5, S7, S8 (Out. sensor poly.) **(b)** S1, S2, S7, S8 (In. sensor poly.)

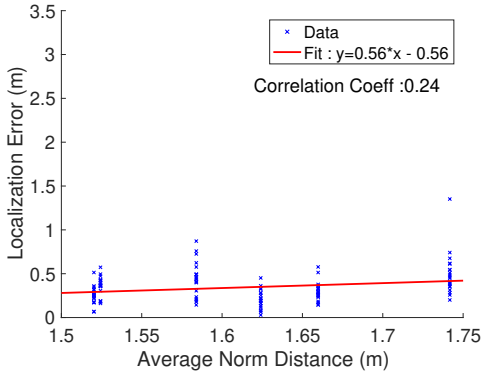

(c) Our sensor selection approach

Figure 4.8: Effect of Distance between Footsteps and Sensors on Localization Accuracy. This figure shows that footsteps out of the polygon (Part (a)) are generally more sensitive to distance than the footsteps inside the polygon (Part (b) and (c)). Furthermore, as the sensor selection chooses the closest sensors, Part (c) shows the smallest the localization errors.

footstep-sensor distance decreases the localization accuracy. To evaluate this effect, we fix the location of the footstep and increase the number of sensors. We employ two approaches for sensor selection: first, to mitigate the effect of distance, we randomly choose the subset of sensors; and second, to choose the optimal set of sensors using our approach, we choose the additional sensors based on the same principle (i.e., minimum distance to the footstep), as described in Section 4.3.2.

Figure 4.9a shows the localization errors using the randomized sensor selection. The localization error decreases when the number of sensors increases up to six sensors, and then the error increases afterwards. Specifically, using four sensors results in 0.99 meters average localization error; whereas, using six sensors and eight sensors results in 0.84 and 1.22 meters average localization error. When we have a lower number of sensors, having sensors far from the footstep affects

the localization results significantly. Due to randomized sensor selection, this is likely to happen and therefore utilizing four sensors results in the higher localization error than using six. On the other hand, if we have many sensors (e.g., eight) some of the sensors will be far from the footstep (regardless of the selection) and this results in large errors. Therefore, using the randomized sensor selection, six sensors result in minimum localization error.

Figure 4.9b shows the localization errors using our sensor selection approach. In this case, by increasing the number of sensors, average localization error generally increases. Specifically, average localization error increases from 0.30 meters using 4 sensors to 1.02 meters using 8 sensors. The reason lies in our sensor selection algorithm which finds the closest sensors to the footstep location. In the four-sensor case, we choose the closest sensors to the footstep, which results in low localization error. Additional sensors will be further from the footstep and generally increase the localization error. Another observation in this figure is that the standard deviation of localization is decreased when we are using eight sensors instead of seven sensors. A similar trend is observed for cases with five and six sensors. This is because, in our experiments, the distance of the i^{th} and the $(i+1)^{th}$ furthest sensors from the footstep where i = 5, 7 are similar to each other, while for for i = 4, 6 the distances are significantly different (e.g., the 7^{th} and the 8^{th} furthest sensors are around the equal distance from the footstep while 6^{th} and the 7^{th} furthest sensors have different distances from the footstep). Therefore, adding the 7^{th} sensor further away from the other 6 sensors increased the estimation uncertainty compared to using 6 closest sensors, while adding the 8^{th} sensor decreased the estimation uncertainty since it adds more sensors without increasing the sensor distance from the 7^{th} sensor.

4.5.4 Robustness to Signal-to-Noise-Ratio (SNR)

To evaluate how our approach performs for different levels of noise, we investigate the relationship between localization performance and SNR relation. For each footstep event, SNR values are found by finding the ratio of the summed squared magnitude of the footstep-induced vibration signal to that of the noise (of the same length) and is described in decibel (db). The noise consists of ambient vibration measurements which does not include impulsive excitation and footstep events.

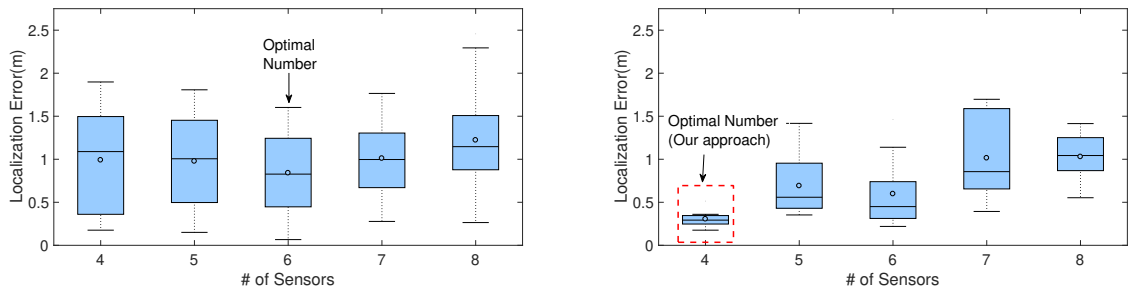

Figure 4.9: Effect of Number of Sensors on Localization Accuracy. Part (a) is the localization results for randomized sensor selection and Part (b) shows the localization results using our sensor selection approach. The difference in the optimal number of sensors is because our approach chooses the closest sensors and therefore, the additional sensors will be further from the footstep and increase the localization error.

To evaluate SNR and to separate the effect of SNR from the effect of distance, we use four sensors and localize footsteps at the same location. The overall SNR value for the system is computed as the average SNR of all the sensors. To consider the effect of different ranges of SNR, we have utilized two sensor configurations with two levels of sensing density.

The dense configuration consists of S4, S5, S7, and S8 and the sparse configuration consists of S1, S2, S7, and S8 as shown in Figure 4.5. For the dense case, the Figure 4.10a depicts the sensitivity of localization error with respect to the average SNR values. For this range of SNR values, the low correlation coefficient of 0.05 shows that localization error does not change significantly for different SNR values. The reason is that the energy (and resolution) of the footstep signals that are received is enough for accurate localization.

The sparser configuration consists of S1, S2, S7, and S8 (as shown in Figure 4.5). The analysis for this case is presented in Figure 4.10b. As discussed in Section 4.5.2, the sparse configuration generally shows larger localization errors due to the larger footstep-sensor distance. Furthermore, the effect of SNR values on the localization error is more significant (with correlation coefficient of -0.19). The reason lies in the fact that, due to higher distance, the footsteps can have lower energy and SNR values (lower than 12 db) for which the localization errors are large. However, low values of correlation coefficients for both cases show that our approach is robust to the noise level with SNR values above 12 db.

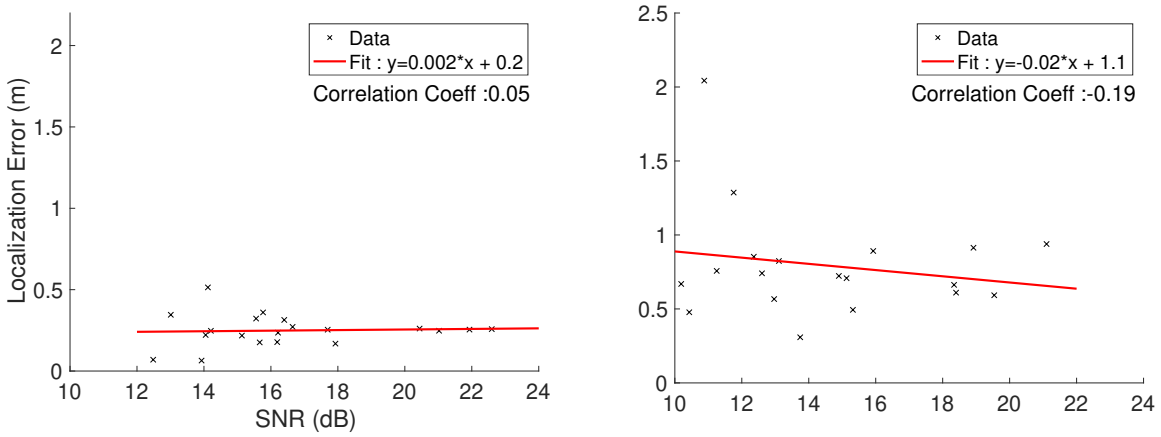

(a) S4, S5, S7, S8 **(b)** S1, S2, S7, S8

Figure 4.10: Effect of SNR on Localization Accuracy. Parts (a) and (b) show the results for the denser and sparser sensor configurations, respectively. Because in the dense configuration the footsteps are generally received with high energy, the effects of SNR is negligible. However, in the sparse, configuration, lower SNRs are possible and the decreasing trend of localization error with SNR is more significant.

Table 4.2: Localization Improvement due to Different Signal Decomposition Methods (using NLS localization approach)

	Original	DecEn		DecSNR		DecCost (ours)	
	Error	Error	Improv.	Error	Improv.	Error	Improv.
Mean	2.03	1.96	1.04X	1.84	1.10X	0.99	2.05X
St. Dev.	1.57	1.78	0.88X	1.81	0.87X	1.33	1.18X
Median	1.14	0.81	1.41X	0.71	1.61X	0.46	2.48X
Quartile	3.04	3.73	0.82X	3.16	0.96X	0.57	5.33X

4.5.5 Dispersion Mitigation Evaluation

By focusing on the same set of frequency components in all the sensors, the wavelet-based signal decomposition approach mitigates the dispersion-related distortions and improves the localization accuracy. Figure 4.11, Table 4.2, and Table 4.3 compare the localization accuracy for the decomposed and raw signals. We estimate the location error using the Euclidean distance between the actual location and the estimated location of footsteps. In this figure, 'Raw' shows the results for the original signal; 'DecEn' shows the results for the extracted signals using the highest energy scales; 'DecSNR' shows the results for the extracted signals using the highest SNR scales; and finally, 'DecCost' shows the results for the extracted signals using the scale which result in the minimum

Table 4.3: Localization Improvement due to Different Signal Decomposition Methods (using our adaptive multilateration approach)

	Original	DecEn		DecSNR		DecCost (Ours)	
	Error	Error	Improv.	Error	Improv.	Error	Improv.
Mean	0.82	0.6	1.37X	0.53	1.55X	0.34	2.41X
St. Dev.	0.4	0.4	1.00X	0.48	0.83X	0.18	2.22X
Median	0.79	0.55	1.44X	0.4	1.98X	0.32	2.47X
Quartile	0.59	0.27	2.19X	0.36	1.64X	0.21	2.81X

localization cost. Specifically, this figure shows that, regardless of the multilateration solution approach (our adaptive approach or conventional nonlinear least square (NLS)) or the decomposition approach (highest energy scale (DecEn), highest SNR scale (DecSNR), or minimum localization cost scale (DecCost)), decomposing the signal improves the localization accuracy. Specifically, it decreases the localization error median between 1.41X and 2.48X (i.e., 41-148 percent[1]) and between 1.44X and 2.44X (i.e., 44-144 percent) using NLS and our solution approach, respectively.

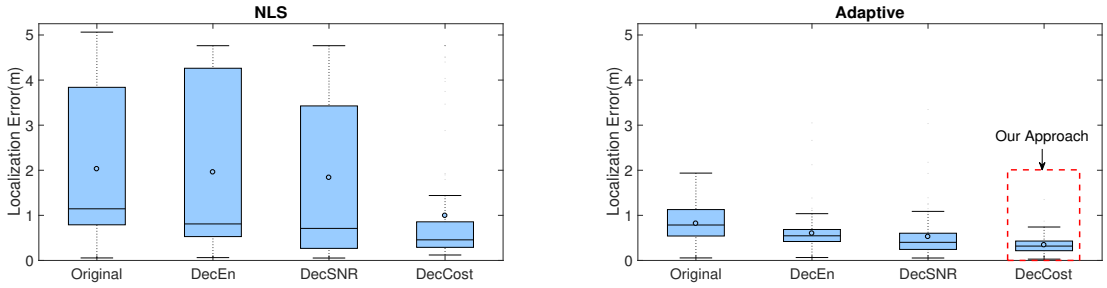

(a) **(b)**

Figure 4.11: Localization Accuracy Evaluation: This figure shows the localization accuracy improvement achieved through signal decomposition. Part (a) displays the results using NLS and Part (b) displays the results using our adaptive solution approach. As can be seen, regardless of the localization and decomposition(i.e., component extraction) approach, signal decomposition improves the accuracy of localization.

An important factor that needs to be decided is the number of scales which are used for occupant localization. The trade-off here is that: 1) using the average of estimated locations for several scale components reduces the effect of noisy estimations and outliers and improves localization performance; however, 2)including scale components that contain large level of noise will result in

[1]As an example, the percentage value in this case is found by calculating $(1.14 - 0.46)/0.46$ which corresponds to the percentage of increase in localization error for the baseline compared to our approach.

large localization error (even after averaging). Figure 4.12 presents this trade-off and shows how the localization accuracy changes with the number of scale components for three structures. It can be seen that, for all three structures, the localization error is relatively similar for 5 to 10 scales. Therefore, choosing any of these numbers does not change the localization accuracy significantly. In this work, we empirically choose 8 scale components to estimate the footstep location through finding the average of estimated locations.

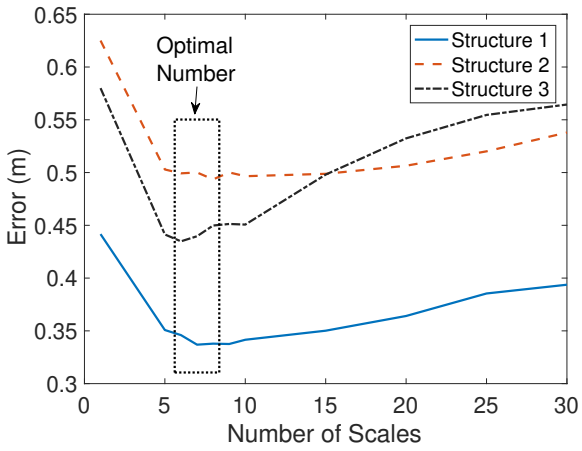

Figure 4.12: Sensitivity to the Number of Scales: This figure shows the changes in the localization performance for different number of utilized scale components. The localization error is minimum for cases with 6-8 components and is fairly similar for cases with 5-10 components used in all the structures. Therefore, we use eight scale components for final estimation of footstep location.

4.5.6 Robustness to Floor Heterogeneity

To validate the robustness of our approach in heterogeneous floors, we compare the performance of our approach with a baseline approach for footsteps in six locations (as shown in Figure 4.5). The baseline approach utilizes the raw signals for TDoA estimation and NLS multilateration solution, as mentioned in Section 4.5.1. This comparison is presented in Figure 4.13 and Tables 4.4-4.5. These results show that our approach outperforms the baseline approach in all the locations. The average localization accuracy using our approach is 0.21-0.5 meters. Compared to the baseline approach, these averages correspond to 3.9X-9.6X improvement. Similarly, our approach reduces the standard deviation (corresponding to the localization precision) by 1.9X-14.3X in different locations. Low

localization error and consistent improvement in all the locations show that our approach performs well in real-world heterogeneous floors.

Table 4.4: Localization Accuracy for Locations 1, 2, and 3 (shown in Figure 4.5)

	L1			L2			L3		
	Base	Ours	Imp.	Base	Ours	Imp.	Base	Ours	Imp.
Mean	0.82	0.21	3.9X	1.00	0.25	4.0X	1.41	0.29	4.9X
St. Dev.	0.21	0.11	1.9X	0.70	0.10	7.0X	0.63	0.11	5.7X
Median	0.88	0.20	4.4X	0.71	0.25	2.8X	1.14	0.29	3.9X
Quart.	0.31	0.16	1.9X	0.37	0.09	4.1X	0.37	0.10	3.7X

Table 4.5: Localization Accuracy for Locations 4, 5, and 6 (shown in Figure 4.5)

	L4			L5			L6		
	Base	Ours	Imp.	Base	Ours	Imp.	Base	Ours	Imp.
Mean	2.55	0.44	5.8X	3.44	0.36	9.6X	2.94	0.50	5.9X
St. Dev.	1.70	0.2	8.5X	1.57	0.11	14.3X	1.68	0.25	6.7X
Median	3.84	0.44	8.7X	4.26	0.37	11.5X	1.82	0.46	4.0X
Quart.	3.2	0.27	11.9X	1.55	0.09	17.2X	3.42	0.22	15.5X

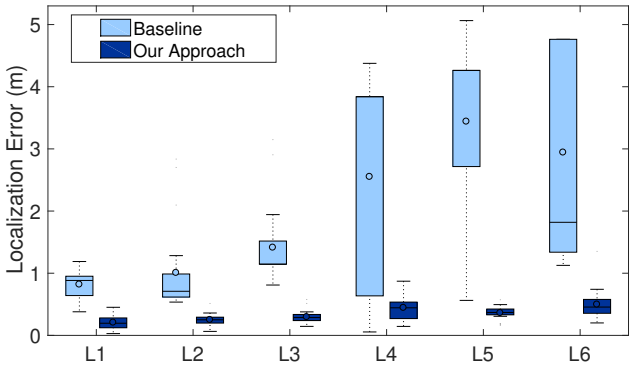

Figure 4.13: Localization Errors for Different Locations.

4.5.7 Robustness in Different Structures

To evaluate the robustness of our approach in different structures, we localized occupants in three structures, as described in section 4.5. Figure 4.14 and Table 4.6 compares the localization accuracy using our approach with that of a baseline approach in each structure. The first structure

is a non-carpeted wooden floor on the second level of a residential building in Pittsburgh, PA. For this case, our approach resulted in 5.97X (i.e., 497 percent) improvement in the average localization accuracy, as well as 7.24X (i.e., 624 percent) improvement in localization precision. The second structure we evaluated is a carpeted concrete metal deck floor on the second level of a senior care facility in Pittsburgh, PA. For this structure, our approach improves the average localization accuracy and precision by an order of 4.66X (i.e., 366 percent) and 7.24X (i.e., 624 percent). The last structure we evaluated is a non-carpeted concrete floor on the ground level of a university campus building in Pittsburgh, PA. In this structure, our approach results in 4.22X (i.e., 322 percent) and 6.08X (i.e., 508 percent) improvement in localization accuracy and precision.

In summary, We improve the localization accuracy between 4.22 and 5.97 times the baseline approach in different structures and also improve the localization precision between 6.08 and 8.72 times. The consistent improvement in a range of structures further shows that our approach is robust to structural differences.

Table 4.6: Localization Results for the Three Structures

	Structure 1			Structure 2			Structure 3		
	Base	Ours	Imp.	Base	Ours	Imp.	Base	Ours	Imp.
Mean	2.03	0.34	5.97X	2.33	0.5	4.66X	1.90	0.45	4.22X
St. Dev.	1.57	0.18	8.72X	1.52	0.21	7.24X	1.52	0.25	6.08X
Median	1.15	0.32	3.59X	1.72	0.46	3.74X	1.15	0.43	2.67X
Quart.	3.05	0.21	14.52X	2.74	0.27	10.15X	2.92	0.29	10.07X

4.5.8 Calibration Evaluation

In this section, we compare our locally adaptive approach with a calibration-based approach which assumes a fixed wave propagation velocity in the floor and obtains its value through a calibration before the run-time occupant localization (fixed-velocity approach) [23]. Figure 4.15 shows the average localization accuracy of the fixed-velocity approach for different wave propagation velocity calibrations and compares it to our adaptive approach. Our approach does not require the wave propagation velocity as an input and hence its localization errors does not change for varying velocity inputs (and hence it is represented by the flat line). However, the performance

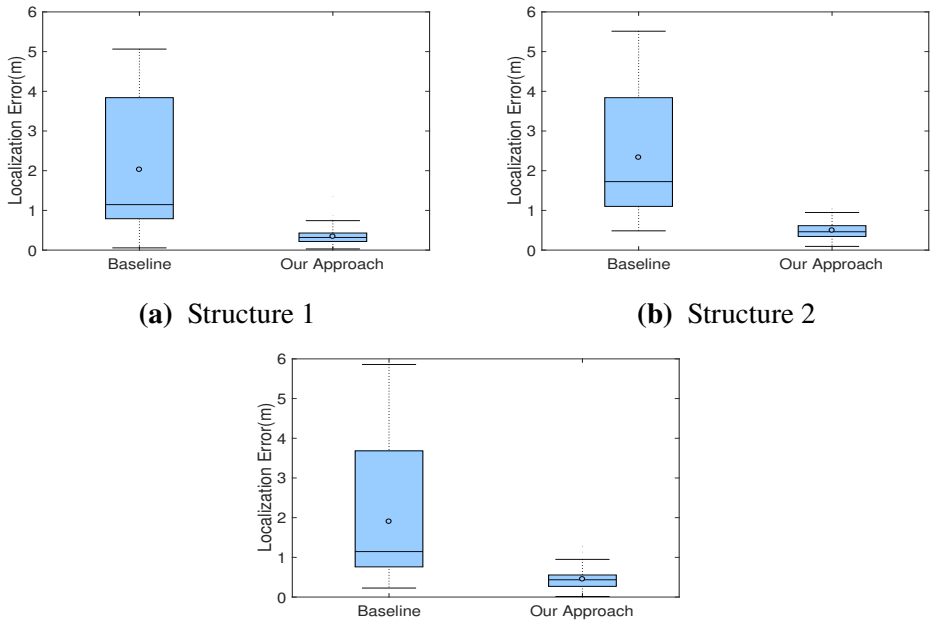

(a) Structure 1

(b) Structure 2

(c) Structure 3

Figure 4.14: Evaluating Our Localization Approach in Different Structures. Part (a), Part (b), and Part (c) evaluates our approach in a non-carpeted wooden floor, a carpeted metal deck floor, and a non-carpeted concrete floor on ground level, respectively. Consistent improvement of localization performance in all the structures suggests that our locally adaptive localization approach is robust in different structures.

of the fixed-velocity approach depends on the assumed velocity input. This figure shows that the fixed-velocity approach results in the minimum localization error of 0.39 meters when the calibrated wave propagation velocity is equal to 152.4 m/s. On the other hand, our approach (with adaptive velocity) results in 0.34 meters of localization error and, as it does not depend on the velocity, it is shown with a constant line. Therefore, our approach outperforms the fixed case regardless of the assumed wave propagation velocity. The reason is that the assumption of a fixed velocity for all the footstep locations does not hold in real-world floors which contain spatial structural variations. Our approach does not make such an assumption and thus can better deal with these structural variations.

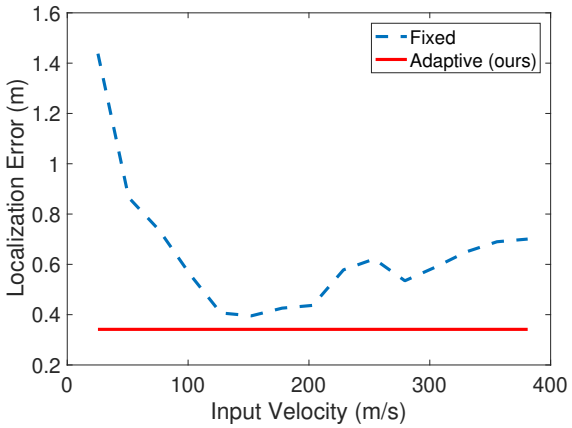

Figure 4.15: Comparing the Adaptive and the Fixed-Velocity Localization Approaches. This figure shows that, regardless of the assumed propagation velocity, our adaptive localization approach outperforms the fixed-velocity approach.

Chapter 5

Modeling the Obstruction Effects on the Vibration Responses

In this section, we characterize the effects of obstructions on footstep-induced floor vibrations to enable obstruction-invariant indoor occupant localization. As mentioned in Chapter 4, prior works have explored non-intrusive human foot-step location estimation using structural vibrations [24]. These approaches assume that the wave propagation velocities between the footstep and the sensors are similar (i.e., isotropic behaviour) and thus, is suitable for open spaces. However, in real life structures, there are various types of obstructions (e.g., walls, furniture, etc.) which affect the floor structural properties and hence the wave propagation velocity [115]. In turn, these changes in propagation velocity can significantly reduce the occupant localization accuracy. Therefore, to maintain the localization accuracy, the prior works require multiple sensors with unobstructed wave propagation path to footsteps in every room which increases the instrumentation and maintenance costs.

We introduce an obstruction-invariant footstep-vibration-based occupant localization approach which considers different wave propagation velocity between the footstep and various sensors depending on the existence and the mass of the obstruction. The main challenges are that 1) the relationship between the wave propagation velocity and the obstruction mass is unknown and structure-dependent and 2) for each footstep, the existence and the mass of obstruction on the

vibration wave path is also unknown. To overcome these challenges, we first characterize the frequency-dependent attenuation of the footstep-induced vibrations to find the existence and mass of the obstruction on the path between the footstep and each sensor using the signal energy. Then, we employ the lamb wave propagation characteristics to model the velocity-mass relationship which is suitable for various structures. This relationship enables finding the obstructed velocities which we then use to locate the occupants using a non-isotropic multilateration approach. To validate the system performance, we use field experiments in multiple structure with human participants. In the rest of this chapter, we first discuss the related works and how our work is distinguished from them (in Section 5.1). Then, we discuss the physical intuition behind lamb wave propagation characteristics and how it is affected by the addition of obstruction mass (in Section 5.2). Next, we discuss our obstruction-invariant occupant localization approach (in Section 5.3). Finally, we describe our evaluation procedure, including the experiments we conducted and the analysis results (in Section 5.4).

5.1 Literature Review

In this section, we explore the related work and the remaining research gap for different aspects of vibration-based occupant localization in obstructed indoor settings. We first discuss the existing approaches for analyzing the addition of mass on the floor. Then, we describe the general source localization and the vibration-based occupant localization approaches.

5.1.1 Mass Addition for Wave Propagation and Structural Vibration Control

Existence of mass on the floor affects the structural dynamic properties as well as the vibration wave propagation characteristics. Based on this effect, adding a series of masses (and mass dampers) in designated locations on the floor have been used to control the structural vibrations and noise of the floors [116–119]. The main goal of this process is to modify the modal characteristics of the floor to attenuate the vibration noise and improve the living condition for the residents. Further, the effect of mass on wave propagation velocity has been studies for guiding and focusing flexural

lamb waves via adding elastic metamaterial masses [120, 121]. However, these approaches are not suitable in our problem. First, they are focused on the forward problem of how the addition of mass affects the structural vibrations, whereas our problem is an inverse problem (i.e., finding mass based on the structural vibration). Second, they develop a physical model which is difficult in real-life floors for which the structural parameters and configuration are often unknown and uncertain. To overcome these limitations, we introduce a physics-guided, data-driven approach to 1) estimate the obstruction mass using the structural vibration and 2) characterize the relationship between the obstruction mass and wave propagation velocity.

5.1.2 Floor-Vibration-Based Occupant Localization

The objective of the floor-vibration-based occupant localization is to estimate the unknown footstep location using the vibration signals received in multiple sensors of known location. The main current approaches for occupant localization include classification-based approaches, TDoA-based approaches, and physical-model-based approaches. The classification approach aims to match the signals received in various locations to a set of signals from known locations [122]. TDoA-based approaches leverage the fact that the vibration waves caused by the footsteps arrive at different sensors at different times. A common approach to leverage these TDoAs is multilateration [23, 24, 123, 124]. Multilateration is based on the fact that the possible locations of the footstep given a specific Time Difference of Arrival (TDoA) between two sensors and wave propagation velocity form a hyperbola. Having more sensors results in additional TDoAs and hyperbolas whose intersection is the footstep location. Alternatively, the sign of the TDoAs can be used to locate the footstep by recurrent division of the search space [125].

However, obstructions such as walls and furniture affect the wave propagation characteristics. This effect results in either extensive calibration requirements, higher sensing requirements, or reduced localization performance for the classification-based and TDoA-based approaches. The physical-model-based approaches compare the vibration measurements with the physical model predictions to estimate the occupant location. Hence, they potentially can handle the obstruction effect by including it in the physical model [26, 126]. However, these approaches require knowing

the structural characteristics for modeling which might not be known in many buildings. In this paper, based on lamb wave properties, we characterize the relationship between the wave propagation velocity and the obstruction mass to enable TDoA-based occupant localization. This approach does not require extensive calibration or knowing the structural characteristics.

5.2 The Physics Behind Obstruction Effect on Footstep-Induced Vibration Wave Propagation

We utilize the footstep-induced floor vibrations to localize the occupants in obstructive indoor settings. In this section, we provide a brief background of the physics of the footstep-induced floor vibration wave propagation and how it is affected by obstructions such as walls and furniture. The footsteps cause elastic vibration waves in the floor which travels outward from the footstep location. These elastic vibration waves can be formulated as Lamb waves because 1) the floors are plates with free surfaces on the top and bottom and 2) due to the low frequency nature of the footstep vibrations, the ratio of wavelength to floor thickness is large in our application [24, 103].

The Effect of Obstruction Mass on the Lamb Wave Attenuation Rate: The attenuation rate of the Lamb waves depends on the floor mass and the frequency (i.e., higher frequency components show higher attenuation rate) [127]. The addition of the obstruction results in larger mass which in turn results in additional frequency-dependent attenuation. In other words, obstructions cause different levels of energy reduction across various frequency components of the vibration wave. For a specific component, this attenuation can potentially be used to estimate the obstruction mass by modeling the relationship between the obstruction mass and the component energies. However, these component energies also depend on the footstep force and thus, it is difficult to find out if the energy reduction is caused by the addition of the mass or a lighter footstep. To negate the effect of the footstep force, we instead model the relationship between the obstruction mass and the ratios of the different frequency component amplitudes. The main intuitions are: 1) the obstruction-induced wave attenuation rate is frequency-dependent and 2) for the small displacements caused by the footsteps, the structure behaves linearly and hence increasing the footstep force results in a similar

increase in all the frequency component amplitudes (e.g., if the footstep force is twice as large, the amplitude of all the frequency components is approximately twice as large). Therefore, by considering the frequency amplitude ratios, we keep the effect of the obstruction while negating the effect of the footstep force. Figure 5.1 shows the changes in a sample ratio for different mass levels (ratio of frequency amplitude at 10 Hz over the amplitude at 60 Hz). This figure shows that addition of the mass results in higher ratio which means that the attenuation at 60 Hz is more significant than the attenuation at 10 Hz.

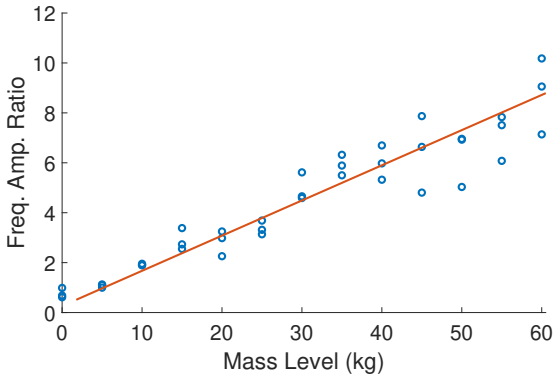

Figure 5.1: The Effect of the Obstruction Mass on the Frequency Amplitude Ratios (ratio of frequency amplitude at 10 Hz over the amplitude at 60 Hz).

The Effect of Obstruction Mass on Lamb Wave Propagation Velocity: In general, Lamb waves show two infinite sets of propagation modes: symmetric (S) and anti-symmetric (A). However, for low frequency footstep-induced vibrations, only the S_0 and A_0 modes can exist and among them, the A_0 modes are most pronounced in magnitude (while S_0 modes are barely visible and hence negligible) [128]. For asymmetrical modes of low frequency (i.e., long flexural waves), the wave propagation velocity is estimated using [129]

$$V^2 = \frac{4}{3}\xi^2 f^2 \frac{\lambda + \mu}{\lambda + 2\mu}\frac{\mu}{\rho} \tag{5.1}$$

where μ and λ are the Lamé constants which describe the material properties, $2f$ is the thickness of the plate, ξ is the wavenumber, and ρ is the material density. This equation shows that for given floor thickness and material properties, the wave propagation velocity depends on 1) the floor

mass which can be affected by the obstruction mass and 2) the frequency (i.e., is dispersive). We use these two principles in designing our obstruction-invariant occupant localization approach, as will be discussed in Section 5.3.1. Figure 5.2 shows that adding more mass results in lower wave propagation velocity. This is shown by reduced ratio of the obstructed velocity to the unobstructed velocity (which does not change across mass levels).

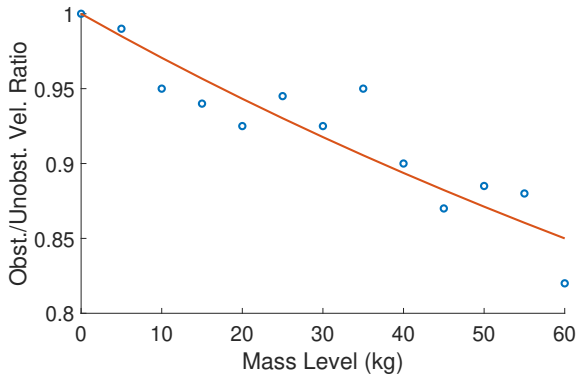

Figure 5.2: The Effect of the Obstruction Mass on the Wave Propagation Velocity.

Figure 5.3 shows an intuitive illustration of the effects of the obstruction on the wave propagation attenuation and velocity. This figure shows the footstep caused by an occupant walking and two sensors of the same distance to the footstep. To reach one of these sensors, the footstep-induced vibration wave propagates through an obstruction. The frequency domain representations of the vibration signals show the frequency-dependent nature of obstruction-induced attenuation. For example, the frequency component of 140 Hz has higher attenuation than the component of 60 Hz. In this figure, we have normalized both signals to have the same maximum to reduce the differences caused by footstep force. On the other hand, the time domain representations of the signals show that the vibration waves reach the obstructed sensor later than the unobstructed sensor. Considering the same footstep-sensor distance, we can conclude that the wave propagation velocity is lower for the obstructed case. This observation is in line with the lamb wave propagation characteristics mentioned in Equation 5.1. These observations and principles form the cornerstone of our obstruction-invariant occupant localization approach which is discussed in Section 5.3.

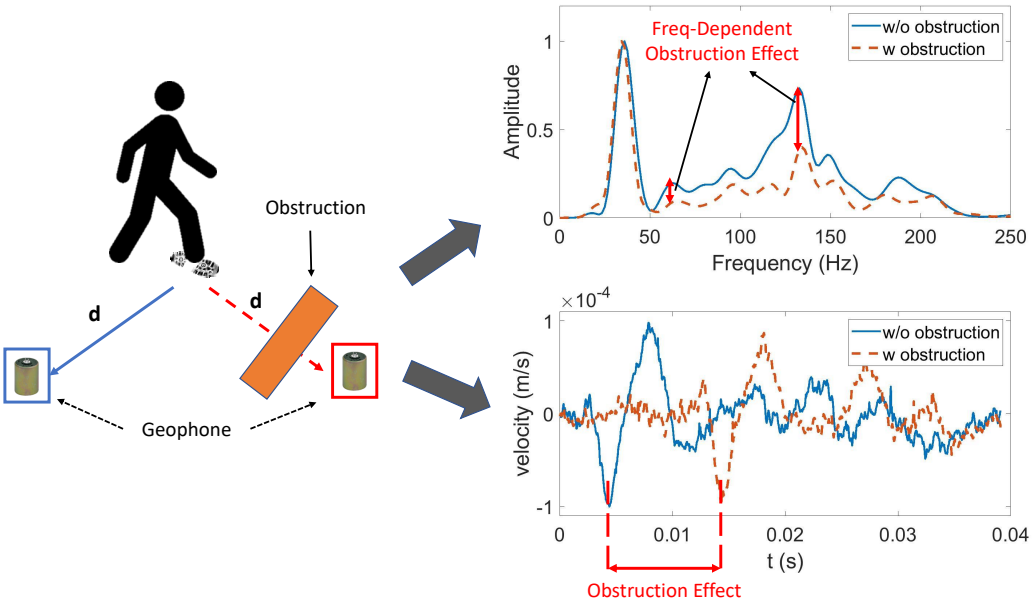

Figure 5.3: The Obstruction Effect Intuition.

5.3 Obstruction-Invariant Occupant Localization

Our approach improves robustness to obstructions by accounting for velocity differences when obstructions of different mass are present. To this end, the approach consists of three main modules: 1) footstep detection, 2) obstruction characterization, and 3) step-level localization. The different stages of this approach are presented in Figure 5.4. We have discussed Footstep Detection in detail in Sections 2 and 3. The other modules will be discussed in the following sections.

5.3.1 Obstruction Characterization Module

Our obstruction characterization module first detects and estimates the obstruction mass and then finds the wave propagation velocities when the wave propagates through the obstruction.

Based on the lamb wave propagation characteristics, this propagation velocity is frequency-dependent (aka, the dispersion effect [23, 24]) and depends on the obstruction mass, as discussed in Section 5.2. Therefore, we first decompose the signal into scale components using a time frequency representation and select a subset of scale components with high energy in all the sensors. Then, for each chosen scale component, we estimate the wave propagation velocity knowing the obstruction

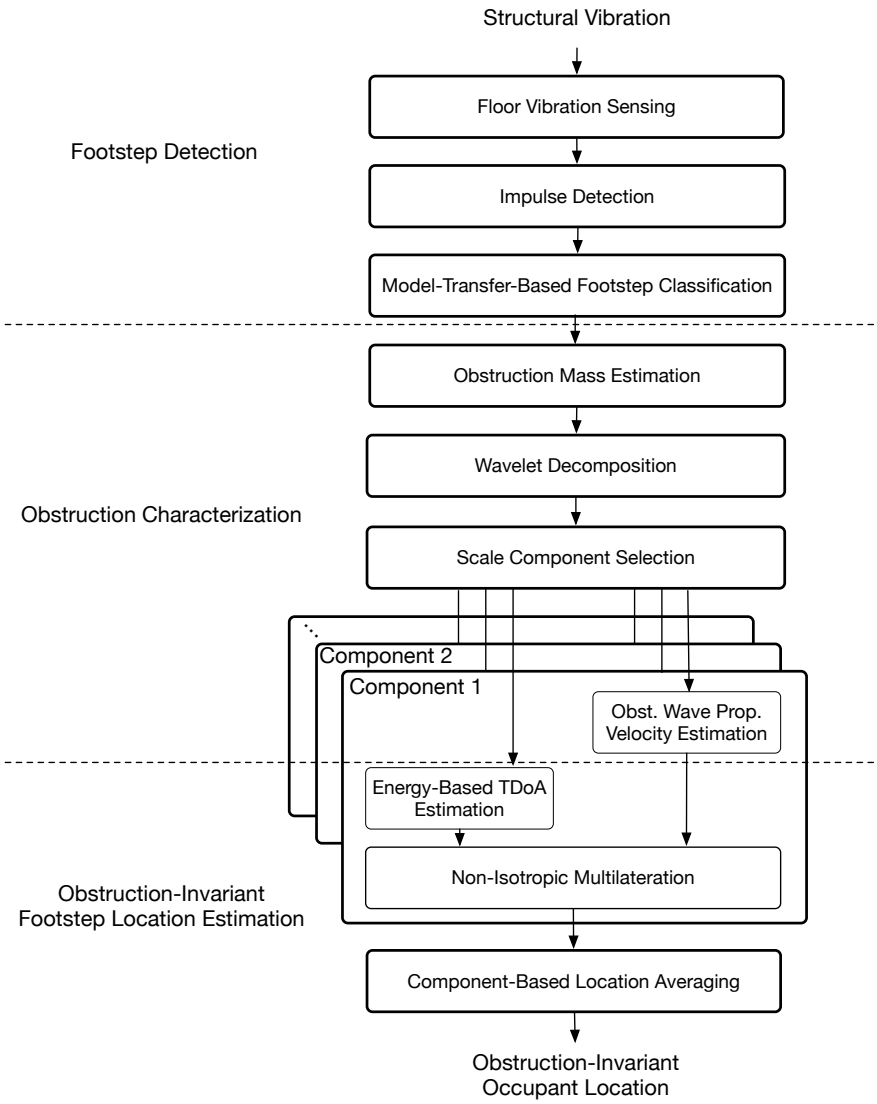

Figure 5.4: Obstruction-Invariant Occupant Localization Approach.

mass.

Obstruction Mass Estimation

To detect and estimate the obstruction mass, we characterize the wave attenuation rates caused by the obstruction. Based on the discussion in Section 5.2, we characterize the relationship between the obstruction mass and the ratios of the amplitude of various frequency components (which are estimated using fft [130]). Further, for the small displacements caused by the footsteps, the structure behaves linearly and thus, we assume a linear relationship between the frequency amplitude ratios

and the mass levels. However, considering the ratios between various frequency components results in a large number of ratio features which in turn increase the chance of model over-fitting. Therefore, we first choose a subset of the ratios for training a mass-ratio model. To this end, we first divide the footstep vibration data into training, validation, and test sets. Then, using the training data, we choose a subset of the ratios which have 1) low standard deviation across the samples in the training set (to improve the robustness) and 2) large correlation coefficient with the mass levels (to ensure the linearity and improve accuracy). Then, among the chosen ratios, we employ a greedy wrapper approach to select the ratio features which result in lower validation error [131]. These remaining feature are then used for training a linear model which is used for detecting and predicting the obstruction mass using the footstep-induced vibration events in the test set. This model is trained for the footsteps that happen in a specific location (e.g., the entrance of the apartment in real-life applications).

Wavelet Decomposition

To characterize the dispersive (i.e., frequency-dependent) wave propagation velocities, we have decomposed the signal using the wavelet transform which is suitable for analyzing and decomposing non-stationary signals (e.g., impulsive signals such as footsteps) [24, 73]. The wavelet decomposition can be described as [107],

$$T(a,b) = w(a) \int_{-\infty}^{+\infty} x(s) \Psi^*_{b,a}(s) ds \tag{5.2}$$

in which $w(a)$ is a weighting function and $\Psi_{b,a}(s)$ is the dilated and time-shifted version of the basis function which is called the mother wavelet $\Psi(s)$. In this paper, we have chosen the Mexican hat wavelet as the mother wavelet because it provides a good representation of the footstep-induced vibration signal characteristics [108]. To select the range of the scales to be analyzed, we have used two notions: 1) geophones are second-degree high pass filters for frequencies lower than 10 Hz [110] and 2) the bandwidth of geophone is 240 Hz [111]. Therefore, the range of the scales we have used for this analysis is between 25 and 300 (i.e., approximately 20 and 250 Hz for sampling

rate of 25.6 kHz and Mexican hat wavelet).

Scale Component Selection

Using all the scale components for localization is not suitable because 1) it is computationally expensive and 2) it decreases the localization performance because the obstruction-induced attenuation potentially causes low-energy scale components with low Signal-to-Noise-Ratio (SNR) which result in large localization errors. Therefore, to overcome the additional obstruction-induced attenuation, we choose a subset of the scale components with high energies in all the sensors for localization. Specifically, we first average the scale component energies across the sensors and then choose the n components with the highest average energy. Choosing the n is an important part of this process. On the one hand, choosing higher n results in reduced effect of noise and outliers. On the other hand, choosing scales of low energy results in large errors in location estimation. This trade-off will be discussed in more detail in Section 5.4.4. In this paper, we have empirically chosen $n = 2$.

Obstructed Wave Propagation Velocity Estimation

We estimate the propagation velocity of the vibration wave travelling through an obstruction based on Lamb wave propagation characteristics. Specifically, based on Equation 5.1, we estimate the obstructed velocity as the ratio of the unobstructed velocity for a given scale (or frequency) component through

$$\frac{V_{obs}^2}{V_{unobs}^2} = \frac{\frac{4}{3}\xi^2 f \frac{\lambda+\mu}{\lambda+2\mu}\frac{\mu}{\rho_a+m_{obs}}}{\frac{4}{3}\xi^2 f \frac{\lambda+\mu}{\lambda+2\mu}\frac{\mu}{\rho_a}} \tag{5.3}$$

where μ and λ are the Lamé constants which describe the material properties, $2f$ is the thickness of the plate, ξ is the wavenumber, ρ_a is the mass of the floor per unit of area, m_{obs} is the mass of the obstruction, and V_{obs} and V_{unobs} are the obstructed and unobstructed velocities. We can simplify this equation because 1) we use specific decomposed scale components and hence the wavenumber is constant, 2) the Lamé constants depend on the Poisson ratio and the modulus of elasticity and hence do not change with obstruction, and 3) we assume that the obstruction does not affect the

effective thickness of the floor because it simply sits on the floor or has minimal connection to the floor and hence, there is no significant structural integrity (which is true for most common obstructions such as furniture and non-load-bearing partition walls). Therefore, we have

$$\frac{V_{obs}}{V_{unobs}} = \sqrt{\frac{\rho_a}{\rho_a + m_{obs}}}. \tag{5.4}$$

Using Equation 5.4, we estimate the obstructed velocity based on the unobstructed wave propagation velocity, the mass of obstruction, and the mass per unit of area of the floor. The unobstructed velocity can be estimated either using additional unobstructed sensors or during the time that the obstruction is not present (through either calibration or our prior calibration-free approach [24]). Further, the mass of the obstruction and the floor can be estimated using the specification sheets and the available structural drawings. Designing an approach to automatically estimate these mass factors is part of our future work plan. Further, in this paper, we have focused on characterizing the effect of mass because we have observed that it is one of the most important factors affecting the wave propagation velocity in our preliminary experiments. We plan to characterize other factors such as footstep-sensor distance and the obstruction area in future work.

5.3.2 Obstruction-Invariant Footstep Location Estimation Module

This module performs step-level and obstruction-invariant occupant localization using our non-isotropic multilateration approach which considers different wave propagation velocities between the footsteps and sensors based on the obstruction mass on the wave path. To this end, we first estimate the Time of Arrivals (ToA) for the vibration signals using an energy-based approach. Then, we utilize these ToAs and the propagation velocities (estimated in Section 5.3.1) for step-level localization through a non-isotropic multilateration approach. We perform this location estimation for the scale components selected in Section 5.3.1 and combine their estimations to find the step-level occupant location.

Energy-Based TDoA Estimation

To find the TDoA between the signals, we have estimated the time where a certain percentage of the energy of footstep-induced vibration happens for each sensor. Generally, current approaches for estimating the TDoA are either threshold-based [24, 27] or similarity-based (e.g., cross-correlation) [84]. This energy-based approach is more robust than the current approaches because it is less affected by 1) missing peaks compared to the peak-based approaches and 2) signal distortions caused by reflections, dispersion, and multipath compared to the similarity-based approaches [112]. In this paper, we have empirically chosen 15% of the energy of the footstep signals as the time of arrival of the signals.

Non-Isotropic Multilateration and Component-based Location Averaging

Our non-isotropic multilateration formulation, which is able to consider various propagation velocities in different directions, has two main steps: 1) the simulation step and 2) the filtering step. The objective of the simulation step is to find the possible TDoA ranges caused by a footstep. To this end, we first define a Possible Location Set (PLS) for the footstep (e.g., inside the boundary of the room). Then, we estimate the sensor-footstep distances for various locations inside the PLS. Finally, we estimate the TDoAs for various sensor pairs for a given wave propagation velocity array. This wave propagation velocity array contains the velocities between the footstep location and each one of the sensors and is achieved from Section 5.3.1. Therefore, the simulation step results in a Possible TDoA Set (PTS) for locations in PLS. The objective of the filtering step is to find the locations in the PLS which result in TDoAs similar to the measured TDoAs. Specifically, we first find the actual TDoA values for various sensor pairs (as discussed in Section 5.3.2) and then, filter the TDoAs in PTS which are similar to the actual TDoAs. Finally, we find the locations in PLS which correspond to the remaining TDoAs in PTS. The detailed steps of our non-isotropic multilateration is presented in Algorithm 2. Finally, to improve the accuracy and robustness of our location estimation approach, we average multiple location estimations from the scale components selected in Section 5.3.1.

Algorithm 2 The Non-Isotropic Multilateration Approach

Define the Possible Location Set (PLS) of the Footstep ▷ Simulation Step ↓
for PLS_i in PLS **do**
    for S_j in sensor-locations **do**
        $d_{ij} = \left\| X_i - S_j \right\|_2$
        $ToA_j = d_{ij}$ / v_j
    end for
    $TDoA_i = ToA - ToA[1]$
    Possible TDoA Set (PTS) ← $TDoA_i$
end for

Estimate the actual pairwise TDoAs (AT) ▷ Filtering Step ↓
Define Required-Number-of-Estimations (RNE), init-thresh, update-thresh;
thresh ← init-thresh
while number-of-estimations < RNE **do**
    for PTS_i in PTS **do**
        if $PTS_i + thresh < AT < PTS_i + thresh$ **then**
            $ELS \leftarrow PLS_i$
        end if
    end for
    number-of-estimations ← number of elements in ELS
    thresh += update-thresh
end while
Estimated Location ← mean(ELS)

5.4 Obstruction-Invariant Occupant Localization Evaluation

To understand the performance of our obstruction-invariant occupant localization approach, we conducted a set of experiments with human participants in real-world structures. We first introduce the experimental setup in Section 5.4.1. Then, we validate the performance of our obstruction-invariant occupant localization approach. This evaluation consists of the general performance as well as the performance of different modules of the approach (in Sections 5.4.2- 5.4.6). Finally, we evaluate the sensitivity of our approach to the changes in the footstep-sensor distance, mass level, scale components, and structure (in Sections 5.4.7- 5.4.10).

5.4.1 Experimental Setup

To evaluate our approach, we have utilized a sensing system which measures the floor vibration via a geophone. Geophone is a sensor which converts the vertical velocity of the floor to Voltage [111]. Figure 2.1 shows a sample sensing node. The collected signals are amplified approximately 200-2000X. After amplification and depending on the structure type and footstep strike energy, the effective sensing range of our system for footstep detection is up to 20 meters in diameter. Amplified signals are then digitized and transferred to a server using a 24-bit A/D converter. To ensure enough time resolution for accurate TDoA estimation, we have chosen sampling frequency of 25kHz.

Sensing Configuration: For the experiments, the subject walks in two different structures to show that our approach is robust in across structures. The structures include a non-carpeted concrete floor on the ground level of a campus building in Carnegie Mellon University and a non-carpeted an elevated wood framed mock floor. The difference between the natural frequencies of these structures (i.e., 23.83 and 29.5 Hz, respectively) make them suitable to show the robustness of our approach over various structures. Figure 5.6 shows the two experimental locations. To mimic the effect of the obstruction mass, we have used a plastic bin filled with sand. Based on the amount of the sand, we have achieved different levels of additional mass between 0 and 60 kg. For each of the 13 mass levels considered, we have collected 5 traces of four steps from each structure. To focus on

the effect of the obstruction, these four step locations are chosen inside the polygon created by the sensors. The reason is that for steps outside this polygon, multilateration performance decreases quickly and hence the results become too uncertain to effectively and accurately study the effect of the obstruction [24]. To obtain the ground truth, we have taped the locations of the footsteps on the floor and asked the subjects to walk on these locations.

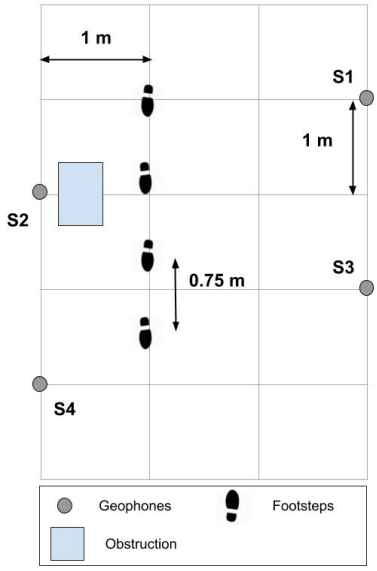

Figure 5.5: The Sensing Configuration.

Unobstructed Velocity: Our obstruction characterization module aims to find the obstructed velocity as a ratio of the unobstructed velocity. This ensures that our approach is able to localize footsteps across various structures. To find the unobstructed velocity, in our prior work, we have introduced a multilateration solution approach which estimates the location and propagation velocity simultaneously [24]. However, the objective of this work is to study the obstruction effects and therefore, to reduce the uncertainties in estimating the propagation velocities, we calibrate for the velocity which results in the minimum localization error in a set of experiments with no obstruction [23].

5.4.2 Overall Footstep Localization Evaluation

To evaluate the performance of our obstruction-invariant occupant localization approach, we compare our localization errors with a baseline approach. The baseline approach 1) averages the

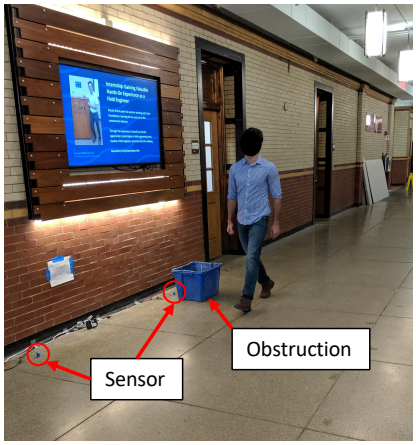

(a) CMU Porter Hall: Concrete Slab on Grade

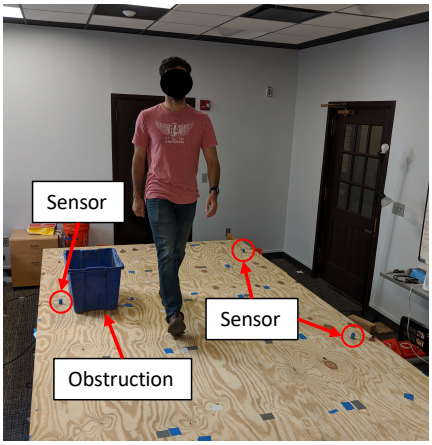

(b) CMU Lab: Mock Wood Floor

Figure 5.6: Experimental Locations

estimations across all the scale components ("AllScale" approach), 2) does not account for the effect of the obstruction ("NoVelCorrect" approach), 3) utilizes a Nonlinear Least Square (NLS) ToA-based multilateration ("ToAMult" approach). Further, we compare our approach with the unobstructed case (i.e., there is no obstruction). The localization error metric is the Euclidean distance between the actual and estimated locations. As shown in Figure 5.7, our approach results in 0.63 meters average error which is equivalent to 1.7X improvement over the baseline approach which has 1.07 meters error. Further, the unobstructed approach has 0.63 meters average error which is similar to our approach. These results show that our obstruction-invariant localization approach 1) successfully negates the effect of the obstruction and results in similar performance to the unobstructed approach and 2) outperforms the baseline approach.

5.4.3 Mass Estimation Evaluation

In this section, we evaluate the performance of our mass estimation module. To this end, we first discuss the mass estimation performance and then study its sensitivity to the number of chosen features.

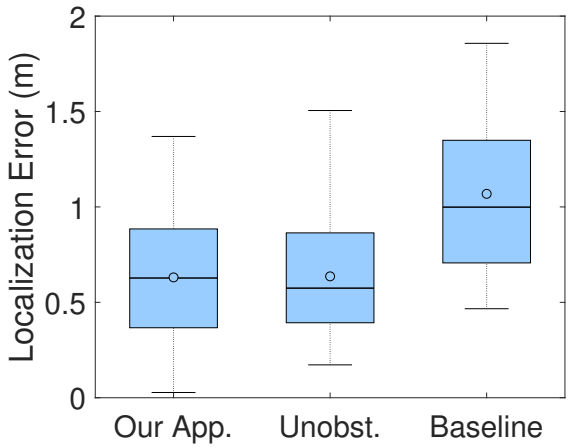

Figure 5.7: The Overall Performance of Our Obstruction-Invariant Occupant Localization Approach.

Mass Estimation Performance

As we discussed in Section 5.3.1, our approach predicts the mass through the ratios between the amplitude of the different frequency components of the vibration signals. To evaluate this approach, we compare the its results with a baseline approach which trains a linear regression model using all the components of the frequency representation of the vibration signals (instead of the ratios). As shown in Figure 5.8a, in the first structure, our approach results in average mass estimation error of 12.7 kg, whereas the baseline approach results in average error of 29.4 kg. This is equivalent to 2.3X improvement in the performance. Moreover, our approach results in estimation standard deviation of 8 kg compared to 23kg using the baseline approach (i.e., 2.9X improvement). In the second structure, as shown in Figure 5.8b, our approach results in average mass estimation error of 3.6 kg which is 4X improvement over the baseline approach which result in 14.8 kg error. With regards to the standard deviation, our approach result in 3.9 kg compared to 14.6 kg using the baseline approach (i.e., 3.7X improvement in robustness). These results show that our mass estimation is both more accurate and robust compared to the baseline approach. In general, the results are better in the second structure. This is because the second structure is a wooden floor and has lower mass. Therefore, the effect of the additional mass is more significant and easier to quantify.

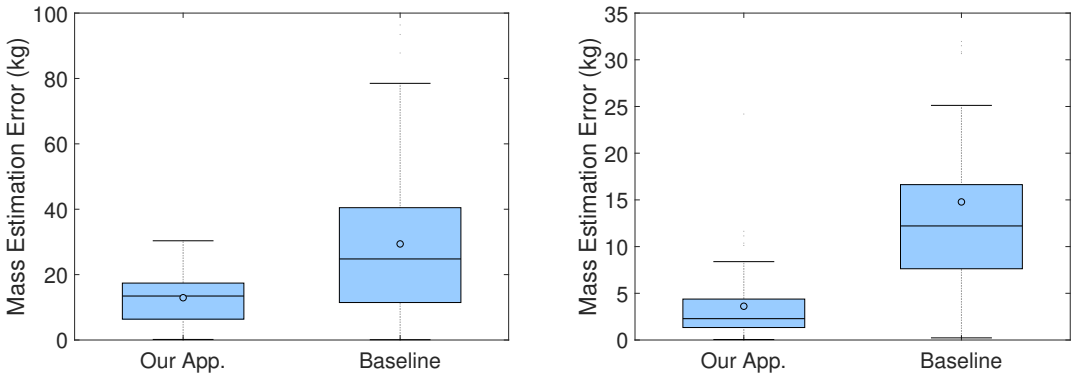

(a) St1: Concrete Slab Floor **(b)** St2: Wooden Floor

Figure 5.8: The Mass Estimation Evaluation.

Mass Estimation Sensitivity to the Number of Chosen Scales

An important factor for mass estimation performance is the number of chosen ratio features. As discussed in Section 5.3.1, we choose a subset of the ratio features for mass estimation to reduce 1) the chance of over-fitting and 2) the computational cost of the model training. To evaluate the sensitivity of our mass estimation approach to this factor, we have estimated the test error for the ratio feature subsets of various size, as shown in Figure 5.9. Based on this figure, the mass estimation performance is robust and consistent when the size of the ratio feature subsets is less than 25. In this paper, we have chosen subset size of 4 for mass estimation to minimize the mass estimation error while reducing the computational cost.

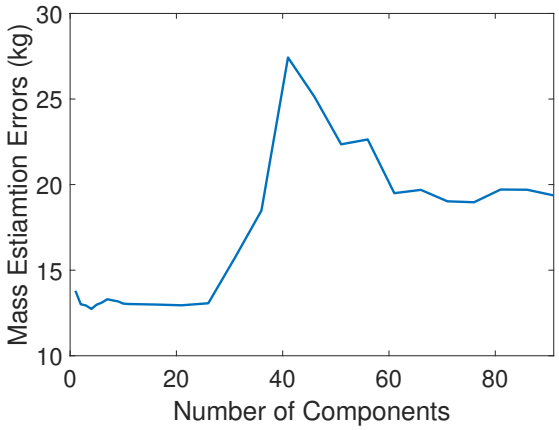

Figure 5.9: Sensitivity of the Mass Estimation Approach to the Number of Chosen Ratio Features.

5.4.4 Scale Component Selection Evaluation

As discussed in Section 5.3.1, the existence of obstruction results in additional attenuation which reduces the Signal-to-Noise (SNR) ratio and hence the localization performance. To overcome this effect, our scale selection approach chooses a subset of scale components with high energies. We first evaluate how the scale selection affects the performance of our obstruction-invariant occupant localization approach (in Section 5.4.4). Then, we discuss the sensitivity of our approach to the number of chosen scale components in Section 5.4.4.

Scale Component Selection Performance

To validate the effect of our scale selection approach, we compare our results with the AllScale approach which averages the location estimation across all the scales. In comparison, our approach averages the location estimation over two of the scale components with the highest energy. The rest of the localization procedure is similar for both of the considered approaches. As shown in Figure 5.10, our scale selection approach results in 0.61 meters average localization error which is 1.3X improvement over the AllScale approach which results in 0.8 meters error. These results show that our scale selection approach chooses a suitable subset of scale components for occupant localization.

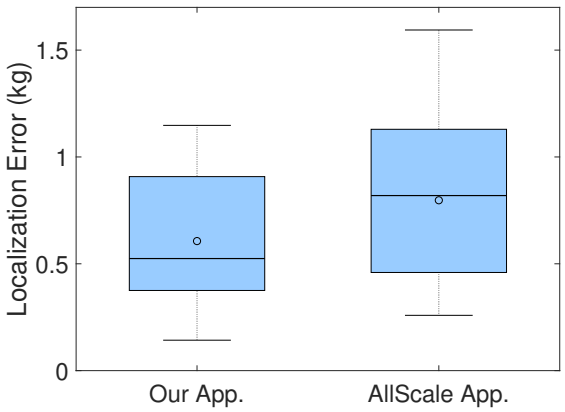

Figure 5.10: Scale Selection Evaluation

Localization Performance Sensitivity to the Number of Chosen Scales

One of the factors that affects the performance of our obstruction-invariant localization approach is the number of the scale components. The trade-off is that: 1) choosing multiple scale components reduces the effect of erroneous and noisy location estimations (by averaging several estimations); however, 2) considering estimations from very low energy signals which mostly contain noise results in lower localization performance. To evaluate this factor, we have evaluated the localization performance across different number of scales. Figure 5.11 shows this evaluation and the trade-off regarding the number of scale components. It can be seen that the localization performance is similar for cases with 2-20 scales. Therefore, in this paper, we empirically average over the location estimations of 2 scale components for footstep localization to ensure accurate localization while reducing the computational cost of the localization.

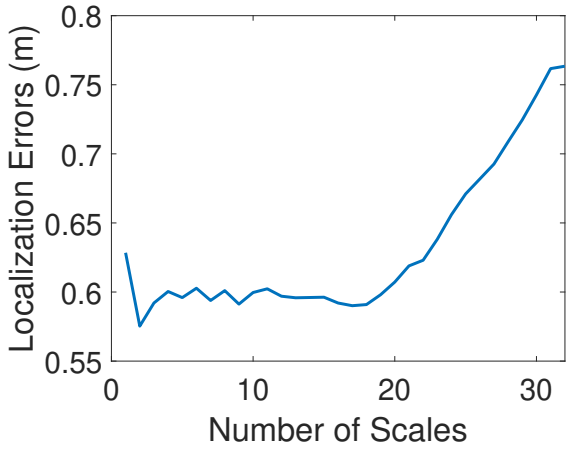

Figure 5.11: The Sensitivity of The Approach to the Number of Chosen Scales.

5.4.5 Obstructed Wave Propagation Velocity Estimation Evaluation

In this section, we study the effect of the Obstructed Wave Propagation Velocity Estimation module. To this end, we compare our localization results with the NoVelCorrect approach which does not consider the effect of the obstruction on the wave propagation velocity. Similar to the

previous sections, the rest of the localization procedure is similar between our approach and the NoVelCorrect approach. As shown in Figure 5.12, our approach results in 0.61 meters average error which is equivalent to 1.2X improvement over the NoVelCorrect approach which results in 0.72 meters error. This improvement in performance shows that our wave propagation velocity estimation approach is effective in reducing the obstruction-induced propagation velocity changes.

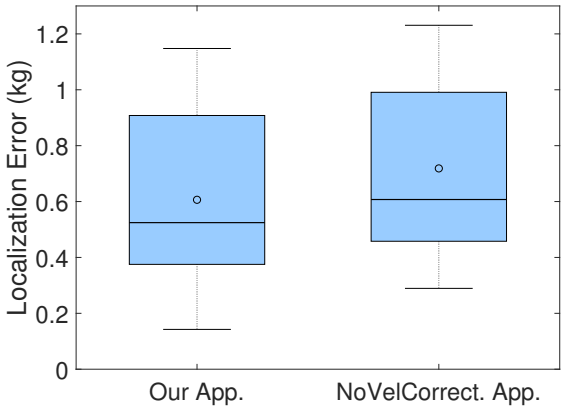

Figure 5.12: Obstructed Wave Propagation Velocity Estimation Evaluation

5.4.6 Non-Isotropic Multilateration Evaluation

Our non-isotropic multilateration approach enables occupant localization when there is different wave propagation velocities between the footstep and various sensors. To evaluate this approach, we compare our results with ToAMult which is a Nonlinear Least Square (NLS) based approach based on the Time of Arrival (ToA) of the vibration signal in the sensors. For the i^{th} sensor, ToAMult defines the following cost function:

$$C_i = \|x - p_i\|_2 - v_i(t_i - t_f) \tag{5.5}$$

where x is the location of the footstep, p_i is the location of the sensor, v_i is the propagation velocities between the footstep and the sensors, t_i is the vibration wave ToAs for the sensors, and finally t_f is the time that the footstep happens. There will be four equations for four sensors and the overall

objective function is,

$$\min_{x,t_f} \sqrt{\sum_i C_i^2} \tag{5.6}$$

Knowing the wave propagation velocities, Equation 5.6 can be solved for 3 unknowns: the 2-d footstep location (x) and the footstep occurrence time (t_f). Further, this formulations is a bounded nonlinear least-squares problem which can be solved using a trust region reflective algorithm [132].

Figure 5.13 shows the results of this evaluation. Based on this figure, our approach results in average localization error of 0.61 meters error which is 2X improvement compared to the ToA-based approach (with average error of 1.23 meters meters). The reason behind this improvement is that adding the t_f as an unknown increases the dimension of the problem which in turn increases the likelihood of the NLS approach getting stuck in a local optimum. In comparison, our approach performs a grid search to find the globally optimum solution while keeping the online computational cost low by separating the offline simulation and online filtering step. The performance improvement shows that our non-isotropic multilateration approach is suitable for the real-life obstructed floors.

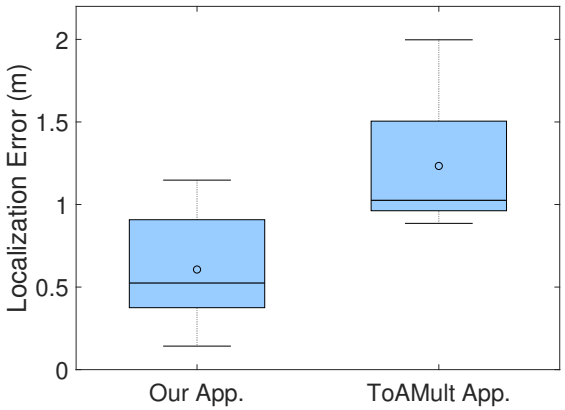

Figure 5.13: Localization Performance of the Non-Isotropic Multilateration.

5.4.7 Localization Performance Sensitivity to Changes in the Footstep-Sensor Distances

Sensor-footstep distance is an important factor in the localization performance. To evaluate this factor, we find the localization errors for footsteps across different locations. Generally, the furthest

sensor has the most effect on the localization error because 1) higher travelling distance between the sensor and the footstep means higher signal distortions and 2) the furthest signals generally have lower SNR which in turn results in lower localization performance. Therefore, to evaluate the effect of distance, the footstep-sensor distance for each footstep is found as the maximum of the Euclidean distances between the footstep and various sensors. Figure 5.14 shows the results of this evaluation for our approach. As expected, the correlation coefficient of 0.63 shows that larger distances result in higher localization error. Specifically, our approach results in errors of 0.31-0.94 meters for the 2.4-3.4 maximum norm distance range.

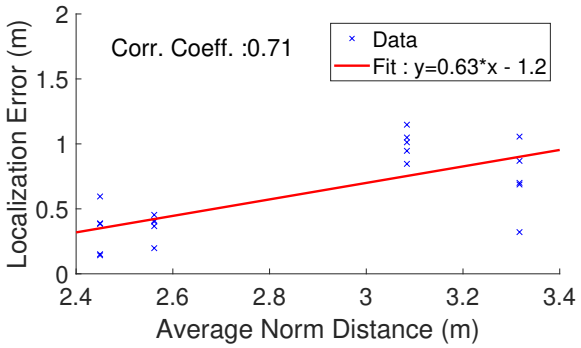

Figure 5.14: Localization Performance Sensitivity to the Footstep-Sensor Distance.

5.4.8 Localization Performance Sensitivity to Changes in the Obstruction Mass

Changing the obstruction mass results in changes in the wave propagation velocity which in turn, affects the localization performance. To evaluate this effect, we have conducted experiments with 12 levels of obstruction mass (each 5 kg between 0 and 60 kg). The localization results for these different added mass levels are presented in Figure 5.15. Based on this figure, our approach outperforms the baseline approach for all the mass levels. Further, the improvements are generally more significant for cases with higher added mass. For example, when there is 5 kg of added mass, our approach outperforms the baseline by 0.25 meters. However, this number is increased to 0.38 meters when there is 60 kg of added mass. The reason is that the higher added mass cause

more significant changes in the wave propagation velocity which, in turn, reduce the localization accuracy of the baseline approach. However, our approach considers this obstruction-induced velocity changes and therefore is less affected by the additional mass. This consistent improvement across all the mass levels shows that our approach efficiently negates the effect of the obstructions.

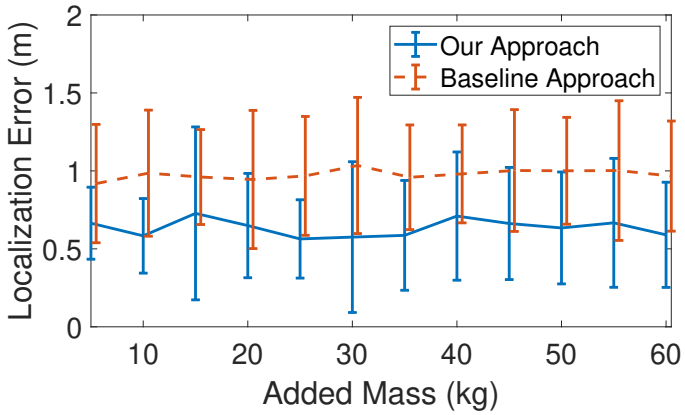

Figure 5.15: The Sensitivity of Our Obstruction-Invariant Occupant Localization Approach to the Obstruction Mass.

5.4.9 Localization Performance Sensitivity to The Scale Components

In this section, we evaluate the improvement resulted from our obstruction-invariant occupant localization approach across various scales. The baseline approach 1) does not account for the obstruction masses and 2) utilizes the ToAMult approach discussed in Section 5.4.6. For this analysis, we have focused on the scale range of 25 to 300 which corresponds to 20-250 Hz for the Mexican hat wavelet. This range is decided by sensing specifications of the Geophone sensor, as discussed in Section 5.3.1. As shown in Figure 5.16, our approach outperforms the baseline approach across all the scales. This shows that our obstruction-invariant occupant localization approach is more robust across all the scale components.

5.4.10 Obstruction-Invariant Occupant Localization Evaluation Across Structures

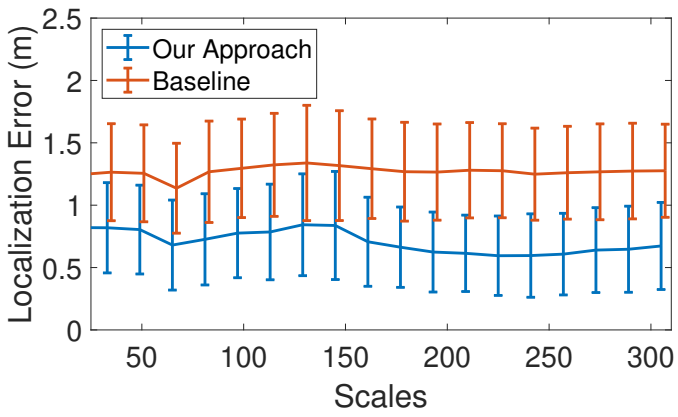

Figure 5.16: Localization Performance across Various Scales. This figure shows that our approach outperforms the baseline approach in all the scales.

By leveraging the lamb wave propagation characteristics, our obstruction-invariant occupant localization is robust across various structures. To evaluate this robustness, we have performed experiments in two different structures. For each structure, we have compared the performance of our approach with the baseline and the unobstructed approach. Figure 5.17a shows the results for the first structure which is a non-carpeted concrete slab on the ground level of a campus building in Carnegie Mellon University in Pittsburgh, PA. This figure shows that our approach results in 0.61 meters average localization error which is equivalent to 1.6X improvement over the baseline approach which results in 0.97 meters average error. Further, in this structure, our approach has comparable results with the unobstructed approach which results in 0.62 meters average error. Figure 5.17b show the results for the second structure which is a non-carpeted elevated mock wooden floor. In this structure, our approach results in 0.65 meters which is equivalent to 1.8X improvements compared to the baseline approach average localization error which is 1.17 meters. Despite the slightly higher localization errors (which is possibly caused by noisy nature of wooden floor vibrations [24]), our approach results in comparable localization performance to the unobstructed approach with 0.65 meters average error. These results shows that our obstruction-invariant occupant localization approach is robust to the changes in the structure which in turn, shows that it is practical in real-life applications.

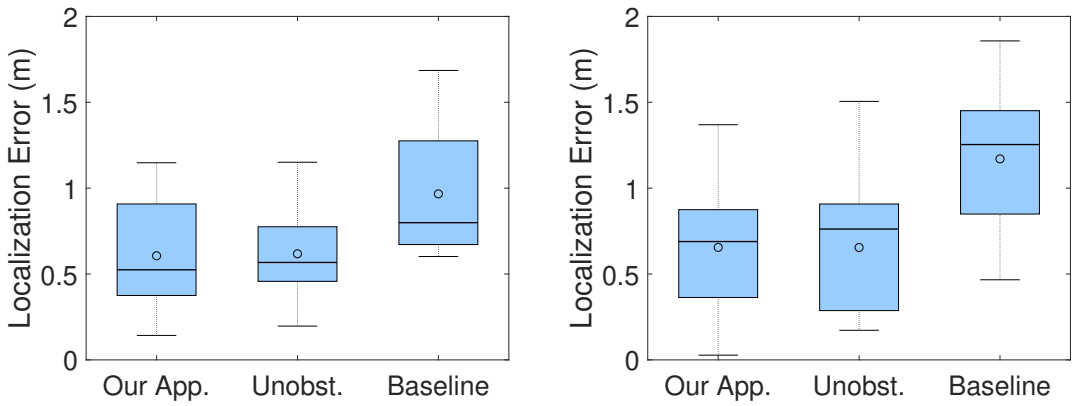

(a) St1: Concrete Slab Floor

(b) St2: Wooden Floor

Figure 5.17: Localization Performance in Different Structures

Chapter 6

Conclusion

In this chapter, I present a brief summary of this dissertation, the key results, and contributions of the projects that constitute this document. Further, I discuss the future work directions and list my publications during PhD.

6.1 Concluding Remarks

The overall objective of this research is to monitor occupants in the indoor settings using their footstep-induced floor vibration. Compared to current sensing approaches, our floor-vibration-based approach enables non-intrusive and sparse sensing. However, the footstep-induced vibration waves propagate through the structure which will result in various research challenges. In this dissertation, I have focused on three main structure-related research challenges: 1) the footstep model changes across various structures (in Chapter 3), 2) the dispersive vibration wave propagation (in Chapter 4), and 3) the obstruction effects on the vibration responses (in Chapter 5).

In Chapter 3, I present a step-level occupant detection which enables detection across different buildings using footstep-induced floor vibrations. To ensure successful transfer across various structures, this approach first projects the original frequency-based features into a feature space in which the structural effects are minimized. We have shown that reducing structural effects can be achieved through minimizing the Maximum-Mean-Discrepancy (MMD) between the source and

target data distributions. Then, a footstep model is trained in this projected feature space using the labeled data from the source structure to predict the samples in the target structure where no labeled data is available. By not requiring any labeled data in the target structure, our model transfer approach significantly reduces the calibration requirements. We have evaluated our approach in three structures and through comparing with Time-Domain-based and Frequency-Domain-based approaches which do not transfer the data. The evaluation shows that: 1) our approach results in up to 29X and 16X improvement compared to the baseline TD-based and FD-based approaches, respectively; 2) when there is only one source structure, our approach outperforms the baseline approaches by up to 3.3X, 4.5X, and 13.5X across the three target structures; 3) our approach requires 240, 55, and 85 samples in the target structures to reach to the maximum accuracy; 4) using 50 or more samples from the source structure results in the F1-score greater than 0.9; 5) our approach results in consistent improvement in the performance across different ranges of SNR and hence is more robust to the SNR.

In Chapter 4, I introduce a robust and fine-grained occupant localization approach based on the footstep-induced floor vibrations for dispersive and heterogeneous floors. The main challenges are signal distortions due to dispersion and wave propagation velocity variation in different floor locations due to heterogeneity. We address dispersion-related signal distortions by decomposing the signal using wavelet transform and extracting specific components with similar propagation characteristics. We have chosen the components which result in highest localization performance. Moreover, we address the velocity variation by introducing an adaptive multilateration solution which does not require prior knowledge of the wave propagation velocity in the floor. Our evaluations show that: 1) regardless of the multilateration and decomposition (i.e., component extraction) approach, signal decomposition improves the accuracy of localization (e.g., 2.41X improvement in localization using our decomposition method compared to using the raw signal); 2) our locally adaptive localization approach for heterogeneous floors outperforms the baseline approach in different locations of the same structure with average errors of 0.21-0.5, which shows up to 9.6X improvement; 3) our approach performs well across different structures (with errors as low as 0.34 meters location estimation error, which corresponds to 6X reduction compared to the baseline

approach); 4) our approach does not assume a constant propagation velocity (i.e., adaptive) and therefore outperforms the calibration-based approach which assumes a fixed velocity.

In Chapter 5, I present an obstruction-invariant occupant localization approach using footstep-induced floor vibrations. Conventional vibration-based occupant localization approaches map the Time Differences of Arrivals (TDoA) between multiple sensors pairs to the footstep location by assuming similar wave propagation velocities between the footstep and the sensors. This assumption, although true in open spaces, does not always hold in real-life situations with various types of obstruction (walls, furniture, etc.). These obstructions add to the mass of the floor on the path of the vibration waves which in turn affect the wave propagation velocity and reduces the occupant localization performance. To overcome the obstruction effect, we characterize 1) the frequency-dependent attenuation rate of the footstep-induced vibrations to find the existence and mass of the obstruction and 2) the mass-velocity relationship based on the lamb wave properties to estimate the wave propagation velocities between the footstep and various sensors knowing the obstruction mass. Finally, we introduce a non-isotropic multilateration approach to leverage these propagation velocities and the TDoA values across the signals for step-level occupant localization. Our approach resulted in a 0.61 meters average location estimation error, which corresponds to a 1.6X improvement compared to the baseline that does not account for obstructions. Further, our approach results in the same localization performance compared to the case with no obstruction which shows that it effectively negates the effect of the obstruction.

In summary, our footstep-induced vibration sensing provides a sparse and non-intrusive alternative occupant sensing and monitoring in future smart buildings. Further, to enable such monitoring without extensive calibration, we have introduced physics-guided learning approaches. In the next section, we discuss some of the main research directions and opportunities that this work opens up.

6.2 Future Work

In this dissertation, we have addressed some of the most pressing research challenges in occupant monitoring using footstep-induced vibrations. However, there are multiple research directions for

future work, including:

- In Chapter 3, we have focused on designing a model transfer approach which detects footsteps from other sources of excitation across different structures. This work can be extended in multiple directions. For example, future work will focus on extending this model transfer approach to design an occupant activity monitoring which is robust across multiple people. This new direction adds the highly complex human factor to the problem. For example, different people might do the same activity (e.g., vacuuming) differently. This human factor is difficult to model and adds to the research challenges.

- As discussed in Chapter 4, the occupant localization approach performs well when the footsteps are inside the polygon formed by the sensors. However, the performance drops when footsteps outside the polygon are considered. As part of our future work, we plan to update the algorithm to improve its performance outside the sensor polygon. Further, the discussed projects only localize one footstep at a time and do not consider a trace of footsteps from one person. However, in real life situations, people tend to walk in certain traces (e.g., they do not tend to suddenly turn around). To further improve the accuracy and robustness of occupant localization, we will incorporate tracking to consider a trace of footsteps.

- In Chapter 5, we focus on the obstruction mass as the main factor affecting the attenuation and wave propagation velocity. However, there are other factors (e.g., structural stiffness and obstruction shape) which might affect these characteristics. Further, the mass effect on the attenuation requires calibration. Future work will 1) study the obstruction effects on other vibration characteristics and 2) reduce the calibration requirements.

- Physicians use gait temporal parameters for diagnosis and prognosis of various medical conditions such as dementia, chronic obstructive pulmonary disease, and muscular dystrophy. As part of our future work, we aim to characterize the human gait using their footstep-induced vibration responses to enable monitoring the progress of these medical conditions. Further, other smart infrastructure applications will be explored (e.g., energy management and space utilization).

6.3 Publications during PhD

Under Review Journal Papers

[1] Mostafa Mirshekari, Jonathon Fagert, Shijia Pan, Pei Zhang, and Hae Young Noh. Obstruction-Invariant Occupant Localization using Footstep-Induced Floor Vibrtions. *Under Review in Sensors*.

[2] Jonathon Fagert, Mostafa Mirshekari, Shijia Pan, Linda Lowes, Megan Lammarino, Pei Zhang, and Hae Young Noh. Gait Balance Symmetry Estimation Using Footstep Induced Structural Floor Vibrations. *Under Review in Mechanical Systems and Signal Processing*.

[3] Asim Smailagic, Pedro Costa, Alex Gaudio, Kartik Khandelwal, Mostafa Mirshekari, Jonathon Fagert, Devesh Walawalkar, Susu Xu, Adrian Galdran, Pei Zhang, Aurelio Campilho, and Hae Young Noh. O-MedAL: Online Active Deep Learning for Medical Image Analysis. *Under Review in Data Mining and Knowledge Discovery*.

Journal Papers

[1] Mostafa Mirshekari, Jonathon Fagert, Shijia Pan, Pei Zhang, and Hae Young Noh. Step-Level Occupant Detection across Different Structures through Footstep-Induced Floor Vibration using Model Transfer. *accepted in Journal of Engineering Mechanics*.

[2] Shijia Pan, Mostafa Mirshekari, Jonathon Fagert, Carlos Ruiz, Hae Young Noh, and Pei Zhang. Area occupancy counting through sparse structural vibration sensing. *IEEE Pervasive Computing*, 18(1):28–37, 2019.

[3] Mostafa Mirshekari, Shijia Pan, Jonathon Fagert, Eve M Schooler, Pei Zhang, and Hae Young Noh. Occupant localization using footstep-induced structural vibration. *Mechanical Systems and Signal Processing*, 112:77–97, 2018.

[4] Shijia Pan, Mostafa Mirshekari, Jonathon Fagert, Ceferino Gabriel Ramirez, Albert Jin Chung, Chih Chi Hu, John Paul Shen, Pei Zhang, and Hae Young Noh. Characterizing human

activity induced impulse and slip-pulse excitations through structural vibration. *Journal of Sound and Vibration*, 414:61–80, 2018.

[5] Shijia Pan, Tong Yu, Mostafa Mirshekari, Jonathon Fagert, Amelie Bonde, Ole J Mengshoel, Hae Young Noh, and Pei Zhang. Footprintid: Indoor pedestrian identification through ambient structural vibration sensing. *Proceedings of the ACM on Interactive, Mobile, Wearableand Ubiquitous Technologies*, 1(3):89, 2017.

[6] Shijia Pan, Susu Xu, Mostafa Mirshekari, Pei Zhang, and Hae Young Noh. Collaboratively adaptive vibration sensing system for high fidelity monitoring of structural responses induced by pedestrians. *Frontiers in Built Environment*, 3:28, 2017

Peer-Reviewed (Journal-Level) Conference Papers

[1] Asim Smailagic, Pedro Costa, Hae Young Noh, Devesh Walawalkar, Kartik Khandelwal, Adrian Galdran, Mostafa Mirshekari, Jonathon Fagert, Susu Xu, Pei Zhang, et al. Medal: Accurate and robust deep active learning for medical image analysis. In *2018 17th IEEE International Conference on Machine Learning and Applications (ICMLA)*, pages 481–488. IEEE, 2018.

[2] Shijia Pan, Ceferino Gabriel Ramirez, Mostafa Mirshekari, Jonathon Fagert, Albert JinChung, Chih Chi Hu, John Paul Shen, Hae Young Noh, and Pei Zhang. Surfacevibe: vibration-based tap & swipe tracking on ubiquitous surfaces. In *Information Processing in Sensor Networks (IPSN), 2017 16th ACM/IEEE International Conference on*, pages 197–208. IEEE, 2017.

Other Conference Papers

[1] Mostafa Mirshekari, Jonathon Fagert, Shijia Pan, Pei Zhang, and Hae Young Noh. Physics-guided model transfer for human gait monitoring using footstep-induced floor vibration. *Structural Health Monitoring 2019*, 2019.

[2] Jonathon Fagert, Mostafa Mirshekari, Shijia Pan, Pei Zhang, and Hae Young Noh. Vibration source separation for multiple people gait monitoring using footstep-induced floor vibrations. *Structural Health Monitoring 2019*, 2019.

[3] Laixi Shi, Mostafa Mirshekari, Jonathon Fagert, Yuejie Chi, Hae Young Noh, Pei Zhang, and Shijia Pan. Device-free multiple people localization through floor vibration. In *Proceedings of the 1st ACM International Workshop on Device-Free Human Sensing*, pages 57–61. ACM,2019.

[4] Yue Zhang, Shijia Pan, Jonathon Fagert, Mostafa Mirshekari, Hae Young Noh, Pei Zhang,and Lin Zhang. Occupant activity level estimation using floor vibration. In *Proceedingsof the 2018 ACM International Joint Conference and 2018 International Symposium on Pervasive and Ubiquitous Computing and Wearable Computers*, pages 1355–1363. ACM,2018.

[5] Mostafa Mirshekari, Jonathon Fagert, Amelie Bonde, Pei Zhang, and Hae Young Noh. Human gait monitoring using footstep-induced floor vibrations across different structures. In *Proceedings of the 2018 ACM International Joint Conference and 2018 International Symposium on Pervasive and Ubiquitous Computing and Wearable Computers*, pages 1382–1391. ACM, 2018.

[6] Tong Yu, Shijia Pan, Susu Xu, Xinlei Chen, Mostafa Mirshekari, Jonathon Fagert, Pei Zhang, Hae Young Noh, and Ole J Mengshoel. Ilpc: Iterative learning using physical constraints in real-world sensing data. In *SmartIoT 2018 Workshop: AI enhanced IoT data processing for Intelligent Applications*, page 120, 2018.

[7] Jonathon Fagert, Mostafa Mirshekari, Shijia Pan, Pei Zhang, and Hae Young Noh. Characterizing left-right gait balance using footstep-induced structural vibrations. In *Sensors andSmart Structures Technologies for Civil, Mechanical, and Aerospace Systems 2017*, volume 10168, page 1016819. International Society for Optics and Photonics, 2017.

[8] Jonathon Fagert, Mostafa Mirshekari, Shijia Pan, Pei Zhang, and Hae Young Noh. Monitoring hand-washing practices using structural vibrations. *Structural Health Monitoring 2017*, 2017.

[9] Shijia Pan, Mostafa Mirshekari, Pei Zhang, and Hae Young Noh. Occupant traffic estimation through structural vibration sensing. In *Sensors and Smart Structures Technologies for*

Civil,Mechanical, and Aerospace Systems 2016, volume 9803, page 980306. International Society for Optics and Photonics, 2016.

[10] Mostafa Mirshekari, Shijia Pan, Pei Zhang, and Hae Young Noh. Characterizing wave propagation to improve indoor step-level person localization using floor vibration. In *SPIE Smart Structures and Materials+ Nondestructive Evaluation and Health Monitoring*, pages 980305–980305. International Society for Optics and Photonics, 2016.

[11] Mike Lam, Mostafa Mirshekari, Shijia Pan, Pei Zhang, and Hae Young Noh. Robust occupant detection through step-induced floor vibration by incorporating structural characteristics. In *Dynamics of Coupled Structures*, Volume 4, pages 357–367. Springer, 2016.

Posters and Extended Abstracts

[1] Jonathon Fagert, Mostafa Mirshekari, Shijia Pan, Pei Zhang, and Hae Young Noh. Structural property guided gait parameter estimation using footstep-induced floor vibrations. In *Dynamics of Civil Structures*, Volume 2, pages 191–194. Springer, 2020.

[2] Jonathon Fagert, Mostafa Mirshekari, Shijia Pan, Pei Zhang, and Hae Young Noh. Gait health monitoring through footstep-induced floor vibrations. In *2019 18th ACM/IEEE International Conference on Information Processing in Sensor Networks (IPSN)*, pages 319–320. IEEE,2019.

[3] Jonathon Fagert, Mostafa Mirshekari, Shijia Pan, Pei Zhang, and Hae Young Noh. Characterizing structural changes to estimate walking gait balance. In *Dynamics of Civil Structures*,Volume 2, pages 333–335. Springer, 2019.

[4] Yue Zhang, Shijia Pan, Jonathon Fagert, Mostafa Mirshekari, Hae Young Noh, Pei Zhang, and Lin Zhang. Vibration-based occupant activity level monitoring system. In *Proceedings of the 16th ACM Conference on Embedded Networked Sensor Systems*, pages 349–350. ACM,2018.

[5] Amelie Bonde, Mostafa Mirshekari, Jonathon Fagert, Shijia Pan, Hae Young Noh, and Pei Zhang. Seat vibration for heart monitoring in a moving automobile. In *Proceedings of the First Workshop on Data Acquisition To Analysis*, pages 7–8. ACM, 2018.

[6] Yue Zhang, Shijia Pan, Jonathon Fagert, Mostafa Mirshekari, Hae Young Noh, Pei Zhang, and Lin Zhang. Occupant-Induced Structure Vibration Dataset in an Office Building. In *Proceedings of the First Workshop on Data Acquisition To Analysis*, pages 7–8. ACM, 2018.

[7] Mostafa Mirshekari, Pei Zhang, and Hae Young Noh. Calibration-free footstep frequency estimation using structural vibration. In *Dynamics of Civil Structures*, Volume 2, pages287–289. Springer, 2017.

[8] Shijia Pan, Kent Lyons, Mostafa Mirshekari, Hae Young Noh, and Pei Zhang. Multiple pedestrian tracking through ambient structural vibration sensing. In *Proceedings of the 14th ACM Conference on Embedded Network Sensor Systems*, pages 366–367,2016.

[9] Mostafa Mirshekari, Pei Zhang, and Hae Young Noh. Non-intrusive occupant localization using floor vibrations in dispersive structure. In *Proceedings of the 14th ACM Conferenceon Embedded Network Sensor Systems*, pages 378–379. ACM, 2016.

[10] Shijia Pan, Mostafa Mirshekari, Hae Young Noh, and Pei Zhang. Structural sensing system with networked dynamic sensing configuration. In *Proceedings of the 14th International Conference on Information Processing in Sensor Networks*, pages 344–345. ACM, 2015.

[11] Mostafa Mirshekari, Shijia Pan, Adeola Bannis, Yan Pui Mike Lam, Pei Zhang, and Hae Young Noh. Step-level person localization through sparse sensing of structural vibration. In *proceedings of the 14th international conference on information processing in sensor networks*, pages 376–377. ACM, 2015.

Presentations and Talks

[1] Mostafa Mirshekari, Shijia Pan, Jonathon Fagert, Pei Zhang, and Hae Young Noh. Calibration-Free Occupant Localization using Structural Vibration through Locally Adaptive Multilateration. In *The Seventh World Conference on Structural Control and Monitoring (7WCSCM)*, Qingdao, China, 2018.

[2] Mostafa Mirshekari, Shijia Pan, Jonathon Fagert, Pei Zhang, and Hae Young Noh. Obstruction-Invariant Indoor Occupant Localization Using Footstep-Induced Structural Vibration. In *Engineering Mechanics Institute (EMI) Conference*, Los Angeles, California, USA, 2019.

[3] Shijia Pan, Mostafa Mirshekari, Jonathon Fagert, Pei Zhang, and Hae Young Noh. Structural Element Modeling for Vibration-based Indoor Human Sensing Configuration. In *The Seventh World Conference on Structural Control and Monitoring (7WCSCM)*, Qingdao, China, 2018.

[4] Mostafa Mirshekari, Jonathon Fagert, Shijia Pan, Pei Zhang, and Hae Young Noh. Buildings as Sensors: Indirect Monitoring of Human Activities through Structural Vibrations. In *Conference on Smart Materials, Adaptive Structures and Intelligent Systems (SMASIS)*, San Antonio, Texas, USA, 2018.

[5] Mostafa Mirshekari, Jonathon Fagert, Shijia Pan, Pei Zhang, and Hae Young Noh. Human Health Tracking through Gait-Induced Floor Vibrations Across Different Structures. In *Engineering Mechanics Institute (EMI) Conference*, Boston, Massachusetts , USA, 2018.

[6] Mostafa Mirshekari, Pei Zhang, and Hae Young Noh. Characterizing Wave Propagation to Improve Indoor Person Localization using Floor Vibration. In *CMU-SNU Student Workshop*, Pittsburgh, PA, USA, 2017.

[7] Mostafa Mirshekari, Jonathon Fagert, Shijia Pan, Pei Zhang, and Hae Young Noh. Occupant Localization in Obstructed Indoor Environments using Floor Vibrations. In *Engineering Mechanics Institute (EMI) Conference*, San Diego, California, USA, 2017.

[8] Mostafa Mirshekari, Pei Zhang, and Hae Young Noh. Structure-Invariant Indoor Person Localization using Structural Vibration. In *Engineering Mechanics Institute (EMI) Conference*, Nashville, Tennessee, USA, 2016.

References

[1] Giovanni Diraco, Alessandro Leone, and Pietro Siciliano. People occupancy detection and profiling with 3d depth sensors for building energy management. *Energy and Buildings*, 92:246–266, 2015.

[2] Christopher M Stoppel and Fernanda Leite. Integrating probabilistic methods for describing occupant presence with building energy simulation models. *Energy and Buildings*, 68:99–107, 2014.

[3] William PL Cully, Simon L Cotton, William G Scanlon, and JB McQuiston. Localization algorithm performance in ultra low power active rfid based patient tracking. In *Personal Indoor and Mobile Radio Communications (PIMRC), 2011 IEEE 22nd International Symposium on*, pages 2158–2162. IEEE, 2011.

[4] William PL Cully, Simon L Cotton, and William G Scanlon. Empirical performance of rssi-based monte carlo localisation for active rfid patient tracking systems. *International Journal of Wireless Information Networks*, 19(3):173–184, 2012.

[5] Henriet Visser. Gait and balance in senile dementia of alzheimer's type. *Age and ageing*, 12(4):296–301, 1983.

[6] Duygu Ilgin, Sevgi Ozalevli, Oguz Kilinc, Can Sevinc, Arif H Cimrin, and Eyup S Ucan. Gait speed as a functional capacity indicator in patients with chronic obstructive pulmonary disease. *Annals of thoracic medicine*, 6(3):141, 2011.

[7] Craig M McDonald, Lana M Widman, Denise D Walsh, Sandra A Walsh, and R Ted Abresch. Use of step activity monitoring for continuous physical activity assessment in boys with duchenne muscular dystrophy. *Archives of physical medicine and rehabilitation*, 86(4):802–808, 2005.

[8] Peter Henry, Michael Krainin, Evan Herbst, Xiaofeng Ren, and Dieter Fox. Rgb-d mapping: Using kinect-style depth cameras for dense 3d modeling of indoor environments. *The International Journal of Robotics Research*, 31(5):647–663, 2012.

[9] Ying Zhang, Chuanjiang Luo, and Juan Liu. Walk&sketch: create floor plans with an rgb-d camera. In *Proceedings of the 2012 ACM Conference on Ubiquitous Computing*, pages 461–470. ACM, 2012.

[10] Chenren Xu, Bernhard Firner, Robert S Moore, Yanyong Zhang, Wade Trappe, Richard Howard, Feixiong Zhang, and Ning An. Scpl: Indoor device-free multi-subject counting and localization using radio signal strength. In *Proceedings of the 12th international conference on Information Processing in Sensor Networks*, pages 79–90. ACM, 2013.

[11] Anindya S Paul, Eric A Wan, Fatema Adenwala, Erich Schafermeyer, Nick Preiser, Jeffrey Kaye, and Peter G Jacobs. Mobilerf: a robust device-free tracking system based on a hybrid neural network hmm classifier. In *Proceedings of the 2014 ACM International Joint Conference on Pervasive and Ubiquitous Computing*, pages 159–170. ACM, 2014.

[12] Jacob T Biehl, Matthew Cooper, Gerry Filby, and Sven Kratz. Loco: a ready-to-deploy framework for efficient room localization using wi-fi. In *Proceedings of the 2014 ACM International Joint Conference on Pervasive and Ubiquitous Computing*, pages 183–187. ACM, 2014.

[13] Domnic Savio and Thomas Ludwig. Smart carpet: A footstep tracking interface. In *Advanced Information Networking and Applications Workshops, 2007, AINAW'07. 21st International Conference on*, volume 2, pages 754–760. IEEE, 2007.

[14] Mihai Andries, Olivier Simonin, and François Charpillet. Localization of humans, objects, and robots interacting on load-sensing floors. *IEEE Sensors Journal*, 16(4):1026–1037, 2016.

[15] Patrick Lazik, Niranjini Rajagopal, Oliver Shih, Bruno Sinopoli, and Anthony Rowe. Alps: A bluetooth and ultrasound platform for mapping and localization. In *Proceedings of the 13th ACM Conference on Embedded Networked Sensor Systems*, pages 73–84. ACM, 2015.

[16] Eladio Martin, Oriol Vinyals, Gerald Friedland, and Ruzena Bajcsy. Precise indoor localization using smart phones. In *Proceedings of the international conference on Multimedia*, pages 787–790. ACM, 2010.

[17] Anshul Rai, Krishna Kant Chintalapudi, Venkata N Padmanabhan, and Rijurekha Sen. Zee: zero-effort crowdsourcing for indoor localization. In *Proceedings of the 18th annual international conference on Mobile computing and networking*, pages 293–304. ACM, 2012.

[18] Krishna Chintalapudi, Anand Padmanabha Iyer, and Venkata N Padmanabhan. Indoor localization without the pain. In *Proceedings of the sixteenth annual international conference on Mobile computing and networking*, pages 173–184. ACM, 2010.

[19] Vincent Lenders, Emmanouil Koukoumidis, Pei Zhang, and Margaret Martonosi. Location-based trust for mobile user-generated content: applications, challenges and implementations. In *Proceedings of the 9th workshop on Mobile computing systems and applications*, pages 60–64. ACM, 2008.

[20] Shijia Pan, Susu Pan Xu, Mostafa Mirshekari, Pei Zhang, and Hae Young Noh. Collaboratively adaptive vibration sensing system for high fidelity monitoring of structural responses induced by pedestrians. *Frontiers in Built Environment*, 3:28, 2017.

[21] Michael Baron. *Probability and statistics for computer scientists*. CRC Press, 2013.

[22] Tony Finch. Incremental calculation of weighted mean and variance. *University of Cambridge*, 4:11–5, 2009.

[23] Mostafa Mirshekari, Shijia Pan, Pei Zhang, and Hae Young Noh. Characterizing wave propagation to improve indoor step-level person localization using floor vibration. In *SPIE Smart Structures and Materials+ Nondestructive Evaluation and Health Monitoring*, pages 980305–980305. International Society for Optics and Photonics, 2016.

[24] Mostafa Mirshekari, Shijia Pan, Jonathon Fagert, Eve M Schooler, Pei Zhang, and Hae Young Noh. Occupant localization using footstep-induced structural vibration. *Mechanical Systems and Signal Processing*, 112:77–97, 2018.

[25] Jeffrey D Poston, R Michael Buehrer, and Pablo A Tarazaga. Indoor footstep localization from structural dynamics instrumentation. *Mechanical Systems and Signal Processing*, 88:224–239, 2017.

[26] Yves Reuland, Sai GS Pai, Slah Drira, and Ian FC Smith. Vibration-based occupant detection using a multiple-model approach. In *Dynamics of Civil Structures, Volume 2*, pages 49–56. Springer, 2017.

[27] Shijia Pan, Mostafa Mirshekari, Jonathon Fagert, Ceferino Gabriel Ramirez, Albert Jin Chung, Chih Chi Hu, John Paul Shen, Pei Zhang, and Hae Young Noh. Characterizing human activity induced impulse and slip-pulse excitations through structural vibration. *Journal of Sound and Vibration*, 414:61–80, 2018.

[28] Ramin Madarshahian, Juan M Caicedo, and Nicholas Haerens. Human activity benchmark classification using multilayer artificial neural network. In *Dynamics of Civil Structures, Volume 2*, pages 207–210. Springer, 2019.

[29] Jonathon Fagert, MOSTAFA MIRSHEKARI, SHIJIA PAN, PEI ZHANG, and HAE YOUNG NOH. Monitoring hand-washing practices using structural vibrations. *Structural Health Monitoring 2017*, (shm), 2017.

[30] Shijia Pan, Tong Yu, Mostafa Mirshekari, Jonathon Fagert, Amelie Bonde, Ole J Mengshoel, Hae Young Noh, and Pei Zhang. Footprintid: Indoor pedestrian identification through ambi-

ent structural vibration sensing. *Proceedings of the ACM on Interactive, Mobile, Wearable and Ubiquitous Technologies*, 1(3):89, 2017.

[31] Jonathon Fagert, Mostafa Mirshekari, Shijia Pan, Pei Zhang, and Hae Young Noh. Characterizing left-right gait balance using footstep-induced structural vibrations. In *Sensors and Smart Structures Technologies for Civil, Mechanical, and Aerospace Systems 2017*, volume 10168, page 1016819. International Society for Optics and Photonics, 2017.

[32] Gökhan Koç and Korkut Yegin. Footstep and vehicle detection using slow and quick adaptive thresholds algorithm. *International Journal of Distributed Sensor Networks*, 2013, 2013.

[33] George P Succi, Daniel Clapp, Robert Gampert, and Gervasio Prado. Footstep detection and tracking. In *Aerospace/Defense Sensing, Simulation, and Controls*, pages 22–29. International Society for Optics and Photonics, 2001.

[34] Jeffrey D Poston, R Michael Buehrer, and Pablo A Tarazaga. A framework for occupancy tracking in a building via structural dynamics sensing of footstep vibrations. *Frontiers in Built Environment*, 3:65, 2017.

[35] SA Alyamkin and SI Eremenko. Pedestrian detection algorithms based on an analysis of the autocorrelation function of a seismic signal. *Optoelectronics, Instrumentation and Data Processing*, 47(2):124–129, 2011.

[36] Michael S Richman, Douglas S Deadrick, Robert J Nation, and Scott Whitney. Personnel tracking using seismic sensors. In *Aerospace/Defense Sensing, Simulation, and Controls*, pages 14–21. International Society for Optics and Photonics, 2001.

[37] Arun Subramanian, Kishan G Mehrotra, Chilukuri K Mohan, Pramod K Varshney, and Thyagaraju Damarla. Feature selection and occupancy classification using seismic sensors. In *Trends in Applied Intelligent Systems*, pages 605–614. Springer, 2010.

[38] Mike Lam, Mostafa Mirshekari, Shijia Pan, Pei Zhang, and Hae Young Noh. Robust occupant

detection through step-induced floor vibration by incorporating structural characteristics. In *Dynamics of Coupled Structures, Volume 4*, pages 357–367. Springer, 2016.

[39] Sinno Jialin Pan, Qiang Yang, et al. A survey on transfer learning. *IEEE Transactions on knowledge and data engineering*, 22(10):1345–1359, 2010.

[40] Jerome Friedman, Trevor Hastie, and Robert Tibshirani. *The elements of statistical learning*, volume 1. Springer series in statistics New York, NY, USA:, 2001.

[41] Wenyuan Dai, Gui-Rong Xue, Qiang Yang, and Yong Yu. Transferring naive bayes classifiers for text classification. In *AAAI*, volume 7, pages 540–545, 2007.

[42] Steffen Bickel, Michael Brückner, and Tobias Scheffer. Discriminative learning for differing training and test distributions. In *Proceedings of the 24th international conference on Machine learning*, pages 81–88. ACM, 2007.

[43] Masashi Sugiyama, Shinichi Nakajima, Hisashi Kashima, Paul V Buenau, and Motoaki Kawanabe. Direct importance estimation with model selection and its application to covariate shift adaptation. In *Advances in neural information processing systems*, pages 1433–1440, 2008.

[44] Tong Yu, Shijia Pan, Susu Xu, Xinlei Chen, Mostafa Mirshekari, Jonathon Fagert, Pei Zhang, Hae Young Noh, and Ole J Mengshoel. Ilpc: Iterative learning using physical constraints in real-world sensing data. In *SmartIoT 2018 Workshop: AI enhanced IoT data processing for Intelligent Applications*, page 120, 2018.

[45] John Blitzer, Ryan McDonald, and Fernando Pereira. Domain adaptation with structural correspondence learning. In *Proceedings of the 2006 conference on empirical methods in natural language processing*, pages 120–128. Association for Computational Linguistics, 2006.

[46] Shai Ben-David, John Blitzer, Koby Crammer, and Fernando Pereira. Analysis of represen-

tations for domain adaptation. In *Advances in neural information processing systems*, pages 137–144, 2007.

[47] Xiao Ling, Wenyuan Dai, Gui-Rong Xue, Qiang Yang, and Yong Yu. Spectral domain-transfer learning. In *Proceedings of the 14th ACM SIGKDD international conference on Knowledge discovery and data mining*, pages 488–496. ACM, 2008.

[48] Sinno Jialin Pan, Ivor W Tsang, James T Kwok, and Qiang Yang. Domain adaptation via transfer component analysis. *IEEE Transactions on Neural Networks*, 22(2):199–210, 2011.

[49] Mostafa Mirshekari, Jonathon Fagert, Amelie Bonde, Pei Zhang, and Hae Young Noh. Human gait monitoring using footstep-induced floor vibrations across different structures. In *Proceedings of the 2018 ACM International Joint Conference and 2018 International Symposium on Pervasive and Ubiquitous Computing and Wearable Computers*, pages 1382–1391. ACM, 2018.

[50] G. Strang and S. Strang. *Linear Algebra and Its Applications*. Thomson, Brooks/Cole, 2006.

[51] Alan V Oppenheim, Alan S Willsky, and Syed Hamid Nawab. Signals and systems 2nd ed. *New Jersey: Prentice Hall*, 1997.

[52] Alex Smola, Arthur Gretton, Le Song, and Bernhard Schölkopf. A hilbert space embedding for distributions. In *International Conference on Algorithmic Learning Theory*, pages 13–31. Springer, 2007.

[53] Arthur Gretton, Karsten M Borgwardt, Malte J Rasch, Bernhard Schölkopf, and Alexander Smola. A kernel two-sample test. *Journal of Machine Learning Research*, 13(Mar):723–773, 2012.

[54] Sinno Jialin Pan, James T Kwok, and Qiang Yang. Transfer learning via dimensionality reduction. In *AAAI*, volume 8, pages 677–682, 2008.

[55] Arthur Gretton. Introduction to rkhs, and some simple kernel algorithms. *Adv. Top. Mach. Learn. Lecture Conducted from University College London*, 16, 2013.

[56] FENG Changyong, WANG Hongyue, LU Naiji, CHEN Tian, HE Hua, LU Ying, et al. Log-transformation and its implications for data analysis. *Shanghai archives of psychiatry*, 26(2):105, 2014.

[57] Arthur Gretton, Karsten M Borgwardt, Malte Rasch, Bernhard Schölkopf, and Alex J Smola. A kernel method for the two-sample-problem. In *Advances in neural information processing systems*, pages 513–520, 2007.

[58] Bernhard Schölkopf, Alexander Smola, and Klaus-Robert Müller. Nonlinear component analysis as a kernel eigenvalue problem. *Neural computation*, 10(5):1299–1319, 1998.

[59] Arthur Gretton, Olivier Bousquet, Alex Smola, and Bernhard Schölkopf. Measuring statistical dependence with hilbert-schmidt norms. In *International conference on algorithmic learning theory*, pages 63–77. Springer, 2005.

[60] Rune Brincker, Lingmi Zhang, and P Andersen. Modal identification from ambient responses using frequency domain decomposition. In *Proc. of the 18*'International Modal Analysis Conference (IMAC), San Antonio, Texas*, 2000.

[61] Yutaka Sasaki et al. The truth of the f-measure. *Teach Tutor mater*, 1(5):1–5, 2007.

[62] Matlab statistics and machine learning toolbox, 2018. The MathWorks, Natick, MA, USA.

[63] James S Hall and Jennifer E Michaels. Model-based parameter estimation for characterizing wave propagation in a homogeneous medium. *Inverse Problems*, 27(3):035002, 2011.

[64] Ajay Raghavan and Carlos ES Cesnik. Guided-wave signal processing using chirplet matching pursuits and mode correlation for structural health monitoring. *Smart Materials and Structures*, 16(2):355, 2007.

[65] Jingpin Jiao, Cunfu He, Bin Wu, Renyuan Fei, and Xiuyan Wang. Application of wavelet transform on modal acoustic emission source location in thin plates with one sensor. *International Journal of Pressure Vessels and Piping*, 81(5):427–431, 2004.

[66] N Toyama, J-H Koo, R Oishi, M Enoki, and T Kishi. Two-dimensional ae source location with two sensors in thin cfrp plates. *Journal of Materials science letters*, 20(19):1823–1825, 2001.

[67] WH Prosser, Michael D Seale, and Barry T Smith. Time-frequency analysis of the dispersion of lamb modes. *The Journal of the Acoustical Society of America*, 105(5):2669–2676, 1999.

[68] Francesco Ciampa and Michele Meo. Acoustic emission source localization and velocity determination of the fundamental mode a0 using wavelet analysis and a newton-based optimization technique. *Smart Materials and Structures*, 19(4):045027, 2010.

[69] Hyunjo Jeong and Young-Su Jang. Wavelet analysis of plate wave propagation in composite laminates. *Composite Structures*, 49(4):443–450, 2000.

[70] Hyunjo Jeong and Young-Su Jang. Fracture source location in thin plates using the wavelet transform of dispersive waves. *Ultrasonics, Ferroelectrics, and Frequency Control, IEEE Transactions on*, 47(3):612–619, 2000.

[71] Fucai Li, Guang Meng, Lin Ye, Ye Lu, and Kazuro Kageyama. Dispersion analysis of lamb waves and damage detection for aluminum structures using ridge in the time-scale domain. *Measurement Science and Technology*, 20(9):095704, 2009.

[72] Alessandro Perelli, Luca De Marchi, Alessandro Marzani, and Nicolò Speciale. Frequency warped cross-wavelet multiresolution analysis of guided waves for impact localization. *Signal Processing*, 96:51–62, 2014.

[73] Mostafa Mirshekari, Pei Zhang, and Hae Young Noh. Non-intrusive occupant localization using floor vibrations in dispersive structure. In *Proceedings of the 14th ACM Conference on Embedded Network Sensor Systems CD-ROM*, pages 378–379. ACM, 2016.

[74] E Dehghan Niri and S Salamone. A probabilistic framework for acoustic emission source localization in plate-like structures. *Smart Materials and Structures*, 21(3):035009, 2012.

[75] Stefano Coraluppi. Multistatic sonar localization. *IEEE Journal of Oceanic Engineering*, 31(4):964–974, 2006.

[76] Elizabeth Hoppe and Michael Roan. Non-linear, adaptive array processing for underwater source localization and sonar interference suppression. In *OCEANS 2009-EUROPE*, pages 1–5. IEEE, 2009.

[77] James J Caffery Jr. *Wireless location in CDMA cellular radio systems*, volume 535. Springer Science & Business Media, 2006.

[78] Si TS Chia. Location determination and handover in mobile radio systems, February 28 1995. US Patent 5,394,158.

[79] Xiaohong Sheng and Yu-Hen Hu. Maximum likelihood multiple-source localization using acoustic energy measurements with wireless sensor networks. *IEEE Transactions on Signal Processing*, 53(1):44–53, 2005.

[80] Michael G Rabbat and Robert D Nowak. Decentralized source localization and tracking [wireless sensor networks]. In *Acoustics, Speech, and Signal Processing, 2004. Proceedings.(ICASSP'04). IEEE International Conference on*, volume 3, pages iii–921. IEEE, 2004.

[81] Francesco Ciampa and Michele Meo. A new algorithm for acoustic emission localization and flexural group velocity determination in anisotropic structures. *Composites Part A: Applied Science and Manufacturing*, 41(12):1777–1786, 2010.

[82] Alessandro Perelli, Luca De Marchi, Alessandro Marzani, and Nicolò Speciale. Acoustic emission localization in plates with dispersion and reverberations using sparse pzt sensors in passive mode. *Smart Materials and Structures*, 21(2):025010, 2012.

[83] Tribikram Kundu. Acoustic source localization. *Ultrasonics*, 54(1):25–38, 2014.

[84] Jean-Marc Valin, François Michaud, Jean Rouat, and Dominic Létourneau. Robust sound source localization using a microphone array on a mobile robot. In *Intelligent Robots*

and Systems, 2003.(IROS 2003). Proceedings. 2003 IEEE/RSJ International Conference on, volume 2, pages 1228–1233. IEEE, 2003.

[85] Kazuhiro Nakadai, Daisuke Matsuura, Hiroshi G Okuno, and Hiroaki Kitano. Applying scattering theory to robot audition system: Robust sound source localization and extraction. In *Intelligent Robots and Systems, 2003.(IROS 2003). Proceedings. 2003 IEEE/RSJ International Conference on*, volume 2, pages 1147–1152. IEEE, 2003.

[86] Tian He, Qiang Pan, Yaoguang Liu, Xiandong Liu, and Dayong Hu. Near-field beamforming analysis for acoustic emission source localization. *Ultrasonics*, 52(5):587–592, 2012.

[87] Joe C Chen, Kung Yao, and Ralph E Hudson. Source localization and beamforming. *IEEE Signal Processing Magazine*, 19(2):30–39, 2002.

[88] Jean-Marc Valin, François Michaud, and Jean Rouat. Robust localization and tracking of simultaneous moving sound sources using beamforming and particle filtering. *Robotics and Autonomous Systems*, 55(3):216–228, 2007.

[89] Stephen P Tarzia, Peter A Dinda, Robert P Dick, and Gokhan Memik. Indoor localization without infrastructure using the acoustic background spectrum. In *Proceedings of the 9th international conference on Mobile systems, applications, and services*, pages 155–168. ACM, 2011.

[90] Martin Azizyan, Ionut Constandache, and Romit Roy Choudhury. Surroundsense: mobile phone localization via ambience fingerprinting. In *Proceedings of the 15th annual international conference on Mobile computing and networking*, pages 261–272. ACM, 2009.

[91] Eddie CL Chan, George Baciu, and SC Mak. Using wi-fi signal strength to localize in wireless sensor networks. In *Communications and Mobile Computing, 2009. CMC'09. WRI International Conference on*, volume 1, pages 538–542. IEEE, 2009.

[92] Qing Fu and Guenther Retscher. Active rfid trilateration and location fingerprinting based on rssi for pedestrian navigation. *Journal of Navigation*, 62(02):323–340, 2009.

[93] Navin Kumar Sharma. A weighted center of mass based trilateration approach for locating wireless devices in indoor environment. In *Proceedings of the 4th ACM international workshop on Mobility management and wireless access*, pages 112–115. ACM, 2006.

[94] Yaming Xu, Jianguo Zhou, and Peng Zhang. Rss-based source localization when path-loss model parameters are unknown. *Communications Letters, IEEE*, 18(6):1055–1058, 2014.

[95] Yifeng Zhou, Jun Li, and Lisa Lamont. Multilateration localization in the presence of anchor location uncertainties. In *Global Communications Conference (GLOBECOM), 2012 IEEE*, pages 309–314. IEEE, 2012.

[96] Dong Liang, Shen-fang Yuan, and Meng-long Liu. Distributed coordination algorithm for impact location of preciseness and real-time on composite structures. *Measurement*, 46(1):527–536, 2013.

[97] Tribikram Kundu, Samik Das, Steven A Martin, and Kumar V Jata. Locating point of impact in anisotropic fiber reinforced composite plates. *Ultrasonics*, 48(3):193–201, 2008.

[98] Ka Wai Cheung, Hing-Cheung So, W-K Ma, and Yiu-Tong Chan. Least squares algorithms for time-of-arrival-based mobile location. *IEEE Transactions on Signal Processing*, 52(4):1121–1130, 2004.

[99] Fredrik Gustafsson and Fredrik Gunnarsson. Positioning using time-difference of arrival measurements. In *Acoustics, Speech, and Signal Processing, 2003. Proceedings.(ICASSP'03). 2003 IEEE International Conference on*, volume 6, pages VI–553. IEEE, 2003.

[100] Giuseppe Destino and Giuseppe Abreu. On the maximum likelihood approach for source and network localization. *IEEE Transactions on Signal Processing*, 59(10):4954–4970, 2011.

[101] Yiu-Tong Chan, H Yau Chin Hang, and Pak-chung Ching. Exact and approximate maximum likelihood localization algorithms. *IEEE Transactions on Vehicular Technology*, 55(1):10–16, 2006.

[102] Gang Yan and Jianfei Tang. A bayesian approach for localization of acoustic emission source in plate-like structures. *Mathematical Problems in Engineering*, 2015, 2015.

[103] Igor Aleksandrovich Viktorov. *Rayleigh and Lamb waves: physical theory and applications*. Plenum press, 1970.

[104] Young Hak Lee and Taekeun Oh. The simple lamb wave analysis to characterize concrete wide beams by the practical masw test. *Materials*, 9(6):437, 2016.

[105] Keith Worden. Rayleigh and lamb waves-basic principles. *Strain*, 37(4):167–172, 2001.

[106] Young Hak Lee and Taekeun Oh. The measurement of p-, s-, and r-wave velocities to evaluate the condition of reinforced and prestressed concrete slabs. *Advances in Materials Science and Engineering*, 2016, 2016.

[107] Paul S Addison. *The illustrated wavelet transform handbook: introductory theory and applications in science, engineering, medicine and finance*. CRC press, 2002.

[108] Michael Edwards and Xianghua Xie. Footstep pressure signal analysis for human identification. In *Biomedical Engineering and Informatics (BMEI), 2014 7th International Conference on*, pages 307–312. IEEE, 2014.

[109] James M Sabatier and Alexander E Ekimov. A review of human signatures in urban environments using seismic and acoustic methods. In *Technologies for Homeland Security, 2008 IEEE Conference on*, pages 215–220. IEEE, 2008.

[110] Musaab Alaziz, Zhenhua Jia, Jian Liu, Richard Howard, Yingying Chen, and Yanyong Zhang. Motion scale: A body motion monitoring system using bed-mounted wireless load cells. In *Connected Health: Applications, Systems and Engineering Technologies (CHASE), 2016 IEEE First International Conference on*, pages 183–192. IEEE, 2016.

[111] I/O Sensor Nederland bv. *SM-24 Geophone Element*, 2006. P/N 1004117.

[112] Joseph A Paradiso and Che King Leo. Tracking and characterizing knocks atop large interactive displays. *Sensor Review*, 25(2):134–143, 2005.

[113] Milton Abramowitz and Irene A Stegun. *Handbook of mathematical functions: with formulas, graphs, and mathematical tables*, volume 55. Courier Corporation, 1964.

[114] Douglas Schwarz. Fast and robust curve intersections. http://www.mathworks.com/matlabcentral/fileexchange/11837-fast-and-robust-curve-intersections, 2010. [Online; accessed 13-September-2016].

[115] Jan Achenbach. *Wave propagation in elastic solids*, volume 16. Elsevier, 2012.

[116] Mehdi Setareh and Robert D Hanson. Tuned mass dampers to control floor vibration from humans. *Journal of Structural Engineering*, 118(3):741–762, 1992.

[117] Jae-Seung Hwang, Hongjin Kim, Dae-Ho Moon, and Hong-Gun Park. Control of floor vibration and noise using multiple tuned mass dampers. *Noise Control Engineering Journal*, 59(6):652–659, 2011.

[118] Anthony C Webster and Rimas Vaicaitis. Application of tuned mass dampers to control vibrations of composite floor systems. *Engineering Journal of the American Institute of Steel Construction*, 29(3):116–124, 1992.

[119] Mehdi Setareh, John K Ritchey, Anthony J Baxter, and Thomas M Murray. Pendulum tuned mass dampers for floor vibration control. *Journal of performance of constructed facilities*, 20(1):64–73, 2006.

[120] X Yan, R Zhu, GL Huang, and FG Yuan. Focusing flexural lamb waves by designing elastic metamaterials bonded on a plate. In *Health Monitoring of Structural and Biological Systems 2013*, volume 8695, page 86952P. International Society for Optics and Photonics, 2013.

[121] Xiang Yan, Rui Zhu, Guoliang Huang, and Fuh-Gwo Yuan. Focusing guided waves using surface bonded elastic metamaterials. *Applied Physics Letters*, 103(12):121901, 2013.

[122] Americo G Woolard, VVN Sriram Malladi, Pablo A Tarazaga, et al. Classification of event location using matched filters via on-floor accelerometers. In *Sensors and Smart Structures Technologies for Civil, Mechanical, and Aerospace Systems 2017*, volume 10168, page 101681A. International Society for Optics and Photonics, 2017.

[123] Alex Pakhomov, Albert Sicignano, Matthew Sandy, and E Tim Goldburt. Single-and three-axis geophone: footstep detection with bearing estimation, localization, and tracking. In *Unattended Ground Sensor Technologies and Applications V*, volume 5090, pages 155–161. International Society for Optics and Photonics, 2003.

[124] Javier Schloemann, VVN Sriram Malladi, Americo G Woolard, Joseph M Hamilton, R Michael Buehrer, and Pablo A Tarazaga. Vibration event localization in an instrumented building. In *Experimental Techniques, Rotating Machinery, and Acoustics, Volume 8*, pages 265–271. Springer, 2015.

[125] R Bahroun, Olivier Michel, François Frassati, Mikael Carmona, and Jean-Louis Lacoume. New algorithm for footstep localization using seismic sensors in an indoor environment. *Journal of Sound and Vibration*, 333(3):1046–1066, 2014.

[126] Slah Drira, Yves Reuland, Sai GS Pai, Hae Young Noh, and Ian FC Smith. Model-based occupant tracking using slab-vibration measurements. *Frontiers in Built Environment*, 5:63, 2019.

[127] Hideo Kasama, Mikio Takemoto, and Kanji Ono. Attenuation measurement of laser excited so-lamb wave by the wavelet transform and porosity estimation in superplastic al-mg plate. *Journal of JSNDI*, 49(4):269–276, 2000.

[128] S Mustapha and L Ye. Non-destructive evaluation (nde) of composites: assessing debonding in sandwich panels using guided waves. In *Non-Destructive Evaluation (NDE) of Polymer Matrix Composites*, pages 238–278. Elsevier, 2013.

[129] Horace Lamb. On waves in an elastic plate. *Proceedings of the Royal Society of London.*

Series A, Containing papers of a mathematical and physical character, 93(648):114–128, 1917.

[130] Matteo Frigo and Steven G Johnson. Fftw: An adaptive software architecture for the fft. In *Proceedings of the 1998 IEEE International Conference on Acoustics, Speech and Signal Processing, ICASSP'98 (Cat. No. 98CH36181)*, volume 3, pages 1381–1384. IEEE, 1998.

[131] Girish Chandrashekar and Ferat Sahin. A survey on feature selection methods. *Computers & Electrical Engineering*, 40(1):16–28, 2014.

[132] Andrew R Conn, Nicholas IM Gould, and Ph L Toint. *Trust region methods*, volume 1. Siam, 2000.